Mohammad Sadegh Shahmirzadi

Evaluation of small-strain Stiffness of Tiller-Flotten Quick Clay and its Anisotropy using Bender Elements

Master's thesis

NTNU
Norwegian University of Science and Technology
Faculty of Engineering
Department of Civil and Environmental Engineering

NTNU
Norwegian University of
Science and Technology

Evaluation of small-strain Stiffness of Tiller-Flotten Quick Clay and its Anisotropy using Bender Elements

Mohammad Sadegh Shahmirzadi

(502385)

Trondheim, July 2020

Supervisor: Steinar Nordal

Preface

This study was performed as a Master's Thesis in the specialization course TBA4900 in Geotechnics. The study is a part of the MSc in civil and environmental engineering with a specialization in Geotechnics. The study is written under the division for Geotechnics at the Norwegian University of Science and Technology (NTNU).

This work has been carried out from February 2020 to July 2020 under the supervision of Steinar Nordal.

This thesis is the continuation of the project thesis on lab testing at the NGTS test site on Flotten, Trondheim. Unfortunately, the experimental program was interrupted due to the Coronavirus outbreak which made it impossible to follow the original plan.

Trondheim, July 2020
Mohammad Sadegh Shahmirzadi

Acknowledgments

Abstract

Small-strain soil properties are of crucial importance in many practical geotechnical problems and seismology aspects. Determination of these parameters, including shear wave velocity (V_s), corresponding small strain shear modulus (G_{max}), and stiffness anisotropy seem to be necessary when describing the behavior of soil in ground movements, and geotechnical modeling. In principle, shear wave velocity measurement can be utilized as a complementary predictor of clay mineralogy and soil classification due to its sensitivity to structure, small-scale heterogeneity, and anisotropy. Moreover, the reasonable correlation of the V_s and G_{max} with the soil mechanical properties provides a useful basis for better evaluation of these parameters. In this research, an experimental study performed to identify the shear wave velocity using the bender element technique incorporated with the triaxial test for Norwegian sensitive soft clay at different orientations. The specimens taken from both mini-block and big-block were isotropically consolidated under various confining pressures. Consequently, the shear wave velocities propagating at three different directions (VH, HH, HV) and polarization were measured by the bender element technique. The results indicate that there are a large number of factors influencing maximum shear modulus, such as consolidation stress, void ratio, depositional angle, and inter-particle bonding. Meanwhile, the relationships between average confining pressure and maximum shear modulus (G_{max}) was also entirely addressed. The vertical shear wave velocity was obtained for big-block within the range of 150 m/s$\leq V_{s(vh)} \leq$173 m/s that was slightly higher than measured values for mini-block 120 m/s$\leq V_{s(vh)} \leq$164 m/s with various mean effective stress after 24-hour consolidation, reflecting the effect of the diameter of the sample on sample quality. Moreover, the influence of the aging on G_{max} and stiffness anisotropy at the small-strain range was investigated using both fresh and old samples. The less dispersion of results followed by a gentle non-linear increase in G_{max} with an increase of isotropic mean stress was observed for the fresh sample (defined as properly extracted, transported, stored under appropriate conditions, and tested as soon as possible), particularly for the fresh sample from the surface with higher OCR. The fresh specimen from mini-block, however, experienced little G_{max} degradation caused by the subsequent three months of storage under appropriate conditions. It was, therefore, concluded that G_{hh} became larger than G_{hv} and G_{vh}. The Shear modulus anisotropy ratios G_{hh}/G_{vh} values at the end of primary isotropic consolidation were found to be within the range of 1.22 and 1.44 in this research. The samples taken from greater depth tended to exhibit a higher degree of fabric anisotropy when subjected to the higher corresponding stress level. Likewise, the degree of fabric anisotropy was higher for fresh samples than old samples that could be due to having higher OCR, and original fabric of the fresh samples. The comparison with previous relevant findings suggests a higher degree of uncertainty at low-stress level than that of high-stress level for G_{max} measurement. Additionally, the measured degree of fabric anisotropy has been reported up to 1.88 when applying higher stress level which is relatively significant for Flotten quick clay.

contents

APPENDIX A – Bender Element Specifications

APPENDIX B – Bender Element Equipment

APPENDIX C –Sample Preparation Apparatus

List of Figures

List of Tables

List Symbols and Abbreviations

Roman letters

A material constant

a attraction

B material constant

b bender element width

b force vector

Bq CPTU pore pressure parameter

c cementation

D diameter of the sample

d effective height

d distance between measurement point

E Young's modulus

$E*$ modified Young's modulus

Eh young's modulus in horizontal direction

Eb elastic modulus

Ev young's modulus in vertical direction

e void ratio

$e0$ initial void ratio

$F(e)$ void ratio function

f frequency

f_c characteristic frequency

$flim$ limiting frequency of near-field influence

fr resonant frequency

fs   CPTU sleeve friction

G shear modulus

GR green tensor

$G1000$ shear modulus measured at T=1000 minutes from the start of the primary consolidation

$Gmax,field$ in-situ small strain shear modulus

$Gmax,primary$ small strain shear modulus at the end of primary consolidation

$Gmax$, $G0$ small strain shear modulus

Gvh small strain shear moduli in the vertical plane

G hv   maximum shear modulus in h,v-plane

G hh   maximum shear modulus in horizontal plane

$Gxy(f)$ cross-power spectrum

Gcon   maximum shear modulus caused by primary consolidation

g gravitational constant

$gmax$ normalized shear modulus

H height of the sample

h bender element thickness

I moment of inertia

IG coefficient of shear modulus increase with time

IL liquidity index

IP plasticity index

K bulk modulus

$K0$ coefficient of earth pressure at rest

k exponent

kb equivalent spring constant

k_h hydraulic conductivity

Lb cantilever length

Ltt tip-to-tip distance between the bender elements

Lu normalized soil suction parameter for sample quality assessment

Lvs normalized shear wave velocity parameter for sample quality assessment

m   total weight of specimen

$m1$ mass of the cup and wet sample

$m2$ mass of the cup and dry sample

mb cantilever mass

mc mass of the cup

md mass of dry specimen

md mass of dry sample

ms   weight of solid

mw mass of water

mwp mass of waterfilled pycnometer

$mwps$ mass of waterfilled pycnometer and the sample

$\bar{m}$ mass per unit length

N number of loading cycles

N near-field coefficient of Stoke's fundamental solution

NG normalized shear modulus increase with time

NP , NS p-related and s-related components of near-field coefficient

n stress exponent

n porosity

nP, nS dimensionless s and p ratios

$n$ap   normalized distance

pa atmospheric pressure

pr reference pressure

p' mean effective stress

$p'c$ pre-consolidation pressure

qc   CPTU tip resistance

qnet   cone net resistance

qt   corrected tip resistance

r radius coordinate

S dimensionless parameter

S salinity

Sr degree of saturation

St sensitivity

$S(\omega, r)$ transfer function for shear movement

sr remoulded shear strength

su undrained shear strength

T   apparent period of selected pulse

Tr   total time length of signal

t shear wave travel time

t time

tg geological age

teop   reference time

u displacement vector

ur soil suction

uP, uS displacement vectors of compressive and shear movements

$V0$ initial volume

Vhh shear wave propagating horizontally with horizontal polarization

Vhv shear wave propagating horizontally with vertical polarization

VP P-wave velocity

Vp volume of voids

$VSCPTU$ in-situ shear wave velocity obtained from the seismic piezocone testing (SCPTU)

$Vs,in\ situ$ shear wave velocity measured in-situ

$Vs,remoulded$ shear wave velocity measured on remoulded sample

Vs shear wave velocity

$Vs0$ shear wave velocity measured on unconfined sample

Vvh shear wave velocity propagating vertically with horizontal polarization

Vhv   shear wave velocity propagating horizontally with vertical polarization

Vhh   shear wave velocity propagating horizontally with horizontal polarization

Vw volume of water

V_s^{lf} low-frequency velocity

V_s^{hf} high-frequency velocity

w water content

wL liquid limit

wP plastic limit

X(T)   signal at receiver

Y(T)   driving signal

Greek letters

α   tortuosity factor

α anisotropy factor

α effective length factor

α inclination of the line

β experimentally determined value

γ shear strain

γ unit weight

γc cyclic strain

γw unit weight of water

$\dot{\gamma}$ strain rate

ΔE   energy dissipated per cycle per unit volume

ΔG change in shear modulus

ΔV volume change

Δe change in void ratio

Δt shear wave propagation time

δ axial deformation

$\delta\varepsilon ij$ Strain increment

$\delta\sigma'ij$ Stress increment

εvol volumetric strain

η mean displacement influence factor

λ Lamé elastic constant

λ wavelength

$\lambda p, \lambda s$ compressive and shear wavelengths

ν Poisson's ratio

$\nu *$ modified Poisson's ratio

νhh Poisson's ratio for vertical strains from a horizontal strain

νhv Poisson's ratio for horizontal strains from a horizontal strain

νvh Poisson's ratio for horizontal strains from a vertical strain

ρ bulk density

ρb bender element mass density

ρs density of solids

ρw density of water

$\sigma'c$ effective confining stress

$\sigma'm$ average effective confining pressure

$\sigma h'$ effective horizontal stress

$\sigma v'$ effective vertical stress

$\sigma v0'$ in-situ vertical effective stress

σ_r' isotropic residual effective stress

ω angular frequency

τ applied shear stress

Abbreviations

BE Bender Element

CR Cross-correlation

CSW Continuous Surface Waves

DAQ Data Acquisition Device

$EOPC$ End of primary consolidation

FFT Fast Fourier Transform

$MASW$ Multichannel Analysis of Surface Waves

$NGTS$ Norwegian Geo-Test Site

$NTNU$ Norwegian University of Science and Technology

OCR Over-consolidation ratio

PC Personal Computer

RES Residual effective stress

$SASW$ Spectral Analysis of Surface Waves

$SCPTU$ Seismic Cone Penetration Test

SDT Seismic Dilatometer Test

Chapter 1

Introduction

1.1 Background

Identification of dynamic properties of Norwegian sensitive soft clay is believed to be as important as its mechanical characteristics for many different reasons. One of the most important of these features is undoubtedly small-strain shear modulus. The determination of small-strain shear modulus has been one of the main areas of interest in recent years due to its wide range of applications in geotechnical engineering, especially in constitutive numerical modeling. Shear wave velocity is highly dependent on particle contact, mineral, and structural composition formed during the depositional process in combination with salt content which substantially contributes to quick clay formation of structure. It would be interesting to determine the distinction between lab and field value of maximum shear modulus which might be attributed to many contributing factors, including hard band (cementation, creep) in the field, the high degree of uncertainty related to sampling practice, stress relief caused by unloading, test errors, applied frequency and strain level among others. A wide variety of combinations of field and lab techniques, however, should be employed to obtain reliable value and reason behind this discrepancy. The stiffness anisotropy at small strain is well known to be also an interesting topic that can be extracted from the variation of shear wave velocity at different bender element orientations, owing to primarily one-dimensional depositional process.

Bender element technique can be treated as one of the most promising complementary approaches to obtain shear wave velocity due to its simplicity, and cost-efficiency. In this study bender element method incorporated in the triaxial device has been utilized to determine maximum shear modulus. Numerous procedures, however, have been proposed to reduce the uncertainty associated with this approach, especially challenging measurement of travel-time, and the distorted received signal. Errors associated with accurate interpretation and determination of shear wave velocity by means of bender element is primarily dominated by applied input frequency and sampling practice. The in-depth understanding of the source of fabric-anisotropy is a crucial factor to determine the degree of anisotropy. It would be interesting to perceive how the key characteristics, ranging from soil fabric, stress history,

particle formation, orientations, and fluid flow contribute to small-strain anisotropy. The sampling process is one of the major sources of concern that raises the question regarding the reliability of the results. To reduce the degree of uncertainty regarding this issue the shear wave velocity measurement will also be carried out for both fresh and old samples, as well as various types of samples to interpret the effect of the aging, and size of the sample on G_{max} respectively. Eventually, the findings will be judged with already existing data on the small strain stiffness inferred from the Flotten Norwegian geotechnical test site indicated by other researchers.

1.2 Objectives

The main aim of this study is to provide a comprehensive basis for the determination of maximum shear modulus and small-strain stiffness anisotropy behavior at Flotten Norwegian geotechnical test site by performing bender element tests. The objectives of this study are as follows:

- ✓ To demonstrate G_{max} and parameters influencing G_{max}, sampling considerations, the concept of stiffness anisotropy at small strain, various techniques to measure G_{max}, and the bender element method.
- ✓ To acquire G_{max} value using the bender element technique.
- ✓ To quantify parameters influencing G_{max}.
- ✓ To obtain the degree of fabric anisotropy utilizing the bender element technique.
- ✓ To evaluate the effect of type of block sample on G_{max} and stiffness anisotropy.
- ✓ To interpret the effect of storage time on G_{max} and anisotropy.

1.3 Limitations

The main limitation would be time constraints caused by the coronavirus outbreak which made it impossible to complete some parts of this research. It is apparent more time is required to assess this concept more precisely. Errors associated with bender element test would be another major challenge which should be taken into account. Inadequate equipment needed especially for anisotropy investigation made the determination of degree of anisotropy more complicated.

1.4 Research approach

This literature review consists of useful information, which provides a theoretical framework for the soil properties at the small strain that helps to get a better insight into this topic. In the following, small strains shear modulus of Tiller-Flotten quick clay was obtained at the different orientation of the sample using shear wave velocity measurement. The fundamental principles of fabric and stress-induced anisotropy were described, and the degree of anisotropy was achieved for Tiller-Flotten quick clay. An ongoing study on sample quality assessment to reduce the degree of uncertainty regarding sample disturbance has been taken into account in this research.

1.5 Research structure

This study consists of following chapters:

- ✓ Chapter 2   The small-strain shear modulus
- ✓ Chapter 3   Technique to measure maximum shear modulus
- ✓ Chapter 4   Bender element
- ✓ Chapter 5   Sampling considerations
- ✓ Chapter 6   Clay particle anisotropy
- ✓ Chapter 7   Tiller-Flotten research site
- ✓ Chapter 8   Sampling and Laboratory Testing
- ✓ Chapter 9   Overview of results
- ✓ Chapter 10   Discussion
- ✓ Chapter 11   Summary and recommendations for further work

Chapter 2

Theory

2.1 The small-strain shear modulus

Stiffness characteristics of the soil are recognized to be important in many geotechnical aspects which makes it necessary to incorporate this soil behavior into numerical modeling. It is apparent that materials with different properties have different stress-strain behavior. Non-linearity characteristics of the soil have been fully recognized, soil stiffness decays with increasing shear strain on a logarithmic scale. The typical stiffness degradation curve is shown in Figure 2.1 in terms of shear modulus G and Young's modulus E, versus typical strain levels

developed in geotechnical practice (Mair,1993) and measurement approaches which can be used to obtain stiffness at different stain level (Atkinson, 2000). Corresponding shear modulus to very small strain range where soil exhibits its linear behavior is known to be maximum shear modulus. As illustrated in Figure 2.1, the stiffness degradation curve can be separated into four zones: (1) linear elastic zone, (2) nonlinear elastic zone, (3) pre-yield plastic zone, and (4) full plastic zone.
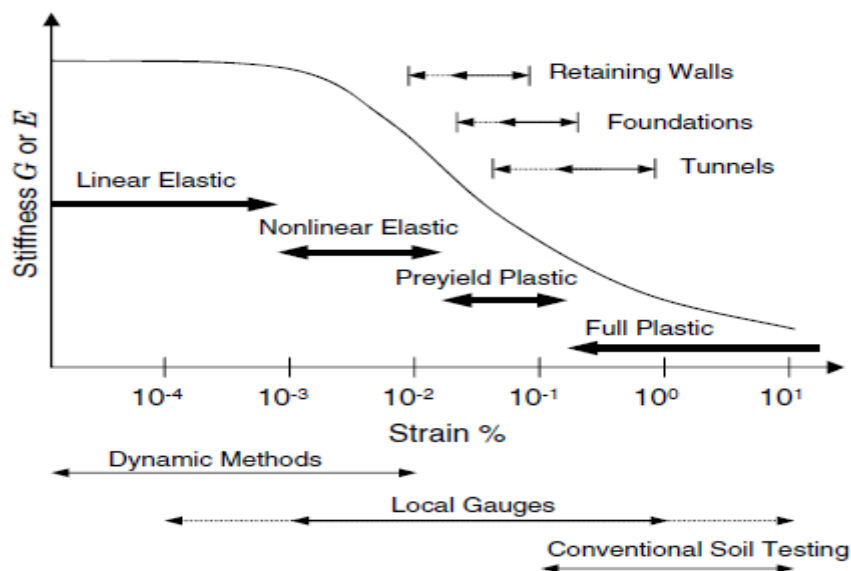
Figure 2.1: Typical strain range for laboratory test (Mitchell, 2005)

In the linear elastic part, soil particles do not slide relative to each other under a small stress increment and the stiffness is at its maximum. It is predominantly due to contact interface,

packing condition and elastic stiffness of solid. Small-strain stiffness is a function of void ratio, mean confining pressure, and other important factors. In principle, coarse-grained soils represent the shorter length of linear zone behaviour, since they lose their contact interface more easily compared to fine-grained soil. This makes them slide to each other and high relative displacement, dissipation of energy is also higher in coarse-grained than fine-grained particles. At high strain range as contact internal friction decreases, damping ratio which is proportional to energy dissipation increases. Small-strain shear modulus decreases significantly with an increase in both shear strain and the cycle of loading while the damping ratio goes up. This reduction in stiffness is expected to occur at even very small strain level approximately .0001 for granular soil and .001 for clay soil. The shear modulus G and damping ratio are utilized to characterize the curves in Figure 2.2, and they are defined by

$$G = \frac{\tau}{\gamma} \tag{2.1}$$

In which τ is the applied shear stress and γ is the corresponding shear strain, and λ is the damping ratio defined as (Mitchell, 2005):

$$\lambda = \frac{1}{2\pi} \frac{\Delta E}{G\gamma^2} \tag{2.2}$$

The area within the hysteresis loop is defined as ΔE the energy dissipated per cycle per unit volume (Figure 2.2) (Mitchell, 2005).
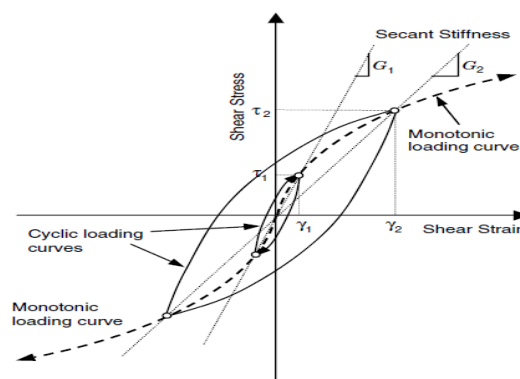
Figure 2.2: Stress–strain hysteresis at different strain amplitudes (Mitchell, 2005)

Stiffness degradation curve can be normalized by the small strain stiffness. A representation of normalized shear modulus degradation curves has been suggested for different soils as shown in Figure2.3 (Kokusho, 1987). This should be primarily a function of grain-size, relative

density and shear strain for gravels and sands, additionally plasticity for clays. As mentioned above, the flatter curve for gravels can be observed than sands and for sands than clays.
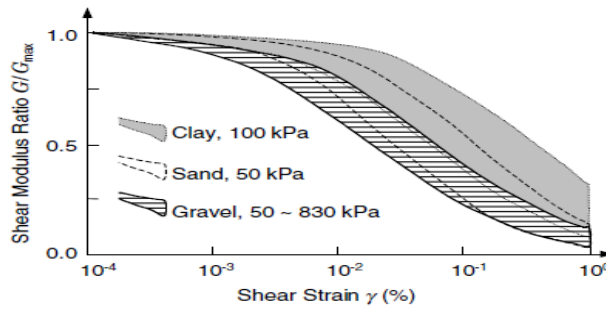
Figure 1

Figure 2.3: Normalized stiffness degradation curves of different types of soils (Kokusho, 1987)

2.2 Determination of G_{max}

To achieve the exact value of maximum shear modulus, taking very small-strain range and linear part into account, the maximum shear modulus G max can be calculated by following equation:

$$G_{max} = \rho v_s^2 \tag{2.3}$$

Where the small-strain shear modulus under isotropic stress condition depends on applied confining stress, packing condition of soil particles, particle stiffness, Poisson's ratio, number of contacts, void ratio, contact force direction, etc. The following empirical equation (Hardin and Black,1966) is often used for isotropic stress conditions, but the existence of anisotropic soil fabric would be more plausible due to stress-induced anisotropy during consolidation process.

$$G_{max} = AF(e)P'^n \tag{2.4}$$

where F(e) is a void ratio function (Yimsiri, 2001), p' is the mean effective stress, and A and n are material constants. In the next section, we evaluate other factors influencing small-strain stiffness more accurately to understand better soil behavior at this strain range. In fact, confining pressure, void ratio, inter-particle electrical and chemical bond concerning clay morphology seems to be more significant in G_{max} determination than other parameters.

2.3 Factors influencing small-strain stiffness

The shear modulus degradation curves are highly dependent on sample quality, over consolidation ratio, soil type, loading procedures, mode of shear, etc. It is therefore not reasonable to expect empirical relationships to give an accurate estimation of G/G0. To understand how empirical and laboratory curves may differ, correlations between index parameters and V_s or G_{max} can provide exact estimate of preliminary design and for confirming in situ and laboratory results. According to Leroueil and Hight (2003) and Hardin (1978), the empirical equation describing the influence of the controlling factors on G_{max} can then be written as follows:

$$G_{max} = SF(e)(\sigma_v'\sigma_h')^n P_a^{(1-2n)} \tag{2.5}$$

where S = dimensionless parameter characterizing the considered soil; F(e) = void ratio function; σ_{0v} and σ_{0h} (kPa) = vertical and horizontal effective stresses, respectively; n = parameter indicating the influence of stress; and P_a (kPa) = atmospheric pressure.

Long and Donohue (2007, 2010) and L'Heureux et al. (2013) believed that for Norwegian clay S is taken to be in the range 500–700, $F(e) = \frac{1}{e^{1.3}}$ (where e = void ratio), $K_0 = 0.6$, n=0.25. The influence of other parameters on maximum shear modulus can be briefly mentioned as Table 2.1 (Dobry and Vucetic, 1991).

Table 2.1: Factors influencing maximum shear modulus for normally and moderately over-consolidated clays (Vucetic and Dobry, 1991)

Influencing factor	G_{max}	G/G_{max}	Damping ratio, ξ
Effective mean confining pressure, σ_m'	Increases with σ_m'	Constant or increases with σ_m'	Constant or decreases with σ_m'
Void ratio, e	Decreases with e	Increases with e	Decreases with e
Geologic age t_g	Increases with t_g	May increase with t_g	Decreases with t_g
Cementation, c	Increases with c	May increase with c	May decrease with c
Overconsolidation ratio, OCR	Increases with OCR	Not affected	Not affected
Plasticity index, I_p	Increases if $OCR > 1$, constant if $OCR = 1$	Increases with I_p	Decreases with I_p
Cyclic strain, γ_c	-	Decreases with γ_c	Increases with γ_c
Strain rate, $\dot\gamma$ (frequency of cyclic loading)	Increases with $\dot\gamma$	G increases with $\dot\gamma$, G/G_{max} probably not affected if G and G_{max} are measured at same $\dot\gamma$	Constant, or may increase with $\dot\gamma$
Number of loading cycles, N	Decreases after N cycles of large γ_c, but recovers later with time	Decreases after N cycles of large γ_c (G_{max} measured before N cycles)	Not significant for moderate γ_c and N

All relationship corresponding maximum shear modulus versus void ratio would be summarized in Figure 2.4 using $G_0 = Af(e)OCR^k(\frac{p'}{p_{ref}})^m$ Hardin and Black (1968) equation for a large variety of applied variables. Where G_0 is the maximum shear modulus in MPa, p' is the mean effective stress in KPa, p_{ref}=100 Kpa is a reference pressure equal to the atmospheric pressure, OCR is the over-consolidation ratio, and A, f(e), k, m are the correlated functions and parameters given in (Benz, 2007).
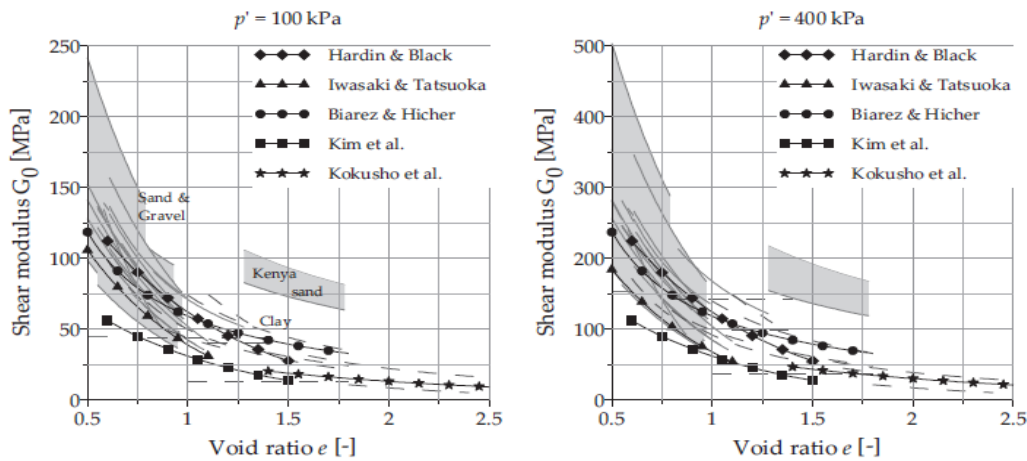
Figure 2.4: Maximum shear modulus versus void ratio (Benz, 2007)

2.3.1 Confining pressure

Consolidation stress is expected to contribute to small-strain shear modulus substantially. Hardin and Richard (1963) suggested maximum shear modulus is proportional to confining pressure as following relationship:

$$G_0 \propto (P')^m \tag{2.6}$$

Viggiani and Atkinson (1995) obtained exponents m for different clays at very small strain based on plasticity index, regardless of effect of void ratio. Hicher et al. (1996) expressed m as a function of liquid limit. Both of them can be observed in Figure 2.5.
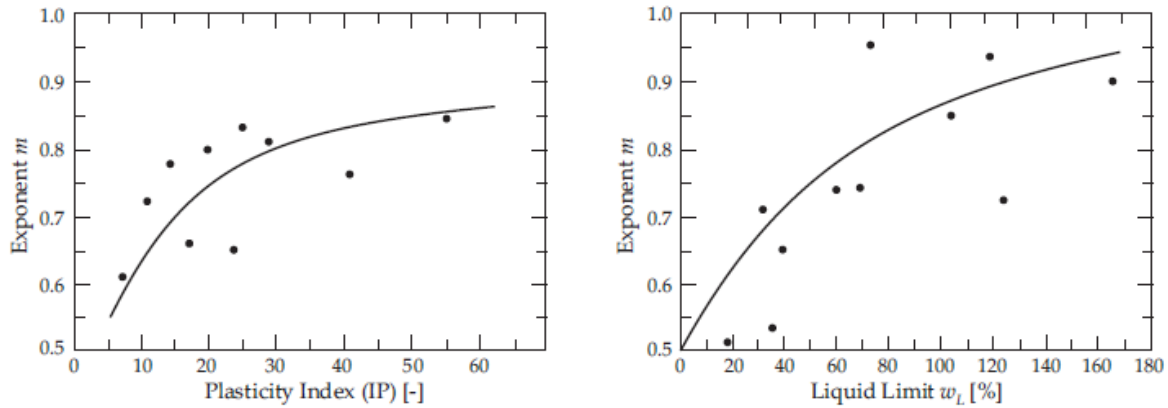
Figure 2.5: Factor of m as a function of plasticity index and liquid limit (Viggiani and Attkinson, and Hicher, 1996)

Hardin and Richard (1963) suggested m=0.5 for both granular and cohesive soil, but other researcher suggested m=0.7-1 for clays, which is consistent well with their findings (Benz, 2007). Brignoli et al. (1996) indicated dependency between shear wave velocity and isotropic confining pressure for different materials using bender element, ultrasonic transducers and resonant column in Figure 2.6.

(a)   (b)
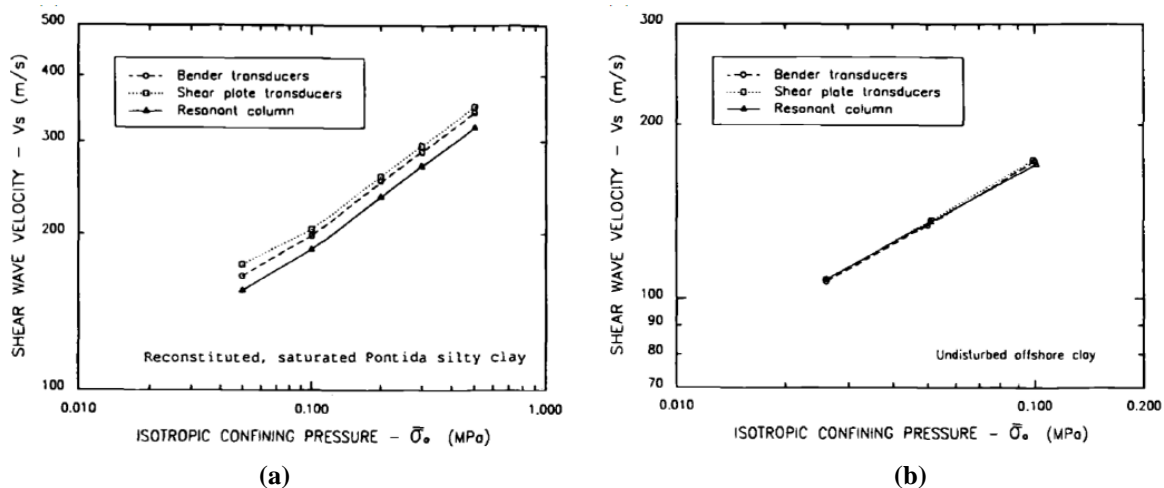
Figure 2.6: Varition of Vs with isotropic confining pressure for (a): reconstituted saturated clayed silt (b): undisturbed offshore clay (Brignoli et al., 1996)

2.3.2   Depth

Depending on different geophysical or laboratory techniques, it is anticipated to have various values inferred from results. V_s values measured with different techniques can be significantly distinctive in heavily over-consolidated clays or layered soils. Teachavorasinskun and lukkunaprasit (2004) suggested a linear equation for shear wave velocity with increasing depth.

$$V_{sz} = V_{sg} + mZ \tag{2.7}$$

Where $V_{sz} = V_s \frac{m}{s}$ at any depth z (m); $V_{sg} = V_s$ close to the ground surface $\left(\frac{m}{s}\right)$; m=slope of the line of V_s versus depth (m/s.m).

L'Heureux et al. (2017) suggested linear relationship between shear wave velocity and effective vertical stress. Results show a clear tendency for in-situ V_s to increase with σ0v. The best approach relationship between v_s and effective vertical stress can be determined as equation (2.7) and Figure 2.7 based on data inferred from all sites in Norway.

$$V_s = 1.11\sigma'_{v0} + 53.24 \tag{2.7}$$
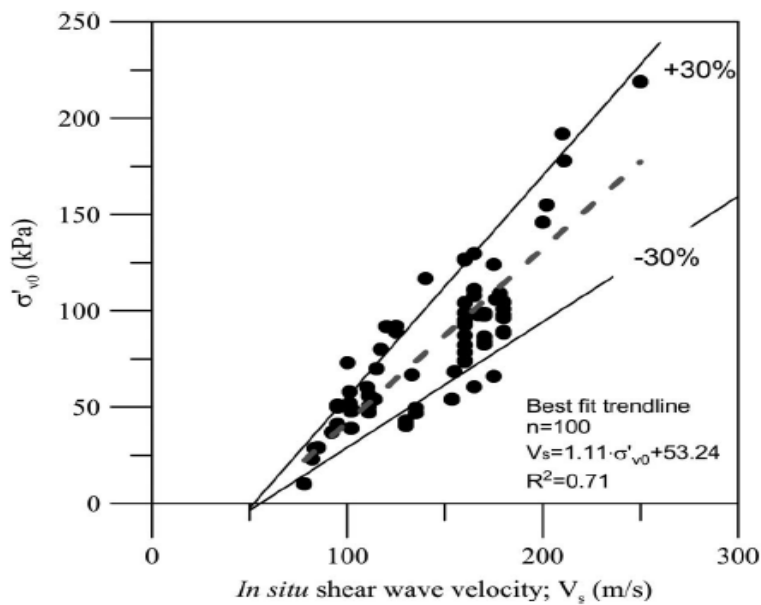
Figure 2.7: In situ shear-wave velocity versus vertical effective stress (L'Heureux and Long, 2017)

They also found the correlation of shear wave velocity with average water content and unit weight and it was concluded that shear wave velocity decreases with increasing water content, and increases with increasing unit weight (L'Heureux et al., 2017).

2.3.3 Plasticity index

For cohesive soil as plasticity increases, the linear part of shear stress-strain continues in longer length (Vucetic and Dorby, 1991). This means that the normalized stiffness degradation curves is inclined to go up and right as soil plasticity index increase. Increasing plasticity leads to increasing contact surface, as particles size decreases. This formation of soil can withstand higher shear load before having particles sliding toward each other. Electrical and chemical inter-particle bond between most thin platy shape of clay particles is reason for this elastic

strength. The contribution of plasticity index on shear modulus to shear modulus degradation curve can also be seen in Figure 2.8 (Vucetic and Dobry, 1991). The effect of plasticity index on maximum shear modulus, however, seems to be minimal for normally consolidated clay (Vucetic and Dobry, 1991).
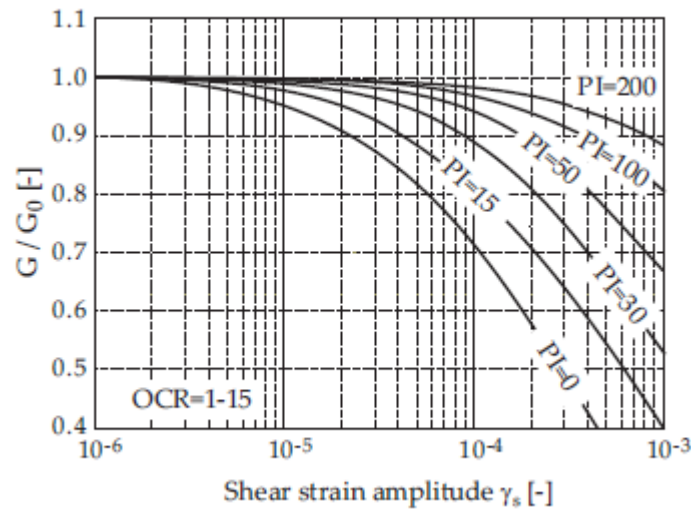
Figure 2.8: Normalized shear modulus versus shear strain for different plasticity index (Vucetic and Dobry, 1991)

2.3.4 Consolidation time

It is worth mentioning that small strain shear modulus is time-dependent, which means confining pressure duration is of great impact on soil maximum shear modulus, leading to logarithmic increase in the stiffness at low strain amplitude (below 0.001%) (Anderson and Stokoe, 1978) (Figure 2.9).
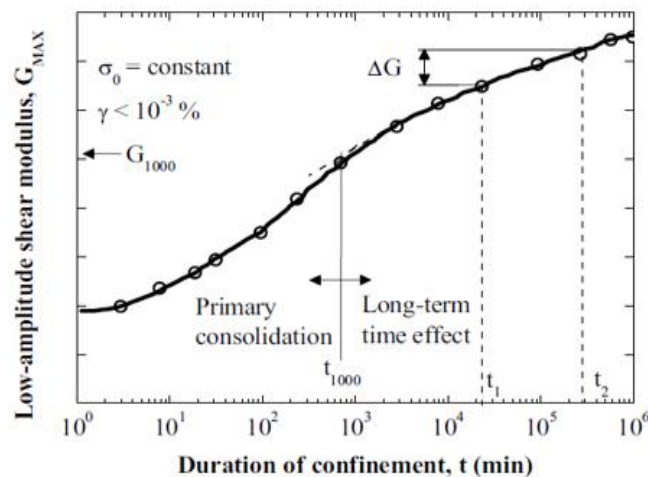
Figure 2.9: Variation of maximum shear modulus versus consolidation time (Anderson and Stokoe, 1978)

This increase during primary consolidation is result of change in void ratio. The second phase consolidation makes soil physical and chemical bond stronger, caused by creep. At this stage the effect of time can be expressed by coefficient of shear modulus:

$$I_G = \frac{\Delta G}{log_{10}(\frac{t_2}{t_1})} \tag{2.8}$$

Where ΔG Logarithmic increase in shear modulus and t2 and t1 are times after primary consolidation. Parameter Ng can be defined as below:

$$N_G = \frac{I_G}{G_{1000}} \tag{2.9}$$

where G1000 is after completion of primary consolidation referred to as the modulus measured after 1000 minutes of constant confining pressure. NG would be a function of plasticity index, increases with increasing soil plasticity. In most cases values of Ng for clays vary between 0.05 and 0.25.

$$\frac{\Delta G}{G_{1000}} = 0.027\sqrt{I_P} \tag{2.10}$$

The relationship between the rate of secondary modulus (NG) and plasticity index (PI) was indicated by Kokusho et al. (1982).

$$N_G \approx 0.027\sqrt{PI} \tag{2.11}$$
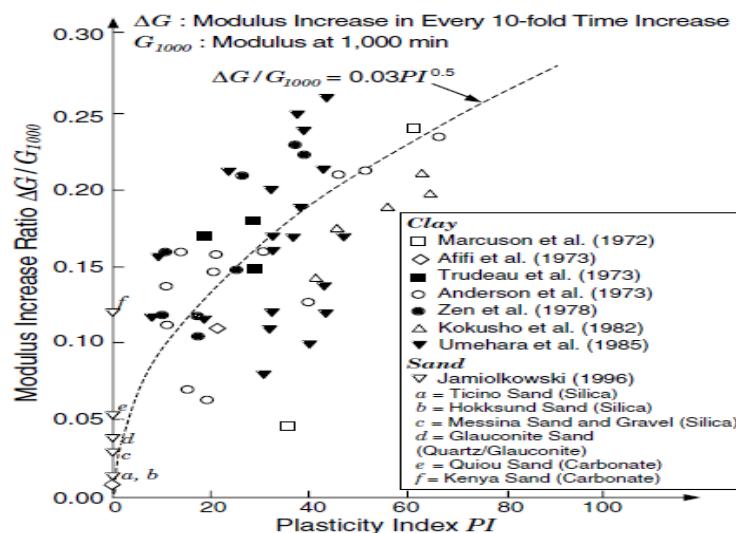
Figure 2.10: Increasing trend of maximum shear modulus for clays (Kokusho, 1987) and sand (Jamiolkowski, 1996)

Plasticity index can be used as a measure of chemical activity of clay minerals. NG, therefore, increases with increasing plasticity index, and decreases with increasing OCR (Kokushu et al., 1982) (Figure 2.10).

Anderson and Woods (1975) believed that NG can be used to modify difference between field and lab-measured G_{max} value.

2.3.5 Void ratio

Small strain shear modulus is expected to be in reverse relationship with void ratio, increasing with decreasing void ratio during primary consolidation.

$$G_0 \propto e^{-x} \tag{2.12}$$

Where the x component would be 1 for sand and clay (Biarez et al., 1994), and $1.1 \leq x \leq 1.5$ for various clays (Presti and Jamiolkowski, 1998). Hardin and black (1968) suggested G_0 in good agreement with $\frac{(2.97-e)^2}{1+e}$ which correlates well for normally consolidated clay (Figure 2.11).
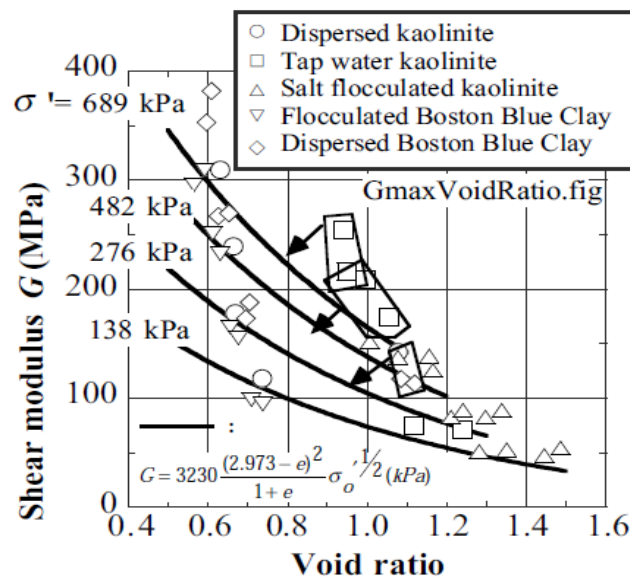
Figure 2.11: Correlation between G_{max} and Void ratio (Hardin and Black, 1968)

2.3.6 Over-consolidation ratio

Over-consolidation ratio is widely believed to be proportional to small-strain shear modulus. Hardin and Black (1968) proposed empirical relationship as below:

$$G_0 \propto OCR^k \tag{2.13}$$

Again the empirical parameter k increases with clay plasticity. For clays with $10 < PI < 40$, (Atkinson and Viggiani, 1995) found $0.20 < k < 0.25$.

Chapter 3

Technique to measure shear modulus

There seem to be numerous various field and lab methods utilized to measure shear wave velocity and corresponding small-strain shear modulus. In terms of geophysical measurement, classification of in-situ shear wave velocity determination can be divided into the invasive and non-invasive approach. The non-invasive method is defined as a procedure in which boreholes or probes are not required. Disturbance of the soil during drilling of the borehole, applied frequency range, dispersion-induced wave property, higher material and geometric damping with increasing distance, and groundwater level effects are disadvantages corresponding to invasive procedures. Common invasive methods include downhole logging (ASTM 2014), cross-hole logging (ASTM 2014), suspension logging, seismic dilatometer (SDMT), and the seismic cone penetration test (SCPTU). Both field and lab approaches can be categorized distinctively as Figure 3.1 (Sitharam et al., 2004).
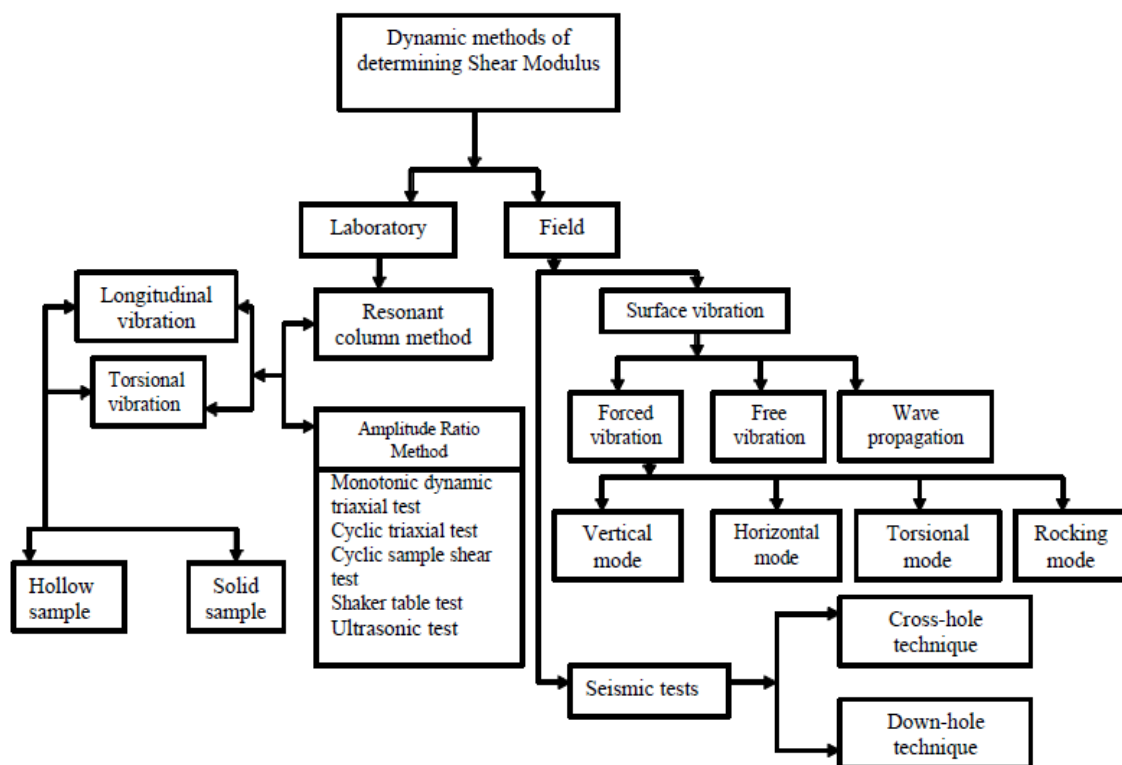
Figure 3.1: Technique to measure shear wave velocity (Sitharam et al., 2004)

3.1 Lab-measurement

Laboratory tests from samples with minimal disturbance and careful test setup give us complementary results corresponding to shear wave velocity. Lab low-strain methods mainly include the Resonant column test, ultrasonic pulse test, and the piezoelectric bender element test are the widely used techniques in this regard. Alternatively, several methods have been introduced to obtain the dynamic properties of the soil. Cyclic triaxial test, cyclic direct simple shear test, and cyclic torsional shear test devices are most popular among them (Sitharam et al., 2004).

3.2 Field-measurement

Dynamic properties of the soil are highly dependent on soil 's stress state, which can be influenced by sampling practice. Field measurement approaches, therefore, are primarily preferred in many geotechnical surveys. Field test measurement is divided into two distinct parts, small and large stain level as well since soil dynamic properties have a dependency on strain level. Some of the low-strain field tests are seismic reflection test, seismic refraction test, suspension logging test, steady-state vibration or Rayleigh-wave test, spectral analysis of surface wave test (SASW), seismic cross-hole test, seismic down-hole (up-hole) test(CHT) and seismic cone test multichannel analysis MASW, continuous surface waves (CSW), frequency wavenumber methods (f-k methods). A standard penetration test (SPT), Cone penetration test (SCPT), Dilatometer test(DMT), and pressure-meter test are the most commonly employed techniques to measure dynamic characteristics of soil at high strain range (Clayton et al., 1995). In the following, a short description of the most crucial field shear modulus measurements has been characterized.

3.2.1 Multichannel analysis of surface wave (MASW)

Multi-Channel Analysis of Surface Waves (MASW) is a non-invasive survey of estimating shear-wave velocity based on applying seismic refraction wave properties to soil subsurface profile. The depth of interest in this method is usually shallower than 30 m. Low-frequency Rayleigh-wave which has longer wavelengths can penetrate the deeper layer. The source of energy is located on the surface generating shot from the impulse energy source in all directions. The wave may either propagate directly parallel to surface, or it may travel down to

earth. The dispersion properties of all types of waves (both body and surface waves) are imaged into transformed energy distribution by inversion technique. The distinction in the amplitude of received wave in geophone and specific dispersion pattern would be utilized to measure travel time and corresponding shear wave velocity. This method is referred to as one of the most reliable and immediate ways of shear wave velocity measurement. One of the main issues associated with this technique is large-scale testing area causes the recording to be adversely influenced by soil 's different layering and anisotropy (L'Heureux et al., 2017). To reduce and isolate unwanted noise and wave interference appropriate data interpretation and complementary tests are highly recommended (Cercato, 2009).

3.2.2 Down-hole test

This method can be applied to measure site compression and shear wave velocity, known as an intrusive technique in geophysical exploration. where only one borehole is needed to place receiver and the wave is sent at a surface level close to the borehole. The arrival of the wave would be registered by geophone. The measurement will be carried out at different depths to obtain higher accuracy. The disadvantage related to this method would be attenuation of the wave, as the distance between receiver and sender increases, and sometimes refracted waves. This survey would be considered as a cost-efficient tool to study soil anisotropy properties, as well as the elastic behavior of the soil (Kramer, 1996).

3.2.3 Cross-hole seismic test

This technique is the same as the Down-hole method, but two or more boreholes are required. One for generating wave and another will be used to place receiver geophone at the same depth. By measuring travel time, since the travel length is clear and consequently shear wave velocity would be achieved. Nowadays, cross-hole tomography is widely utilized, instead of the conventional one, where we use a large number of receivers instead of just one. An additional number of achieved values for shear wave velocity and corresponding maximum shear modulus can improve our accuracy. This method can be considered probably as the most appropriate survey to measure shear wave velocity, since both G_{hv} and G_{hh} at particular favourable layer can be obtained from this method (Hoar et al., 1978). Likewise, the results are less likely to be affected by the wave propagating in a variety of layers, and non-homogeneities.

3.2.4 Seismic cone penetration test (SCPT)

The SCPT test is developed to measure shear wave velocity in the category of Down-hole test using a single sounding (Campanella et al., 1986). A seismic wave is produced at a surface level near the corresponding hole, and arrival times will be measured at geophones within the penetrometer which can be repeated at different depths. Mayne (2000) proposed utilizing two geophones which give more accuracy and reliability than using a single horizontal geophone. He also suggested the implementation of the seismic piezocone pressuremeter test (SPCPMT) which enables us to determine the soil properties at small, intermediate, and large strain.
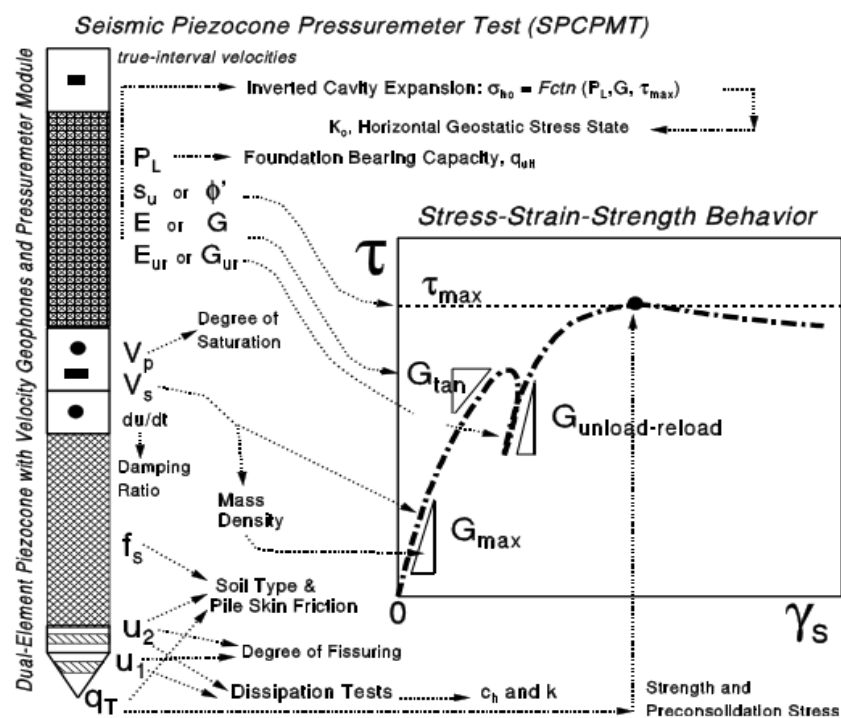
Figure 3.2: The Seismic Piezocone Pressure-meter (Mayne, 2000)

Utilization of SCPTU gives supplementary information of soil properties and stratigraphy at different layer derived from CPTU combined with seismic data, including CPTU tip resistance (qc), corrected tip resistance (qt), water content (w), cone net resistance (qnet), sleeve friction (fs), pore pressure parameter (Bq), effective stress (σ0v), and void ratio (e). It is believed that some parameters present better estimates and are more reliable when correlating well with shear wave velocity depending on soil classification (L'Heureux et al., 2013). And of course, sleeve friction seems to be a less reliable factor than to be used for this purpose, especially for clay. L'Heureux et al. (2013) proposed the below equation as the best fit for Norwegian clay.

$$V_s = 71.7(q_{net})^{0.09}(\frac{\sigma'_{v0}}{w})^{0.33} \qquad (3.1)$$

Where water content, cone net resistance and effective stress are in acceptable agreement with shear wave velocity using 0.89 for coefficient of determination(R^2)and a total of 101 datasets in the analyses. Mayne et al. (1995) presented shear wave velocity as a function of cone resistance(q_c) and void ratio(e) for clayed soil derived from 31 sites while the coefficient of determination(R^2) equal to .832 and 339 for the number of datasets were set.

$$V_s = 9.44(q_c)^{0.435}(e_0)^{-0.532} \text{ (V}_s \text{ m/s and } q_c \text{Kpa)}$$ (3.2)

Long et al. (2010) proposed below relationship for Norwegian clay using high-quality sample by taking high variability of numerous sites into account since sleeve friction is not reliable in soft clays (R^2=0.63) (Figure 3.3).

$$V_s = 2.944 q_t^{0.613}$$ (3.3)
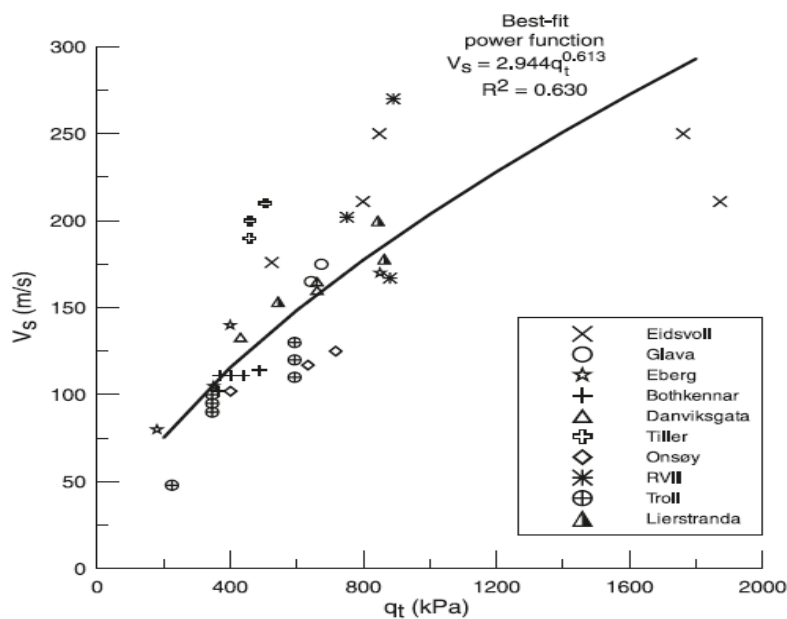
Figure 3.3: Correlation between measured and estimated value of Vs (Long et al., 2010)

They also found that Mayne and Rix (1995) relationship can be modified for Norwegian soft clay by using B_q instead of e_0(void ratio) and corrected cone resistance as a substitute for measured one as it can be observed in the below equation (R^2=0.777).

$$V_s = 1.961(q_t)^{0.579}(1 + B_q)^{1.202}$$ (3.4)

Chapter 4

Bender element

4.1 Basic principle

The bender element technique is of particular interest in detecting shear wave velocity in the laboratory test in the range of small shear strain. The maximum shear strain generates by the bender element found to be in the order of 0.001 % or below using the tip deflection equation of the bender element (Dyvik et al., 1985) and (Pennington et al, 1999). Seismic waves should be utilized to determine shear wave velocity and in consequence maximum shear modulus strain stiffness can also be measured from the shear wave velocity in the laboratory similar to invasive and non-invasive measurement methods used in the field. This method was first introduced by (Shirey et al., 1978). The magnitude of induced strains lies within the linear elastic part of the stiffness response. Bender elements were first mounted into standard triaxial test equipment by (Dyvik et al, 1984), and also have been applied to other sorts of laboratory test such as oedometer tests, (Comina et al., 2008), resonant column tests (Dyvik & Madshus, 1985), and simple shear apparatus (Kuwano et al., 1999). Great care needs to be taken due to errors associated with the orientation of bender element, wave reflection, wave interference, damping, near field effect, etc.

The equation which governs the bender element motion is more like a cantilever beam. It consists of a two-layer piezoelectric transducer and a conductive metal shim at the center. There are two types of bender elements: series and parallel. In the series type, the poling directions of the two piezoelectric layers are opposite to each other, while in the parallel type, the two piezoelectric layers have the same poling direction as shown in Figure 4.1. It is recommended to have parallel one as sender and series one as a receiver since parallel one can undergo twice displacement than series-type for the same input voltage (Lee and Santamarina, 2005).

In terms of penetration depth, Yamashita et al. (2009) stated that embedded depth of bender element into the soil is proportional to the height of specimen, indicating too long penetration causes sample disturbance, while the generation of the too weak shear wave would be anticipated when using too short embedded depth. They also indicated an average value of approximately 4.7 mm for embedded depth.
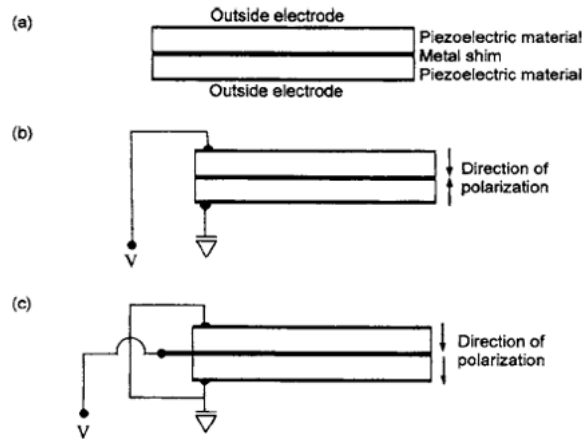
Figure 4.1: Bender element: (a) Technical illustration of bender element, (b) series type, and (c) parallel type (Lee and Santamarina, 2005)

Conventionally, both transmitter and receiver piezoelectric transducers are attached to the structure of interest to detect shear wave velocity at different directions, which can be achieved by changing the orientation of the bender element (Figure 4.2).

$V_{s(hh)}$ = shear wave propagating horizontally polarized horizontally.

$V_{s(hv)}$ = shear wave propagating horizontally polarized vertically.

$V_{S(vh)}$ = shear wave propagating vertically polarized horizontally.
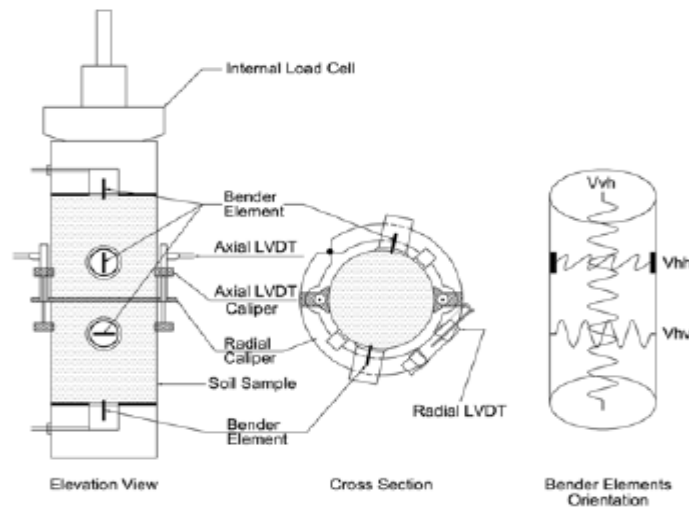
Figure 4.2: Bender element incorporated with the triaxial device (kim et al., 2014)

When dealing with propagation of the shear wave in anisotropic media, it should be mentioned that with a $S_{(vh)}$ wave mode the wave propagates vertically, particles oscillate within the horizontal plane; and with a $S_{(hh)}$ wave mode where the particles oscillate within the horizontal

plane traveling according to their polarization, and $S_{(hv)}$ wave mode, where polarization is perpendicular to propagation horizontal direction. These properties give a framework to assess maximum shear modulus anisotropy utilizing different orientations of bender element and polarization direction (Figure 4.3).
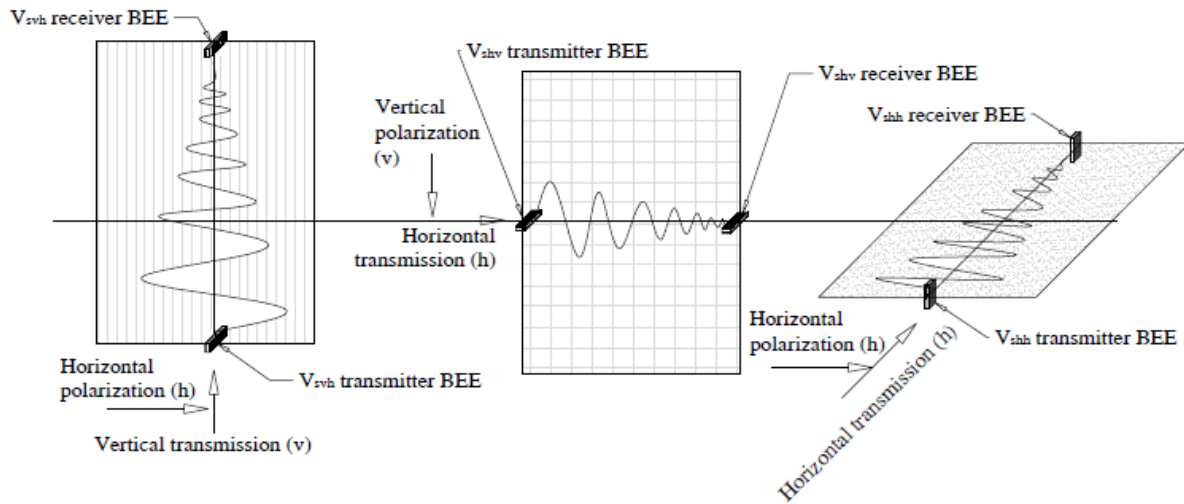
Figure 4.3: Direction of shear wave polarization for anisotropy study (Hasan, 2016)

The dispersive properties of the wave near its source, especially in bounded limited medium would be the major challenge concerning the bender element. What is more, the poor quality of the received signal would make it ambiguous to estimate travel time accurately. The main characteristics which play an important role to receive high-quality signal are, applied input frequency, waveform, and voltage magnitude. Leong et al. (2005) indicated for the sinusoidal input signal and first deflection travel time determination that the quality of the received signal can be modified by ratio travel length to wavelength higher than 3.33 to reduce the near-field effect, and signal to noise ratio higher than 4dB for receiver signal. Accurate interpretation of travel time would be considerably demanding due to the unwanted high noise ratio (Clayton, 2011). They also suggested that less distortion was observed for sinusoidal wave than square wave at the start of the received signal. The main issues associated with the bender element will be addressed with more details in the following.

4.2 Uncertainty in the bender element test

When a voltage is applied, the crystal deforms. The sign of the voltage output or the direction of the mechanical deformation depends on the poling or polarization direction of the crystal. Accurate determination of shear wave velocity appears to be highly dependent on applied frequency, sample geometry, and type of signal. Indeed, the reliability of BE technique might

be adversely affected by these factors, such as near-field effects, directivity, waveguide effect, cross-talking, and consequently poor result. Additionally, alignment of bender element, contact between the BE and the soil especially under unconfined condition, which might cause poor coupling should be taken into consideration. In the following, we describe some of these abovementioned disturbing factors briefly which might cause an unreliable result.

4.2.1 Near field effect

The near field is a phenomenon in which wave propagates at different amplitudes and phase lag, which can be responsible for much of result uncertainty associated with bender element. The near-field effect is defined in terms of the ratio of travel distance La to wavelength λ, La/λ. Its amplitude rapidly decays with an increasing number of wavelengths between the source and the receiver, i.e. with increasing frequency. Both Brignoli et al. (1996) and Sanchez-Salinero et al. (1986) gave evidence to near-field effects masking the first arrival of the wave while Arroyo et al. (2003) showed that signal distortion is not only due to near-field effects, but also P wave contribution might cause overestimation of shear wave velocity (Arroyo et al., 2003). Sanchez-Salinero et al. (1986) conducted a cross-hole test with numerous receivers in an isotropic elastic medium propagating single sinusoidal pulse. They suggested the following limit for the best receiver placement:

$$2 < \frac{d}{\lambda} = n_{ap} < 4 \tag{4.1}$$

$$\lambda = v_s * \text{T} \tag{4.2}$$

They also mentioned that n_{ap} is normalized distance, d distance between measurement point T is apparent period of selected pulse, and λ is the wavelength. The upper limit let pulse attenuate due to both geometrical and material damping ratio. Jovicic et al. (1996) showed that For n_{ap} value less than 2 there would be an initial downward deflection in the received signal due to near field effect. Material damping arises from friction between particle resulting in loss of energy, while geometric damping is amplitude reduction with increasing distance from the center. They also suggest that signal type affects the initial bump caused by the near-field effect. For a single sine pulse, there would be an approximately 10 percent increase based on (Arroyo et al., 2003). As can be seen in Figure 4.4 near-field-induced bump height reduces as the normalized distance increases for various signal shapes. For the single sin-shape pulse with normalized distance higher than 2, the near-field effect can be neglected regardless of low initial bump (Arroyo et al., 2003).
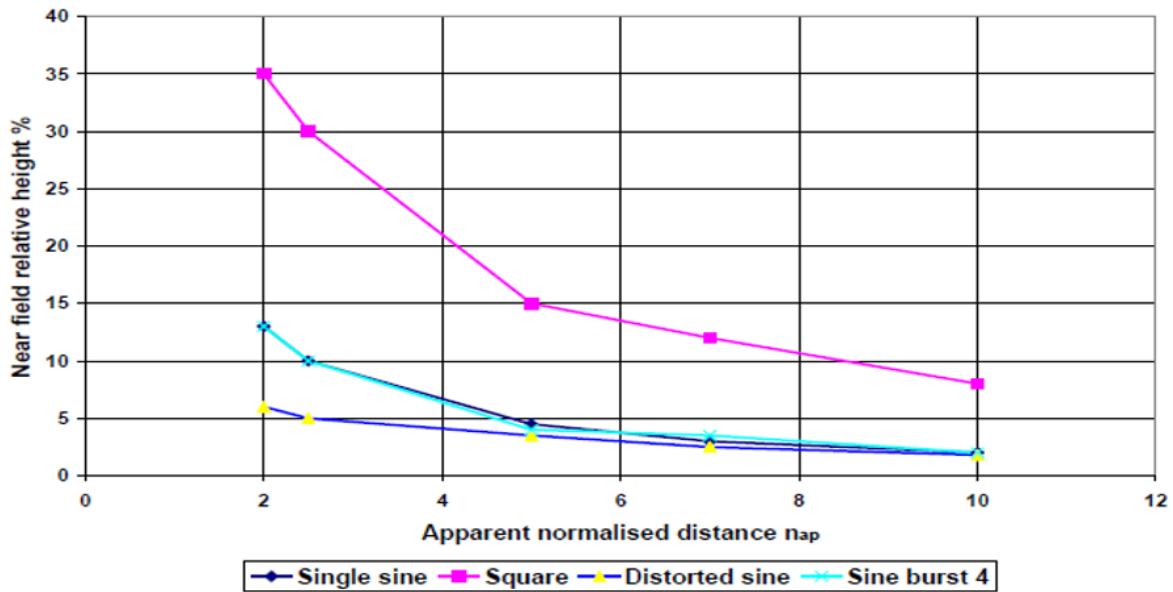
Figure 4.4: Signal type effect on the near field magnification (Arroyo et al., 2003)

The arrival of the shear wave is stronger when a low excitation frequency is used. This component tends to fade away as the excitation frequency increases, that is when the number of shear wavelengths between the bender elements goes from about one to four or more (Brignoli et al., 1996).

4.2.2 Sample geometry

Boundary reflection appears to be one of the major sources of concern regarding the bender element method. The first arrival is more likely to be masked by reflection in a bounded medium while dealing with boundaries. It is therefore necessary how to prevent energy from turning back into the sample. Wave reflection is dependent on wave properties and interface media. As it is commonly recognized the solid medium is capable of propagating P and S waves, depending on elastic properties and density of sample for p-wave and shear modulus and density of sample for s-wave respectively, a fluid medium is capable of propagating P waves and in a vacuum no wave propagation is possible. P wave has its complexity, as might be reflected as both P and S waves. Reflected waves might have different amplitude, phase lag, and angle, depending on Poisson's ratio, and incident angle (Rio, 2006). The properties of the reflected wave from a solid-vacuum interface are enough for simulation of this type of reflection. The main issue associated with dispersion-induced uncertainty would be material

inhomogeneity most notably for granular soil, frequency-dependent parameters, sample geometry concerning sample boundaries, leading to inaccurate estimation of arrival time.

The main purpose would be to make a medium similar to an unbounded situation, in which the wave components traveling between receiver and transducer, can be assumed are propagating in an unbounded condition. As the sample becomes slender, increasing sample height, less dispersion would be expected due to the near-field effect and more dispersion due to wave reflection. For the Bulk samples, on the contrary, there would be less effect of wave dispersion due to reflection, unlike slender samples behaving as waveguides, but we should be careful about the near-field effect, and samples with intermediate geometries, behaving in a transient, more erratic, way (Rio, 2006). Moreover, these geometric limits which affect adversely sample behavior are likely to be enhanced by test setup, confining pressure during the consolidation phase, and many important parameters (Rio, 2006).

4.2.3 Signal effect on dispersion

As it is well-known, bender element generates two p wave approximately in normal direction of s wave near its source which intensifies intrusive nature of device (Lee and Santamarina, 2005) (Figure 4.5). The effect of directivity on quality of received signal, and consequently first arrival should be taken into consideration. The ratio between p wave and s wave can be expressed as below:

Directivity of bender element and consequences of transverse directivity on measured signals: (a) transverse and in-plane directions; (b) and (c) measured signals in dry specimen and partially saturated specimen (input: 2.5 V step signal. Tip-to-tip distance: L=32 mm; oedometer cell diameter=70 mm).
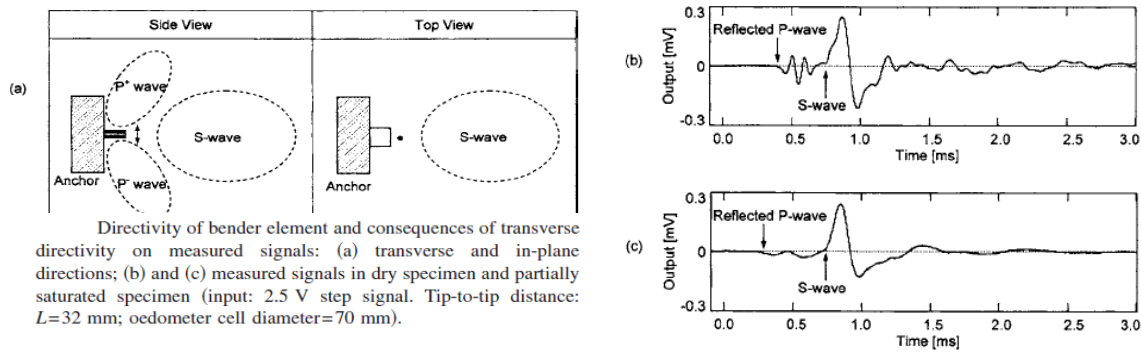
Figure 4.5: (a) Transverse directivity, (b) Effect of transverse directivity on quality of received signal (Lee and Santamarina, 2005)

$$\frac{V_p}{V_s} = \sqrt{\frac{2(1-v)}{1-2v}}$$

(4.3)

P wave hitting interface of sample and cell make the wave reflect, generating p wave and s wave. This distorting phenomenon is known as a transverse directivity, regardless of near-field

effect predominantly caused by p and s wave interference. Both Poisson's ratio and stress state are contributing factors to this phenomenon.

The input signal characteristics, including frequency, amplitude, and others have also profound effect on the reliability of the result. In terms of input signal frequency, for input signals with lower frequencies, the excitation signal would be emulated by the receiver transducer, leading to a reduction in travel time. For input signals with a frequency much higher than the resonance frequency, because of inertia force, there would be a significant phase difference between the input and the response (Rio, 2006) (Figure 4.6).

Brignoli et al. (1996) found that with an exciting frequency higher than resonance frequency, the output frequency reduces concerning input frequency due to energy-absorbing behavior of the soil when the number of wavelengths is increasing between transmitter and receiver.
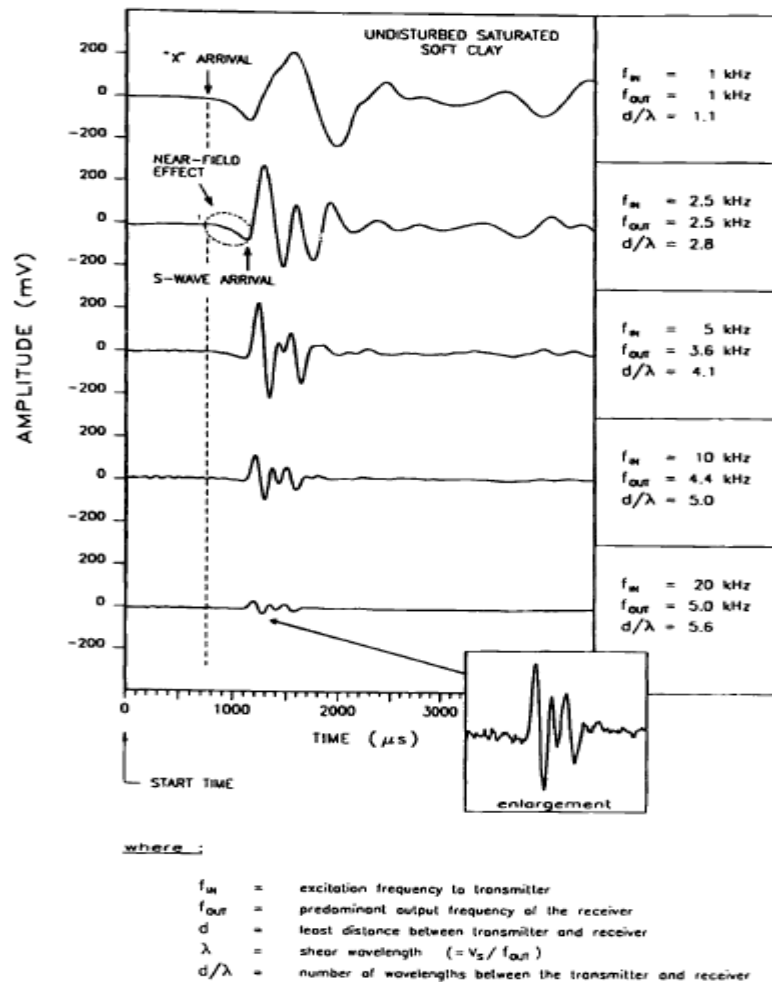
Figure 4.6: Effect of wave dispersion on first arrival (Brignoli et al., 1996)

4.2.4 Resonant frequency

The determination of the resonant frequency of the bender element system seems to be important for signal interpretation and data processing. The bender-soil system resonant frequency in the air is more function of the bender element characteristics when the cantilever length is short (L_b<4mm), whereas it is dominated by the soil properties when the cantilever length is long (L_b>4 mm). The typical mode shapes of the cantilever beam and their natural frequency which are properly consistent with transmitter bender element in the air can be observed in Figure 4.7. The natural frequency of the bender element in the air is related to the inverse square of the height. Therefore, the resonant frequency for the bender element in the air for the first mode can be illustrated as (Meirovitch, 1967).
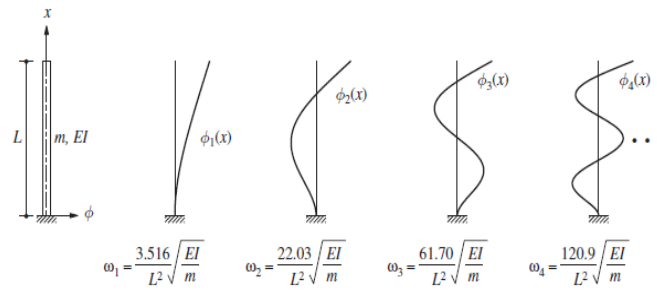
Figure 4.7: Representation of cantilever beam natural frequency at different modes (Chopra, 2012)

$$f_r = \frac{w}{2\pi} = \frac{1}{2\pi}\sqrt{\frac{k_b}{m_b}} = \sqrt{\frac{1.875^4 E_b I}{m(\alpha L_b)^4}} \tag{4.4}$$

After substituting material properties for piezo-ceramic the resonant frequency of an anchored bender element held in the air can be illustrated as:

$$f_r = 464[Hz.m]\frac{h}{(\alpha L_b)^2} \tag{4.5}$$

Where h=thickness and L_b=cantilever length

<u>Bender element in soil</u>

The resonant frequency of bender element in the soil in addition to bender element properties is also dependent on the soil density, stiffness, damping ratio, and even confining stress also affect bender element resonance frequency in the soil. By combining equivalent stiffness and mass and replacement of values found that resonance frequency of the whole system would be expressed as an equation, where β=experimentally determined value, η approximately equal to 2 (Lee and Santamarina, 2005) (Figure 4.8).

$$f_r = \frac{1}{2\pi} \left[\frac{1.875^4 \dfrac{E_b I}{(\alpha L_b)^3} + 2\eta V_S^2 \rho_s (1 + \upsilon) L_b}{\rho_b bh(\alpha L_b) + (\rho_s b^2 L_b)\beta} \right]^{1/2} \tag{4.6}$$
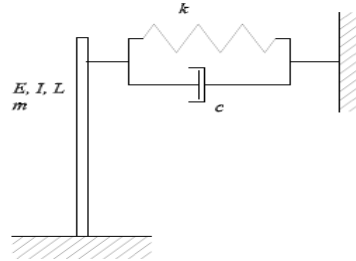
Figure 4.8: Bender element embedded in the soil (Rio, 2006)
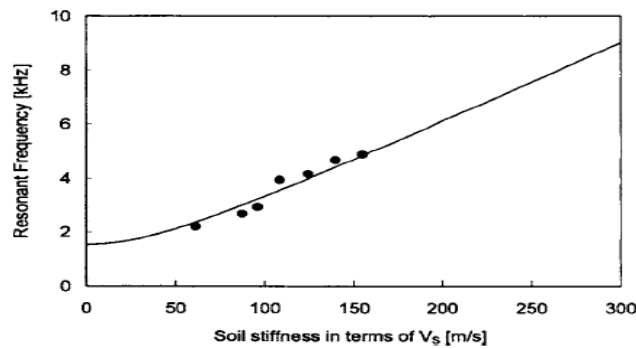
Figure 4.9: Effect of soil density in terms of shear wave velocity on resonant frequency (Lee and Santamarina, 2005)

For the soil with higher stiffness, there would be higher resonance frequency as effective stress increases (Lee and Santamarina, 2005) (Figure 4.9). It should be noted that the maximum tip defection of the bender element would be a function of applied voltage amplitude (Leong et al,2005).

4.3 Determination of travel distance

The length needed for waves effectively to reach the receiver transducer from the sender can be defined simply as travel distance. The exact determination of travel distance is of crucial significance for the determination of shear wave velocity, especially in the small-scale laboratory test. However, uncertainty associated with travel distance is considered to be less problematic than the determination of travel time (Arroyo et al., 2003). Incorporating bender element with the triaxial test, travel distance should be the height of the sample minus the protrusion of each of the bender elements, expressed as a tip to tip distance (Lee and Santamarina, 2005). More accurately, travel distance can be expressed as the length between

the center of the transmitter and receiver bender element. The result indicated by Rio (2006) showed that the distance between the centers of the dynamic pressure of the transducers should be taken as travel distance more precisely.

4.4 Determination of travel time

Accurate determination of travel time is undoubtedly one of the most problematic issues corresponding to the bender element test which affects the reliability of our result. The time required for the wave to reach receiver transducer would be a function of soil properties, bender element system, test setup, and more importantly signal characteristics. These factors heavily affect the complexity of correct interpretation. There are numerous various time-domain (TD) and frequency domain (FD) interpretation methods between the transmitted and received signal which can be applied to obtain the reasonable value of travel time.

4.4.1 First arrival method

The first arrival method is one of the procedures which can be utilized to determine the time needed for the wave to reach the receiver from the transmitter. The arrival of this shear wave at the other end of the sample is picked up by the receiver bender element. It is significantly important to make sure the alignment of the sender and transmitter transducer at the straight line to have the shortest distance.
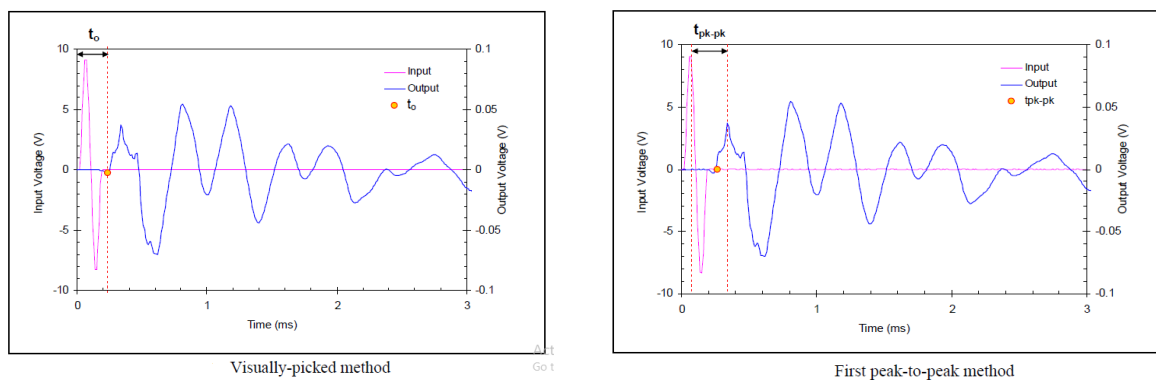
Figure 4.10: Illustration of first arrival method (Chan Chee-Ming, 2010)

This method is known as a time-domain procedure introduced by (Dyvik et al, 1985; Madshus et al,1985; Viggiani et al, 1995a; Brignoli et al, 1996; Jovicic et al,1996; Lohani et al, 1999; Pennington et al, 2001; Lee and Santamarina, 2005; Leong et al., 2005). The results might be adversely affected by wave dispersion near-field effect alternative problems associated with wave interference, which tends to mask the first shear wave arrival.

A comparison of travel times at the different characteristic points of the input signal and the corresponding output signal would be carried out as shown in Figure 4.10. This represents the start of energy transmitted from the bender to the soil. This procedure should be repeated for different points to make sure that acceptable value is identified. This method is widely used in bender element data interpretation. To get high accuracy of the result, wider frequency range, good sample quality, and appropriate signal processing seem to be essential.

4.4.2 Cross-correlation method

Cross-correlation is an alternative signal processing method introduced by Viggiani and Atkinson (1995) and Arulnathan et al. (1998). The cross-correlation function $CC_{xy(t)}$:

$$CC_{xy}(t) = \lim_{T_r \to \infty} \frac{1}{T_r} \int_{T_r} X(T)Y(T+t)dT \tag{4.7}$$

where is the T_r is the total time length of the signal X(T) is the signal at the receiver, Y(T) is the driving signal, and t is the time shift between the signals. Time shift tcc corresponding to the maximum value of equation 4.7. The above equation gives us cross-correlation T_{cc} represents travel time between receiver and source. For an impulse wave that has been recorded at two space points, the CC_{xy} will hit the peak at (CC_{xymax}) known as time-shift t that equals the travel time of the impulse between the two points (Figure 4.11). In fact, according to Santamarina and Fam (1997), the determination of the travel time using the cross-correlation method is only valid if both input and output signals are of the same "nature" and, according to Jovicic and Coop (1997), if the shape of the input and output wave remains unchanged. The fulfillment of these conditions, however, appears to be challenging due to wave distortion and near field effect.
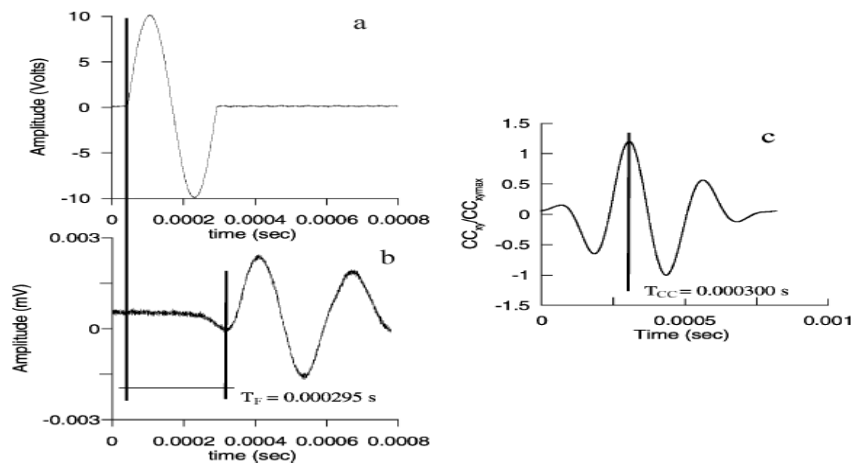
Figure 4.11: Representation of cross-correlation method (Mitaritonna et al., 2010)

Chapter5

Sampling considerations

Sampling disturbance is an important issue when interpreting the accuracy of bender element results. The utilization of the high-quality undisturbed sample seems to be crucial to ensure the reliability of our results. A variety of sampling procedures and sample quality evaluations has been introduced for this purpose.

5.1 Effect of sampling and sample disturbance chain on G_{max}

It should be noted that errors associated with bender element, including wave reflection, near-field, cannot be alone responsible for the discrepancy between field and lab result. It would seem reasonable to take the effect of other distorting factors corresponding to sample disturbance into consideration to understand better the source of error. In terms of sampling, it is widely accepted that there are several reasons associated with poor agreement between field and lab small-strain data, such as sample disturbance, disturbance chain (extraction, transport, storage, preparation, and re-consolidation) which strongly affects degradation curve as can be seen in Table 5.1 proposed by Wood (2016). High silt content, leading to high sensitivity and inhomogeneity, intensifies disturbance problems for low plasticity sensitive clay (Long, 2019). The distinction between in situ shear wave velocities and laboratory data might be also attributed to aging or long storage time for the soil with the same stress state and void ratio, as less discrepancy would be expected for fresh samples (Ferreira., 2008). In principle, stress relief after extraction decreases shear wave velocity followed by storage that might reform some physical and chemical bonds related to small strain property of soil. This decreasing trend, however, seems to be more pronounced for a sample from a larger depth. Samples from large depths are expected to be more affected by storage time (Landon et al., 2007). The main issues which may occur to sample, leading to changes in fundamental soil characteristics during sampling or in the lab can be mentioned as follows (wood, 2016):

- ✓ Stress state alteration
- ✓ Change in soil 's stiffness matrix
- ✓ Change in moisture content distribution
- ✓ Chemical and microbiological effects during storage
- ✓ Mineral alteration

Table 5.1: Sample disturbance chain (wood, 2016)
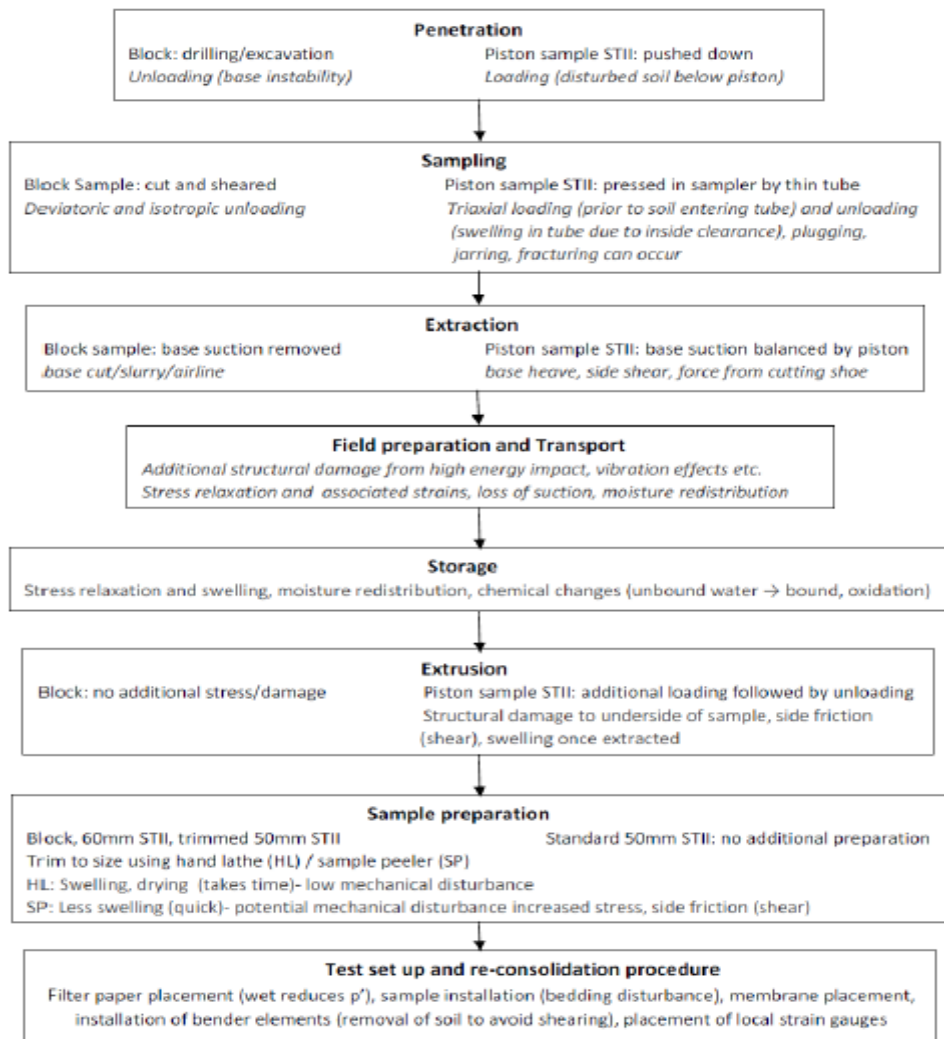
The block sample referred to as a less-disturbed sample, given the low volumetric strain during consolidation. To have a sample that might best represent an in-situ condition in the small-strain range, we should take into account the effect of sampling method, stress relief, sample preparation, sample dimension, aged or fresh sample, etc.

Amundsen et al. (2017) for 54 mm fixed piston sample low plasticity sensitive clay found that storage will reduce undrained shear strength and pre-consolidation pressure. Amundsen et al. (2016) were also expressed that it is fact that block samples represent better quality than the tube samples, but due to stress relief leading to swelling, loss of suction, handling and storage time it might not be a good indicator in many cases, especially for low plastic soft clay. It was observed that sample quality deteriorated with the reduction of the residual stress in less than 10 min after sampling. In principle, stress relief would be an issue, especially for block sample

extracting from a great depth. For the tube sample, however, this trend may be delayed by the support of the tube. Additionally, block samples showed higher undrained shear strength, stiffness, and pre-consolidation stress. Ladd and DeGroot (2003) mentioned that for slightly over-consolidated clay undrained shear strength increases with increasing strain rate.

Findings have been already done exhibit even when disturbances related to soil are kept to a minimum level, there will be still a discrepancy between filed and lab result, considering all contributing factors corresponding to sample disturbance chain, errors influencing lab result, and data interpretation. It would be, on the whole, concluded that the results derived from the in-situ test represent higher stiffness measurement than a laboratory test. Figure 5.1 represents this discrepancy based on studies conducted in both the USA and JAPAN.
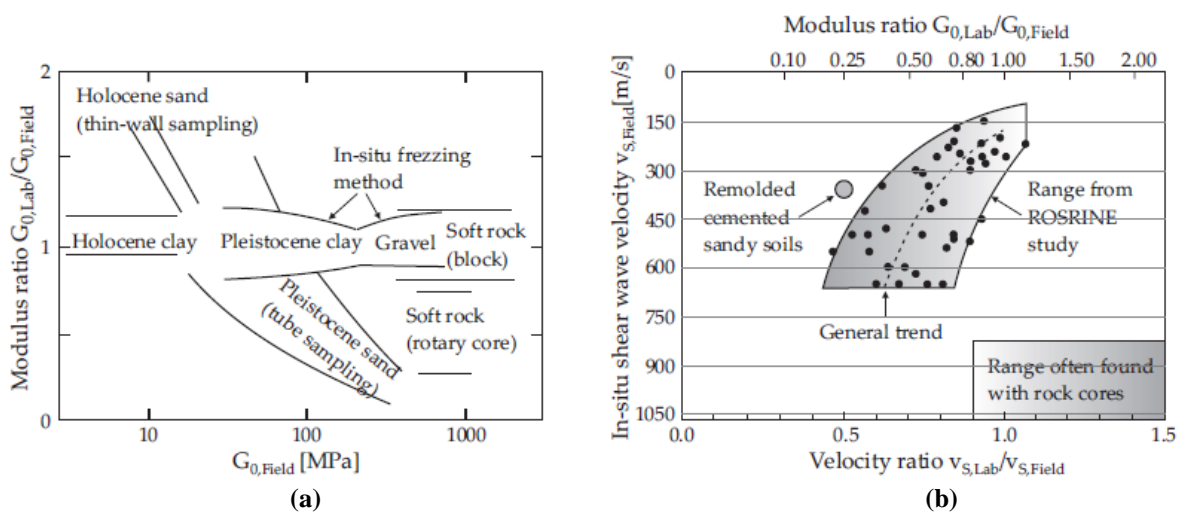
Figure 5.1: Difference between lab and field result based on (a) Japan Toki et al (1995) (b) USA study (Stokoe and Santamarina, 2000).

5.2 Sample quality assessment

The reliability of laboratory data can be adversely affected by the quality of the sample of interest. The most significantly important mechanical parameters, including soil stiffness, pre-consolidation stress, undrained shear strength, and clay sensitivity would be reduced by sample disturbance during sampling techniques, sample transport, or a long period of storage time (Emdal et al., 2016). Not surprisingly, effective techniques seem to be essential to have more reliable results and representative parameters from low plastic sensitive clay while improvements in sampling methods. There are numerous methods utilized to measure sample quality.

Laboratory method

Water expulsion during drained consolidation can be used to measure a high-quality undisturbed sample. Andersen and Kolstad (1979) utilized water expulsion criterion during consolidation as a sample quality indicator. The classification has been shown in Table 5.2.

$$\varepsilon_{vol} = \frac{\Delta V}{V_0} \tag{5.1}$$

Table 5.2: Sample quality assessment based on volumetric strain (Andersen and Kolstad, 1979)

OCR σ_c'/σ_{v0}'	Depth	Perfect quality $\varepsilon_{vol} <$	Acceptable quality $< \varepsilon_{vol} <$	Disturbed quality $\varepsilon_{vol} >$
-	m	%	%	%
1-1,2	0-10	3,0	3,0-5,0	5,0
1,2-1,5	0-10	2,0	2,0-4,0	4,0
1,5-2	0-10	1,5	1,5-3,5	3,5
2-3	0-10	1,0	1,0-3,0	3,0
3-8	0-10	0,5	0,5-1,0	1,0

It is also proposed to use the void ratio $\frac{\Delta e}{e_0}$ as a criterion for sample disturbance (Lunne et al., 2006), where Δe is the change in void ratio and $e0$ is the initial void ratio. The values for this ratio lower than 0.03 - 0.04 imply high-quality undisturbed samples Table 2.5. This method should be employed for marine clays with plasticity index 6-43%, water content 20-67 %, OCR 1-4, and depth below ground level 0-25 m (Lunne et al., 2006) (Table 5.3).

Table 5.3: Sample quality assessment based on $\frac{\Delta e}{e_0}$ (Lunne et al., 2006)

OCR	$\Delta e/e_0$ Sample quality category			
	Very good to excellent (1)	Good to fair (2)	Poor (3)	Very poor (4)
1-2	<0,04	0,04-0,07	0,07-0,14	>0,14
2-4	<0,03	0,03-0,05	0,05-0,10	>0,10

Application of shear wave velocity in sample quality evaluation:

Landon et al. (2007) proposed a non-destructive method for sample quality assessment of soft clays using portable bender element devices immediately after sampling. The ratio between this in-situ unconfined Vs_{vh} and corresponding value from seismic piezocone Vs_{cptu} can be used as an immediate, reliable, and non-destructive measure of sample quality. This non-destructive criterion showed an acceptable correlation with conventional laboratory-based evaluation (Figure 5. 2).
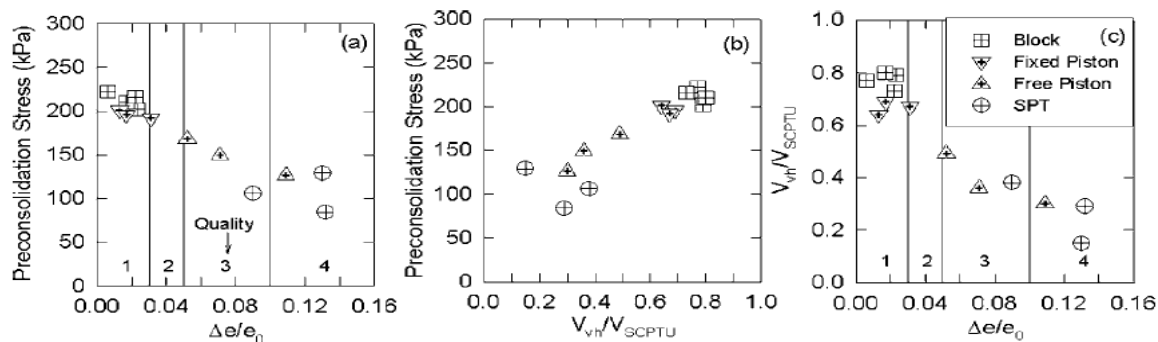
Figure 5.2: Sample quality comparisons (Landon et al., 2007)

As expected, block samples showed higher pre-consolidation stress and quality, representing $\frac{\Delta e}{e_0} < 0.04 \; and \; \frac{Vs_{vh}}{Vs_{cptu}} > 0.6$. The comprehensive classification was incorporated according to Table 5.4.

Table 5.4: Sample quality assessment based on $\frac{Vs_{vh}}{Vs_{cptu}}$ (Landon et al., 2007)

Sample quality		
Very good to excellent (1) Fair to good (2)	Poor (3)	Very poor (4)
$V_{vh}/V_{SCPTU} \geq 0{,}60$	$0{,}35 \leq V_{vh}/V_{SCPTU} < 0{,}60$	$V_{vh}/V_{SCPTU} < 0{,}35$

Donohue and Long (2010) used unconfined shear wave velocity (V_s) and suction (ur) measurements to evaluate sample quality for soft clay. They proposed following normalized parameters to quantify disturbance by using Figure 5.3.

$$L_{vs} = \frac{V_S \, in \, situ - V_{S0}}{V_S \, in \, situ - V_S \, remoulded} \tag{5.2}$$

$$L_u = \frac{0.2 \, \sigma'_{v0} - u_r}{0.2 \sigma'_{v0}} \tag{5.3}$$
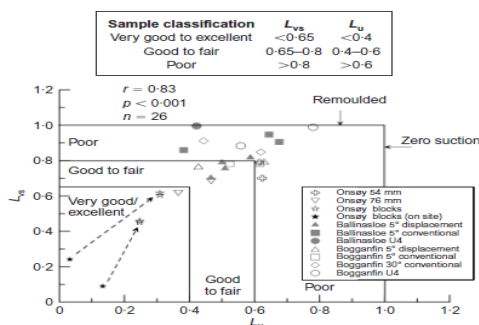
Figure 5.3: Proposed sample quality assessment parameters (Donohue et al., 2010)

Chapter 6

Clay particle anisotropy

Anisotropy properties of Clay emerge from particle arrangement and morphology induced by the depositional process during sedimentation or stress condition referred to as clay 's crucial behavior should not be neglected. This section is dedicated to stiffness anisotropy at small-strain to obtain an in-depth understanding of this soil behavior.

6.1 Anisotropy concept

The anisotropy in a small-strain shear modulus can be characterized as the unique property of the soil comparing other engineering materials. Therefore, there has been a dramatic increase in the number of soil constitutive models on small-strain behaviors in recent years. The main aim of anisotropy investigation is to obtain more accurate analytical results for geotechnical problems, especially for low-plastic sensitive soft clay. It is of crucial significance to determine stiffness parameters, which is a function of stress and strain relationship. When the soil is considered to show identical properties in any horizontal direction, Cross-anisotropic properties in terms of stress and strain increments can be expressed as the following matrix (lings, 2001).

$$
\begin{bmatrix} \Delta\varepsilon_{xx} \\ \Delta\varepsilon_{yy} \\ \Delta\varepsilon_{zz} \\ \Delta\gamma_{yz} \\ \Delta\gamma_{zx} \\ \Delta\gamma_{xy} \end{bmatrix} = \begin{bmatrix} \frac{1}{E'_h} & -\frac{v'_{hh}}{E'_h} & -\frac{v'_{vh}}{E'_v} & . & . & . \\ -\frac{v'_{hh}}{E'_h} & \frac{1}{E'_h} & -\frac{v'_{vh}}{E'_v} & . & . & . \\ -\frac{v'_{hv}}{E'_h} & -\frac{v'_{hv}}{E'_h} & \frac{1}{E'_v} & . & . & . \\ . & . & . & \frac{1}{G'_{hv}} & . & . \\ . & . & . & . & \frac{1}{G'_{hv}} & . \\ . & . & . & . & . & \frac{1}{G'_{hh}} \end{bmatrix} \begin{bmatrix} \Delta\sigma'_{xx} \\ \Delta\sigma'_{yy} \\ \Delta\sigma'_{zz} \\ \Delta\tau_{yz} \\ \Delta\tau_{zx} \\ \Delta\tau_{xy} \end{bmatrix}
\tag{6.1}
$$

Where E'_v and E'_h is young 's modulus in the vertical and horizontal plane respectively, ϑ'_{vh} and ϑ'_{hh} are Poisson's ratios for horizontal strain given the vertical strain, and for horizontal strain given the horizontal strain respectively, and ϑ'_{hv} is Poisson's for vertical strain given the horizontal strain. G'_{hv} is the shear modulus in the vertical plane, and G'_{hh} is the shear modulus in the horizontal plane. From Plane isotropy characteristic and symmetry of the matrix the following equations can be obtained (Yamashita et al., 2006).

$$\frac{\nu_{vh}}{E_v} = \frac{\nu_{hv}}{E_h} \tag{6.2}$$

$$G_{hh} = \frac{E_h}{2(1+\nu_{hh})} \tag{6.3}$$

Transverse isotropy assumption leads to $G_{vh} = G_{hv}$, and the coefficient of anisotropy can be

expressed as follows:
$$\alpha_G = \frac{G_{hh}}{G_{vh}} \tag{6.4}$$

$$\alpha_E = \frac{E_h}{E_v} \tag{6.5}$$

$$\alpha_\nu = \frac{\nu_{hh}}{\nu_{vh}} \tag{6.6}$$

Anisotropic stress condition, as well as anisotropic soil fabric, gives different values depending on many important contributing factors. where inherent small-strain shear modulus anisotropy is believed to be a result of particle arrangement due to stress-strain history, deposition (horizontal bedding planes), and post-depositional processes such as aging and cementation (Jamiolkowski et al., 1995). The stress-induced anisotropy can be attributed to existing stress state and stress changes (Nash et al., 1999). The direction of the confining effective stress with respect to the direction of wave propagation is key factors for getting the exact value of shear wave velocity in different directions. The effect of confining pressure on fabric-induced stiffness anisotropy on reconstituted London clay specimens investigated where the shear wave velocities measured in the horizontal and vertical direction and corresponding polarization under the same confining pressures. The results represented under isotropic stress condition, the values of G_{hh} are larger than those of G_{vh} and G_{hv}, which means the soil is inherently stiffer horizontally than vertically due to its soil fabric (Jovicic and Coop., 1998) (Figure 6.1). This distinction in value varies according to soil fabric, principal stress value, and other contributing parameters. Hardin and Blandford (1989) indicated the following equations 6.7 and 6.8 for maximum shear modulus at vertical and horizontal orientations caused by inherent and stress-induced anisotropy. Where Pr reference stress (1 atm), S_{vh}, S_{hh} material stiffness constant in the vertical and horizontal directions, and other parameters are the same as previously defined.

$$G_{0(vh)} = S_{vh}F(e)OCR^k p_r^{(1-nv-nh)}(\sigma'_v)^{nv}(\sigma'_h)^{nh} \tag{6.7}$$

$$G_{0(hh)} = S_{hh}F(e)OCR^k p_r^{(1-2nh)}(\sigma'_h)^{2nh} \tag{6.8}$$
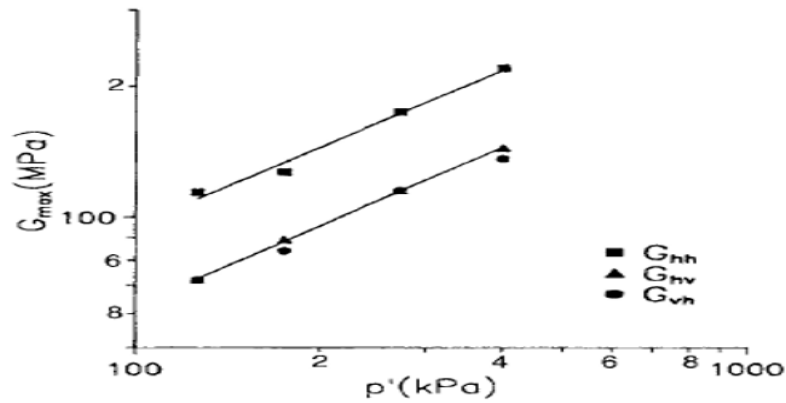
Figure 6.1: Anisotropy study for London clay under isotropic stress conditions (Jovicic and Coop, 1998)

Indeed, the anisotropy behavior of clay particles emerges from the prevalent orientation of platy clay particles and anisotropic stress conditions to the soil during the depositional and consolidation process and soil structure. Nishimura (2005) stated that when the stiffness anisotropy has been developed as the inherent property of soil, it would not be suddenly disappeared during isotropic consolidation.

Table 6.1: Anisotropy study using bender element at different consolidation phase (Nishimura, 2005)

Depth [m]	Test	Before isotropic re-consolidation			After isotropic re-consolidation			After anisotropic re-consolidation		
		G_{vh} [MPa]	G_{hh} [MPa]	G_{hh}/G_{vh}	G_{vh} [MPa]	G_{hh} [MPa]	G_{hh}/G_{vh}	G_{vh} [MPa]	G_{hh} [MPa]	G_{hh}/G_{vh}
5.3	TE5	32	62	1.9	38	79	2.1	41	84	2.1
8.2	TE4	42	71	1.7	54	96	1.8	58	109	1.9
10.6	TE7	48	86	1.8	57	113	2.0	57	125	2.2
13.6	TE6	-	-	-	-	-	-	71	144	2.0
16.1	TE2	58	110	1.9	61	109	1.8	61	109	1.8
20.9	TE1	73	136	1.9	78	155	2.0	77	158	2.1
27.9	TE3	74	133	1.8	84	152	1.8	87	162	1.9
28.2	TE9	77	143	1.9	88	173	2.0	88	173	2.0
29.1	TE8	77	139	1.8	83	153	1.8	83	169	2.0

Nishimura (2005) conducted the bender element test on London clay to assess the degree of anisotropy after isotropic and anisotropic consolidation. He found that the degree of anisotropy caused by isotropic or anisotropic consolidation, is predominantly attributed to clay initial anisotropy, and hence the influence of isotropic or anisotropic stress condition during consolidation is negligible on anisotropy investigation (Table 6.1). Brosse et al. (2017) conducted stiffness behavior study on medium-plasticity, highly over-consolidated four different clays by bender element equipped triaxial experiments. The result regarding anisotropy and non-linear properties interpretation has been shown in Figure 6.2. As seen for all kinds of clays represent consistent anisotropy ratio approximately 2 at a different maximum

depth of buried. Anisotropy is also shown in undrained and drained young modulus. They eventually concluded that stiffness characteristics of the soil are substantially anisotropic, pressure-dependent, and non-linear.
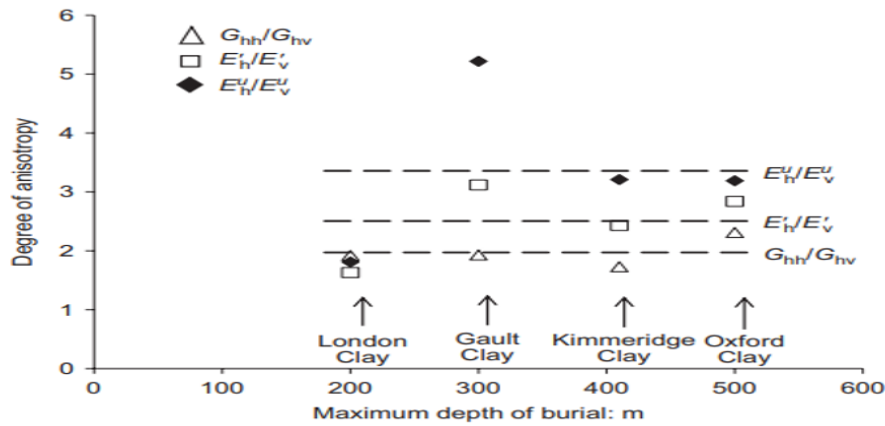
Figure 6.2: Degree of anisotropy based on burial depth for different clays (Gasparre et al., 2007)

Wang et al. (2007) investigated anisotropy study using laboratory bender element and numerical simulation discrete element method, and they found that stiffness anisotropy at small strain is controlled by both directions of inter-particle contact force and contact normal corresponding to major principal stress direction. This analysis confirms the assumption of clay 's cross-anisotropy characteristics. Laboratory results, however, do not agree with this assumption in many cases. As can be seen in Figure 6.3 anisotropy appears once clay 's particle arrangements transform from single spherical to three and four aggregated modes.
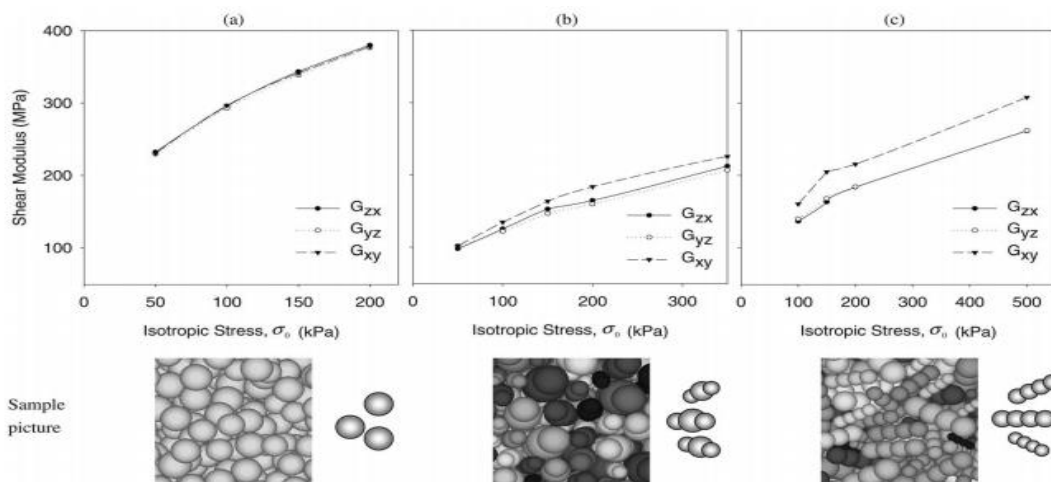
Figure 6.3: Anisotropy study for different states under confining pressure (a) spherical; (b) three-particle aggregated; and (c) four-particle aggregated particles (Wang et al., 2007)

Pennington et al. (1998) used both reconstituted and natural samples of Gault Clay to investigate anisotropy using bender element at different orientations with increasing K0 while

keeping effective vertical stress constant. Anisotropy ratio was found to be highly dependent on the stress state. Inherent anisotropy ratios for both natural and reconstituted clay under anisotropic stress conditions are plotted in Figure6.4. where the distinction between G_{vh} and G_{hv} was negligible, at a stress ratio of 0.4, G_{hh} and G_{hv} become relatively close to each other. It can be observed that the anisotropy ratio decreases with decreasing stress ratio, and escalating with increasing stress state. The distinction between natural and reconstituted clay is believed to be a result of void ratio, a variation of stress state, fabric, aging, and contact bonding. They also expressed cross-anisotropic characteristics of gault clay entails a further assessment.
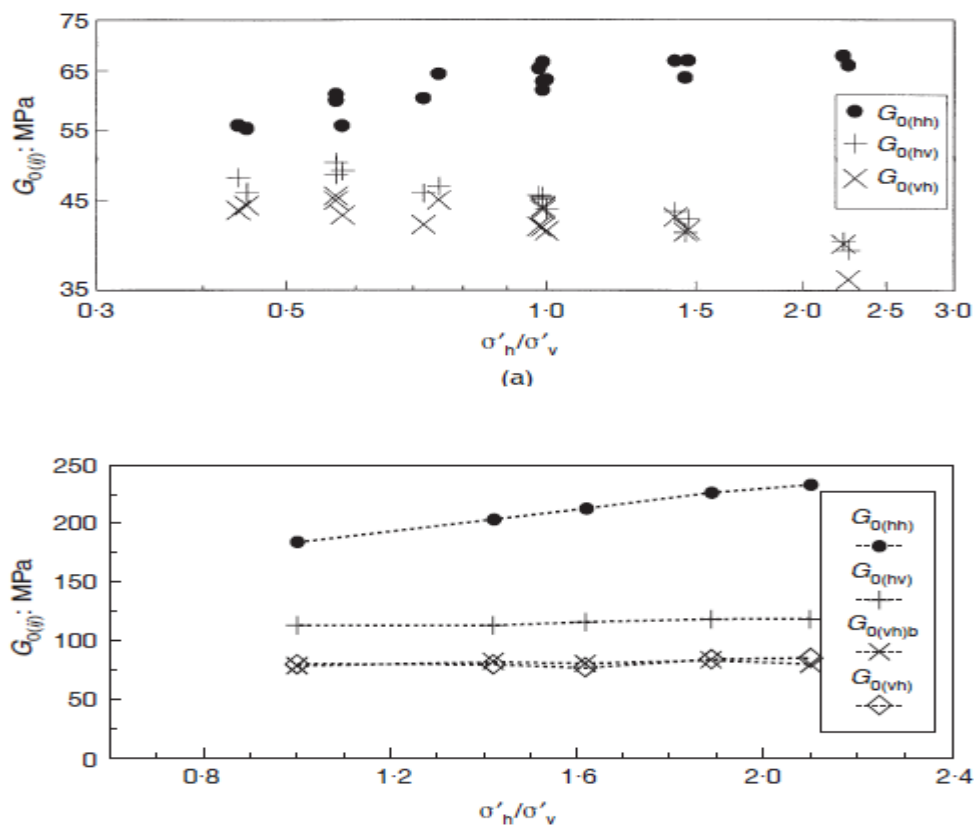
Figure 6.4: Anisotropy evaluation for anisotropic consolidated clay under specific condition (a) OCR=6, effective confining pressure=100 Kpa, Void ratio=1.09 (b) OCR>30, effective confining pressure=120 Kpa, Void ratio=0.84 (Pennington et al., 1997)

On the whole, Shear modulus anisotropy ratios (G_{hh}/G_{vh}) found to be in the literature for clays, such as 1.5 for Pisa and Panigaglia clays (Jamiolkowski et al., 1995); 1.7 for Gault Clay (Pennington et. al., 1997), 1.0 and 1.3 for Both Kennar clay respectively and 1.88 to 2.7 (in situ) and 1.5 (laboratory) for heavily over-consolidated London clay (Leroueil and Hight, 2003). The G_{hh}/G_{vh} values for BBC equal to 1.68 and $G_{hh}/G_{vh} = 1.55$ for Onsøy clay, and approximately one for Burswood clay (Landon et al., 2006).

Chapter 7

Tiller-Flotten research site

In this chapter, the main features of the Tiller-Flotten quick Clay Site will be characterized, developed as a research field by the Norwegian GeoTest Site project (NGTS). An extensive site investigation has been carried out in this region. Some investigation data will be mentioned in the following as well. Obtained soil characteristics results emerge from geotechnical, geological, and geophysical explorations will be illustrated and evaluated in this section.

7.1 Quaternary Geology

The area of study is located in the Flotten research site situated nearby Trondheim in mid-Norway (Figure 7.2). A marine clay deposit of sediment has covered this area with thickness around 50m (L'Heureux et al., 2019). An intense evidence of heterogeneity and anisotropy can be observed in this site resulting from laminations, varved, fissures, variation of clay content in depth and unknown geological factors. A large number of landslides have occurred in this region, especially slopes towards Nidelva which are more susceptible to landslide. This is primarily due to erosion or other triggering factors acting on thick marine deposit. Hence, this zone can be recognized as a high-risk quick Clay in terms of the landslide as three particularly salient examples events at Rissa (1978) nearby this site, Kattmarka (2009) and Esp (2012) can be mentioned in Trondheim (L'Heureux et al., 2019).
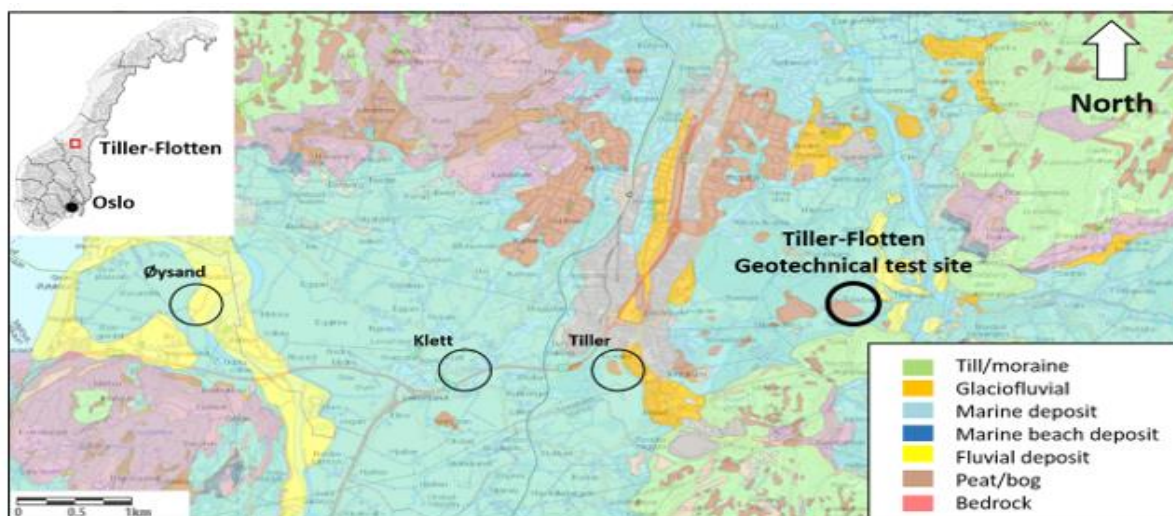
Figure 7.1: Detailed Quaternary geology map Flotten research site (ngu.no)

7.2 Field and laboratory data

Numerous in-situ investigation and laboratory testing have been carried out to acquire geological characteristics and soil properties in this region. A variety of complementary soundings and samplings procedures in addition to geophysical approaches were performed to obtain acceptable level of randomness regarding site characterization (L'Heureux et al., 2019).

7.2.1 Stress State

The depth of the groundwater table is approximately between 1 and 2 from the surface level according to data derived from installed piezometers. The most particularly important site characterization is that pore pressure is below hydrostatic condition, linearly increasing trend with depth from 5m depth to down which might be attributed to dramatic elevation change or local drainage. The estimated over-consolidation ratio was found to be above 2 at first10 m from ground level, and between 1.5-2 from 10 m to depth using odometer tests on the mini-block samples (Figure 7.2) (L'Heureux et al., 2019).
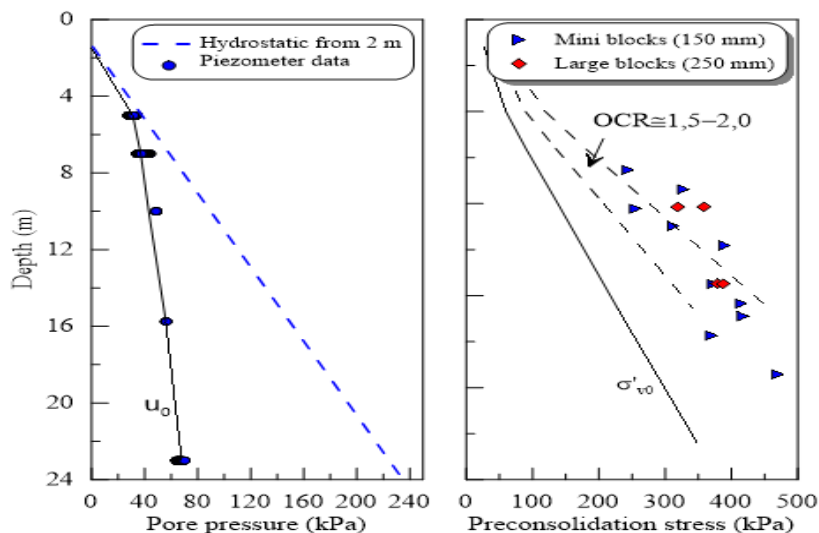
Figure 7.2: In-situ pore pressure and effective stress profile (L'Heureux et al., 2019)

7.2.2 Soil layering and Index properties

Determination of soil layering, relative stiffness in addition to index parameters have been also carried out by L'Heureux et al. (2019). The results will be summarized in the following. Two-meters dry crust mainly consists of desiccated and weathered clay above sensitive clay with variation of sensitivity and clay content in depth. Sensitivity exhibits an upward trend in-depth,

particularly from 7.5 m below ground level where up to 100sensitivity can be observed which emerges from ion change and salt content during the leaching process leading to soil with an unstable structure. The particle density was found to be from 2.83 to 2.88 g/cm3 utilizing a fluid pycnometer method. Salt contents were observed to be 2.1 g/l and 2.6 g/l at both 8 and 15 m below the ground surface, representative of leached clay. Natural water content most dominantly between 40% and 50%, dropped suddenly to approximately 30-35% at 20m depth. The average value of bulk density appears to be 18.0 kN/m3. Variation, however, at different depths can be observed in Figure 7.3. Based on results derived from Atterberg limits tests the soil is classified as low to medium plasticity sensitive clay.
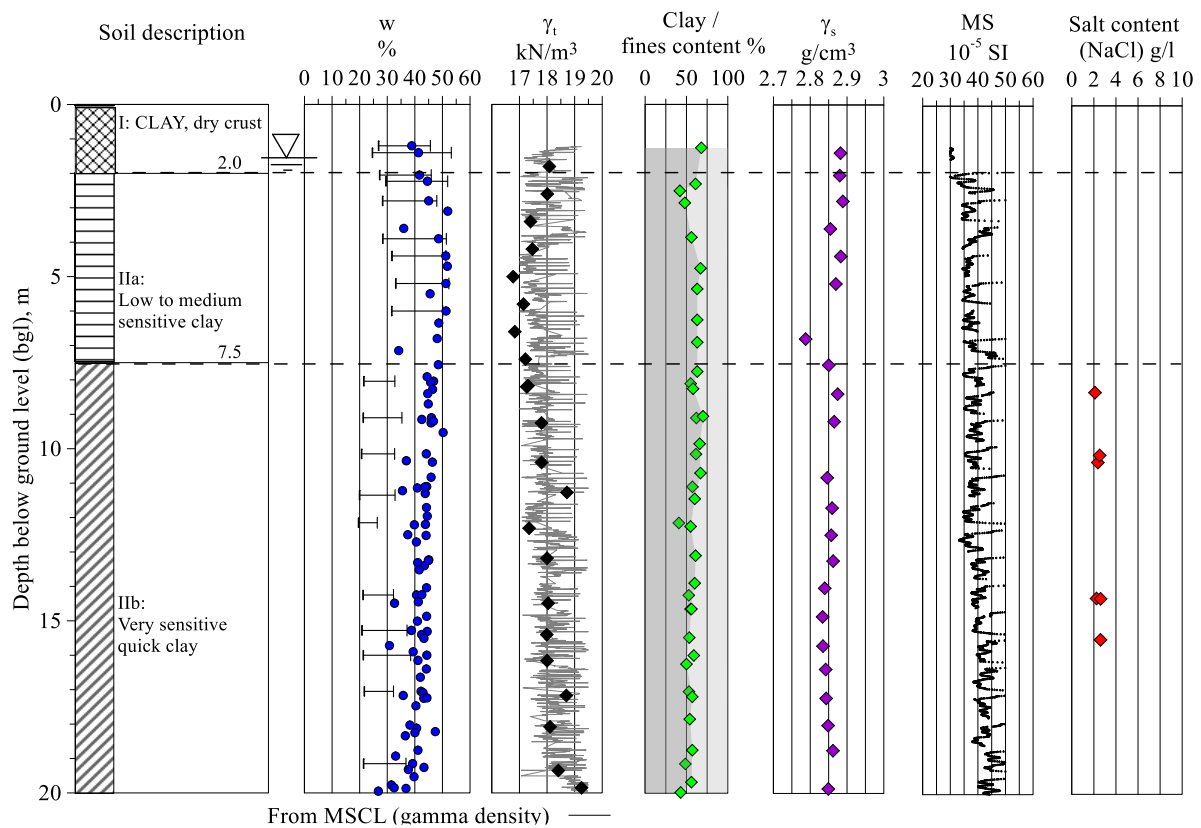
Figure 7.3: Soil layering and index properties at the Tiller-Flotten site. w = water content, γt = bulk unit weight, γs = particle density, MS = magnetic susceptibility (L'Heureux et al., 2019)

7.2.3 Shear wave velocity and G_{max}

In-situ shear wave velocity measurement has also been performed using a variety of field survey. As can be seen in Figure 7.2 V_s increases from 120m/s to 225 m/s between the dry crust and 20m depth. This value is properly consistent with measurements from other sites in the Trondheim area (L'Heureux et al., 2019).
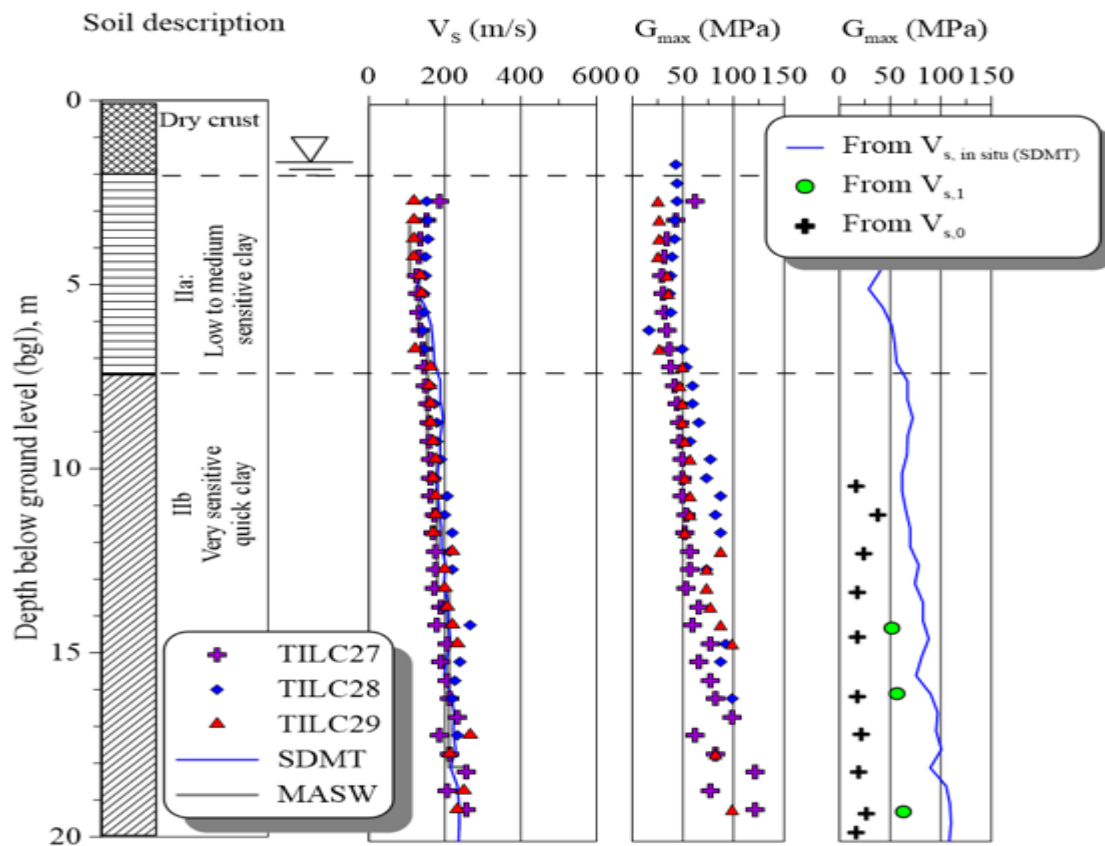
Figure 7.4: In-situ G$_{max}$ and corresponding shear wave velocity (L'Heureux et al., 2019)

7.3 Mineralogical composition and Fabric

L'Heureux et al. (2019) found that the clay content seems to decrease slightly with depth, from 70% at 7.5 m to a value of 50% at 19 m. They also suggested that Tiller-Flotten quick Clay is laminated with thin light and dark layers using X-ray analyses (Figure 7.4). It is considered to be representative of varved clay which compromises lighter-colored deposited during summer indicative of clayey silt stratified into a darker winter-deposited silty clay (Mitchell, 2005). Varved clay is known to be formed during a cyclical deposition and sedimentary process which is more likely to contributes to subsurface small-scale heterogeneity and intrinsic anisotropy of deposited soil. This variability of clay is believed to leave its mark on soil micro and macro-structure characteristics. Hydraulic conductivity, for example, is much higher in the horizontal direction than that of the vertical direction.
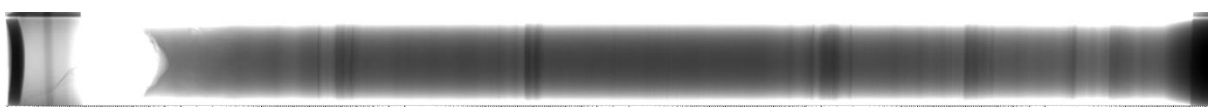
Figure 7.5: X-ray analysis from a 54 mm sample representative of varved clay (L'Heureux et al., 2019)

Chapter 8

Sampling and Laboratory Testing

A complementary combination of index testing, bender element under unconfined condition, and mounted in the triaxial cell under the confined condition at the end of primary consolidation and after 24-hour isotropic consolidation should be implemented to obtain a satisfactory knowledge of stiffness characteristics of Norwegian sensitive clay. In this chapter, the test performance stages will be described more accurately, such as the test equipment, laboratory sample preparation, methodology, test procedures, and Index testing description.

8.1 Sample preparation

Samples required in this research were taken from Flotten NGTS quick Clay Test Site at different depths using NTNU's block sampler. However, the sample was wrapped in several layers of plastic film to maintain moisture and prevent swelling. The loss of moisture and structure would be expected due to the aging for the old sample. This implies the sample should be tested immediately after extraction, and also when dividing the block into smaller specimens. To prevent sample disturbance, and absorb energy as well, caused by transportation or any possible vibration, between sample and container was filled with styrofoam spheres. The samples were then stored under appropriate temperature and humidity before installation.

Four mini-block samples and one big-block were then used for this research. The samples were unwrapped and studied visually, taking fabric, and lamination into account. The peripheral areas of block samples were not to utilize due to sample disturbance, particularly loss of moisture, and structure. The mini-blocks were divided into two parts from half-length. Four vertical specimens from the top and two horizontal ones from the bottom of mini-block samples were trimmed afterward with the aim of anisotropy study. Four tops for $V_{s(vh)}$ at mean effective stress and two bottoms were cut for determination of $V_{s(hv)}$ and $V_{s(hh)}$ as well. And of course, the more specimens were taken from big-block with approximately 25 cm diameter. The remaining parts of block samples were utilized for index testing after trimming. Note that all the fresh samples were tested immediately after a couple of days sampling, except the remaining part of mini-block (3) which made it possible to include the devastating effect of three months in addition to long-term storage into this research. The existence of varved clay

was obvious while cutting samples, indicating the high degree of variability of clay. This property of marine stratified clay might be the main plausible cause for heterogeneity and anisotropy behavior of clay in addition to clay 's micro and macro-structure properties, such as soil content, particle orientation, inter-particle bonding, and electrolyte concentration, etc.
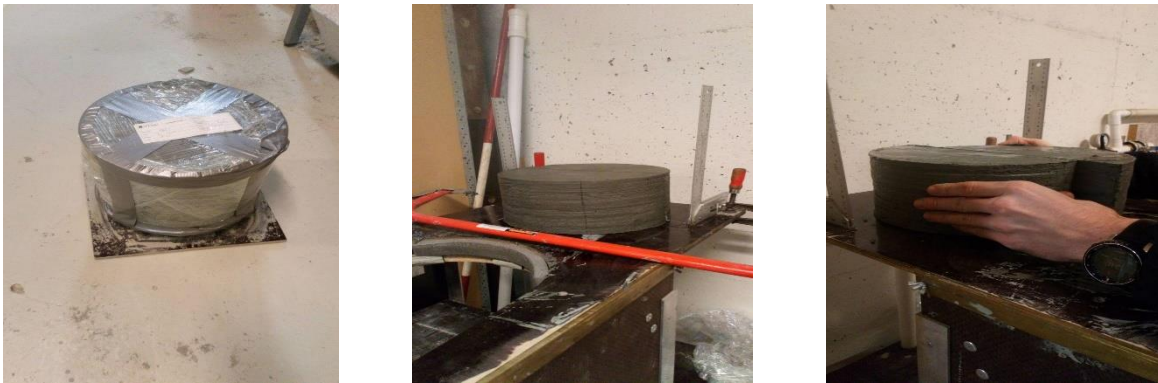
Figure 8.1: Representation of cutting big-block

In figure 8.1 the stages for cutting big-block sample is illustrated. The wire saw was used for cutting and trimming specimens. Finally, the samples were trimmed to the diameter of 54 mm and a height of 100 mm for mounting on the triaxial test. The saturated filter paper was placed on the top and bottom of the sample prior to putting a specimen on the triaxial device incorporated with the bender element receiver and sender. The rubber membrane to prevent water penetrating into the sample was applied. The cell needs to be filled with water in order to start the isotropic consolidation process.

8.2 Index testing

Index testing can be employed for soil classification, and to understand and quantify soil behavior more accurately. Moreover, there is a close link between soil small-strain properties and Index parameters, so it was reasonable to perform the following index tests.

- ✓ Density
- ✓ Water content
- ✓ Atterberg limits
- ✓ Fall cone

Density

Bulk density can be obtained based on standard ISO 17892-2 (ISO, 2014b). A small calibrated cylindrical ring with known mass and volume was pushed into a prepared sample. The weight of the sample and corresponding density was obtained as follows:

$$\gamma = \frac{m \cdot g}{V} \quad \left(\frac{kN}{m^3}\right)$$

(8.1)

γ is unit weight, g=9,81 $\frac{m}{s^2}$, and V is the volume of the sample. After trimming sample wet unit weight, and after drying into oven dry unit weight of specimen can be estimated to obtain satisfactory estimate of water content of specimen using equation:

$$\gamma_n = \gamma_d(1 + \omega)$$

(8.2)

A calibrated pycnometer was used for determination of grain density according to ISO 17892-3 (ISO, 2015). The equation can be used to determine grain density:

$$\rho_s = \frac{m_d \cdot \rho_w}{m_{wp} + m_d - m_{wps}} \quad \left(\frac{g}{cm^3}\right)$$

(8.3)

Where md is the mass of dry sample, ρw is the density of water (g/cm3), mwp is the mass of waterfilled pycnometer, and $mwps$ is the mass of waterfilled pycnometer and the sample ρw is the density of water and g =9.81 m/s2.

Water content

The water content determination was performed for all the specimen used for shear wave velocity measurement according to the standard ISO 17892-1 (ISO, 2014a). This value was obtained using below equation:

$$w = \frac{m_w}{m_s} \cdot 100 = \frac{m - m_s}{m_s} \cdot 100 \quad [\%]$$

(8.4)

Where the m_w is weight of water and m_s is weight of solid, and m is the total wet weight of specimen.

Atterberg limits

The Casagrande test was carried out to determine liquid limit of the clay according to section 5.3 in NS8001 (Norge, 1982). The plastic limit was also obtained using procedures according to section 5.3 in ISO/TS 17892-12 (ISO, 2004a). The plasticity index (IP) and liquidity index can then be calculated as follows:

$$I_p = w_L - w_p \quad (\%)$$

(8.5)

$$I_L = \frac{w - w_p}{w_L - w_p} \quad (-)$$

(8.6)

Fall cone

The fall cone method was utilized to estimate both undisturbed and remoulded undrained shear strength of samples according to ISO 17892-6 (ISO, 2017). The sensitivity then can be calculated using below equation:

$$S_t = \frac{S_u}{S_r} \quad (-)$$

(8.7)

Degree of saturation, porosity and void ratio

The degree of saturation can be obtained using below equation:

$$S_r = \frac{V_w}{V_p} = \frac{w \cdot \gamma}{\gamma_w \left(1 + w - \frac{\gamma}{\gamma_s}\right)} \quad (-)$$

(8.8)

where Vw is the volume of water (m3), Vp is the volume of voids (m3), γw is the unit weight of water (kN/m3). The porosity was achieved by the equation 5.10.

$$n = \frac{V_p}{V} = \left(1 - \frac{\gamma}{\gamma_s(1 + w)}\right) \cdot 100 \quad (\%)$$

(8.9)

The void ratio was calculated using equation 5.11.

$$e = \frac{V_p}{V_s} = \frac{\gamma_s(1+w)}{\gamma} - 1 \quad (-)$$

(8.10)

8.3 Bender elements testing

The application of the bender element has become one of the most popular and promising tools to measure shear wave velocity, indicative of soil skeleton configuration. The quality of the received signal, however, might be distorted by many devastating factors and a high degree of uncertainty which makes interpretation method more complicated, so it would seem reasonable to have a good understanding of this apparatus and test procedures.

8.3.1 Methodology

The bender element system has been developed at NTNU whose specifications can be found in APPENDIX A. The system consists of bender elements, power supply, data acquisition (DAQ) device added to the triaxial device, and LabVIEW program. LabVIEW program was employed to monitor input and received signal characteristics that were sent and received by DAQ. A single sine wave firstly was generated to measure shear wave velocity under unconfined condition. The measurements were also carried out repeatedly during the consolidation stage every 10 seconds by synchronizing the bender element with the triaxial test at the next stage. The determination of travel time is undoubtedly one of the most problematic parts of the bender element test. For this purpose, the time-domain technique has been utilized to match the received signal with a matched signal, and consequently obtain corresponding travel time (Figure 8.2). The bender delay is referred to as travel time. And of course, data can be transferred to EXCEL for more and detailed analysis using output file, including time, bender element delay (ms), effective height (mm) and received signal (mV).

To obtain received signal with high-quality the amplitude and frequency of the input signal should be changed at different stages to avoid signal distorting effects, such as noise, over-shooting, near-field, etc. The voltage was found to be 5V to avoid noise caused by the low amplitude of the received signal. The increasing trend for frequency was chosen from 1 kHz until 3 kHz according to the test characteristics which will be described in the next chapter at the same time with increasing resonance frequency caused by soil stiffness escalation.
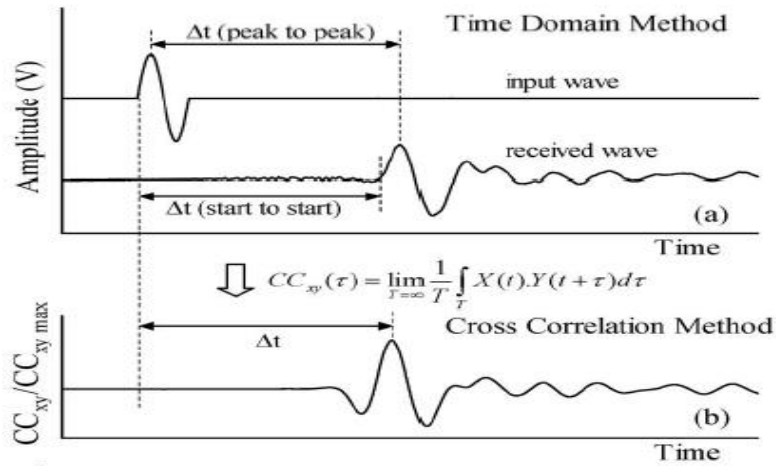
Figure 8.2: Time domain technique for determination of travel time (Yamashita et al., 2009)

8.3.2 Test procedures

To obtain small-strain shear modulus first sample was mounted on the cell under unconfined condition, and then shear wave velocity measurement was performed at this stage. At the next stage, the cell was filled with water to be able to apply the load to the sample. Measurement should be carried out during consolidation, at the end of primary consolidation (EOP) according to ISO (2004b), defined as when the volume change is less than 0.1 % of the specimen volume per hour or 0.1 cm3/hr (ml/hr), whichever is greater, until 24-hour after consolidation. The measurement of shear wave velocity can be carried out by obtaining travel time and travel distance as mentioned before. Travel time or bender delay would be calculated by the bender element device during the consolidation stage which would be the difference between the peaks of sent and match signal. The travel distance or efficient height can be defined as the height of sample minus 5mm which is embedded depth of transmitter and receiver transducers into the sample in addition to the reduction of sample height during the consolidation process (equation 8,11).

$$V_s = \frac{Efficient\ height(mm)}{Travel\ time(ms)} = \frac{h(100mm) - 5mm - axial\ deformation(mm)}{Bender\ delay(ms)} \tag{8.11}$$

During test performance, the applied frequency was increased with increasing soil stiffness. As confining pressure increases, bender element resonance frequency appears to increase, which means that the frequency of the induced signal should be increased to obtain an appropriate

measurement. The consolidation load was varied depending on sample characteristics and in-situ stress conditions. The small strain shear moduli can be calculated using measured propagation velocities at the different orientations of the bender element.

$$G_{vh} = \rho V_{vh}^2 ; \qquad G_{hv} = \rho V_{hv}^2 ; \qquad G_{hh} = \rho V_{hh}^2 \qquad \text{Mpa} \qquad (8.12)$$

Where ρ is the bulk density from the index testing (g/cm3). The values were recorded under 3 following conditions:

- ✓ Unconfined specimen,
- ✓ At the end of primary consolidation (EOPC),
- ✓ After 24 hours from the beginning of consolidation,

During the tests expelled water (cm3), shear wave velocity(m/s) and applied frequency (kHz) should be taken into account. The crucial and problematic part of this study is anisotropy investigation which can be carried out by changing bender element orientation or cutting sample horizontally concerning the direction of bedding plane or lamination (Figure 8.3). The measurements were carried out at different three following states:

- ✓ $V_{s(vh)}$ - shear wave propagating perpendicular to bedding plane with parallel polarization to bedding plane,

- ✓ $V_{s(hv)}$ - shear wave propagating parallel to bedding plane with vertical polarization to bedding plane,

- ✓ $V_{s(hh)}$ - shear wave propagating and polarization parallel to bedding plane,
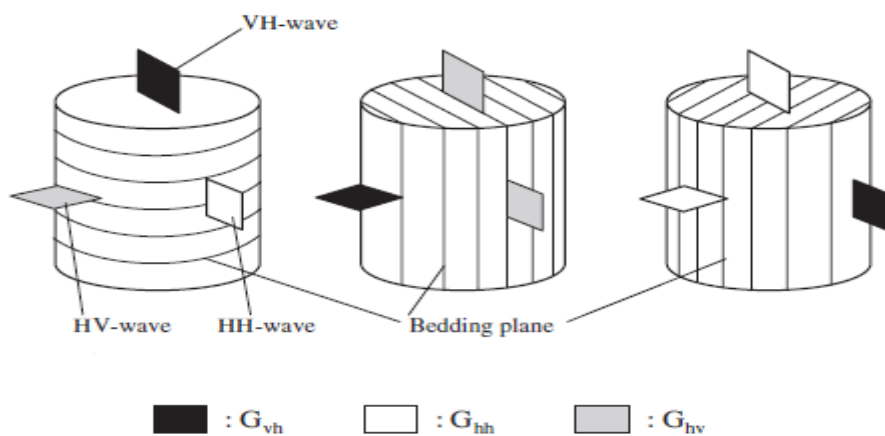
Figure 8.3: Orientation of bedding plane with respect to bender element for anisotropy study (Hori., 2006)

Note that in this research horizontally-cut specimen has been used for the measurement of shear wave velocity parallel to the depositional plane (Ghv and Ghh). The specimens would need to be handled cautiously to avoid sample disturbance during preparation and manipulation, especially when dealing with a fresh sample.

Chapter 9

Overview of results

This chapter is dedicated to a summary of initial results from Index-testing and bender element testing in addition to some basic principles of soil particle-fluid interaction. Sample quality assessment has been carried out at the end. Detailed discussions will be presented in the following chapter.

9.1 Index testing results

Index testing was carried out for mini-block with a diameter of approximately 16 cm and a height of 25–30 cm and big-block with a diameter of about 25 cm. Both fresh and aged samples were used for this research. Fresh sample referred to as cautiously extracted, transported, stored under appropriate humidity and temperature, and tested as soon as possible. Both the average water content and the void ratio are thought to be the most crucial parameters which correlate more precisely with maximum shear modulus. The summary of index test results is presented in Table 9.1.

Table 9.1: Index testing results

Sample no	unit	Miniblock(1)	Storblock	Miniblock(2) Fresh	Miniblock(3) Fresh	Miniblock(4) Fresh
Depth	m	7.5	12.8	6.8	6.5	13.2
Density, ρ	g/cm^3	1.82	1.84	1.83	1.83	1.83
Density of solids, ρs	g/cm^3	2.83	2.7	2.8	2.8	2.73
Average water content, w	%	45	43	46	46	43
Degree of saturation, sr	(-)	98	97	1	1	98
Void ratio, e	(-)	1.3	1.2	1.3	1.3	1.2
Porosity, n	%	56	54	56	56	54
Plastic limit, wp	%	19	24	15	15	25
Liquid limit, wl	%	33	31	35	36	32
Plasticity index, Ip	%	14	7	20	21	7
Liquidity index, IL	%	1.9	2.7	1.6	1.5	2.5
Undrained shear strength, Su	Kpa	38	45	45	43	42
Remoulded shear strength, Sr	Kpa	3	0,6	4	4,5	1.4
Sensitivity, St	(-)	13	75	11	10	30

Quick clay is known as clay with a remoulded shear strength of less than 0.5 Kpa. However, the only big-block tended to show somewhat quick clay properties with 0.6 Kpa remoulded shear strength, high sensitivity, and low plasticity. It would seem reasonable to assume that the

rest of the samples were likely to present properties close to clay to silty-clay at least in terms of mechanical properties and visual inspection. Some of the samples reflected inhomogeneous clay with a thin silt layer, varved, and laminations which makes it challenging, especially when the investigation of anisotropy ratio.

9.2 The influence of frequency change on V_s

In this section the effect of applied frequency of input signal on measured shear wave velocity and corresponding G_{max} will be discussed. The necessity and the significance of applied input frequency for granular soil can be described by the Biot (1956) theory which was indicated to investigate the interaction between viscous fluid flow and soil particle caused by wave propagation in the poroelastic medium. On the one hand, the existence of any small scale heterogeneity and disturbance in the medium containing particles with flat aspect ratios flocculated in the viscous fluid affects bulk elastic and shear modulus. On the other hand, elastic wave propagation in such a medium is likely to be affected by wave attenuation and dispersion. This theory provides a basis to evaluate the effect of excitation frequency on shear wave velocity in the soil specimen. Santamarina (2001) indicated that this theory can be summarized by three parameters, such as characteristic frequency f_c, low-frequency velocity V_s^{lf}, and high-frequency velocity V_s^{hf} when the stiffness of the skeleton Gsk is much smaller than material stiffness that makes up the particles Gg. The characteristic frequency which is the boundary between low and high-frequency velocity can be defined as:

$$f_c = \frac{ng}{2\pi k_h} \tag{9.1}$$

Where g=9.81 m/s2 gravitational acceleration and k_h is the hydraulic conductivity (m/s), n is the porosity of the medium.

If applied frequencies are low (f<0.1f_c) movements will not occur between soil and fluid, since motion is dominated by the viscosity of the fluid. Where the inertia of the fluid and soil particles is merged into each other. Therefore, total mass density can be used when measuring shear wave velocity which can be expressed as follow:

$$V_s^{lf} = \sqrt{\frac{G_{sk}}{(1-n)p_g + np_f}} \tag{9.2}$$

Conversely, if f>f_c the motion is controlled by inertia force, when the soil particle reaches the yield point, and consequently soil particle begins to move. Hence, the measurement of shear wave velocity can be done using mass density in terms of soil particle:

$$V_s^{hf} = \sqrt{\frac{G_{sk}}{(1-n)p_g+n(1-\frac{1}{\alpha})p_f}}$$

(9.3)

Where α tortuosity factor can be expressed as a function of porosity α=$\frac{1+n}{2n}$.

The high value of characteristics frequency will result in a wide low-frequency velocity range, while a wide high-frequency velocity range can be obtained with a low value for characteristics frequency. Increasing confining pressure causes hydraulic conductivity to reduce where characteristics frequency increases. This situation accounts for a wide range of low-frequency velocity, which means high excitation frequency is required for the movement between soil particle and viscous fluid to occur. The impact of other contributing parameters, such as percent of fine-grain, fluid viscosity can also be measured using this theory in granular soil. For the clay, however, with substantially low hydraulic conductivity depending on silt content the Biot theory would not seem to be the case. It just provides a basis for the reason behind the change of frequency during the test with increasing mean effective stress. Such behavior can also be observed in the bender element movement with consolidation time for fine-grained material. In this method, as the sample becomes more consolidated and densified, soil stiffness will increase, reflecting higher resonance frequency of the bender element. This means the excitation frequency should be enhanced to imitate the movement of the receiver transducer and obtain a reliable measurement. In Figure 9.1 the increment of the frequency change of input signal with increasing confining pressure during the test and measured shear wave velocity has been plotted. Thus, the higher consolidation pressure accelerates the trend of increasing shear wave velocity in terms of stiffness, particularly for samples taken from a great depth, experiencing higher swelling after sampling. Moreover, the rate of increasing excitation frequency is expected to be higher for horizontally-cut samples due to the higher water expulsion rate. The frequency of input signal in terms of the consolidation time was meant to vary from 1KHz until 3KHz until 24-hour consolidation. The shear wave velocity eventually was found to be approximately 120m/s≤$V_{s(vh)}$≤164 m/s for mini-block and 150m/s≤$V_{s(vh)}$≤173 m/s for big-block samples depending on the applied stress level.
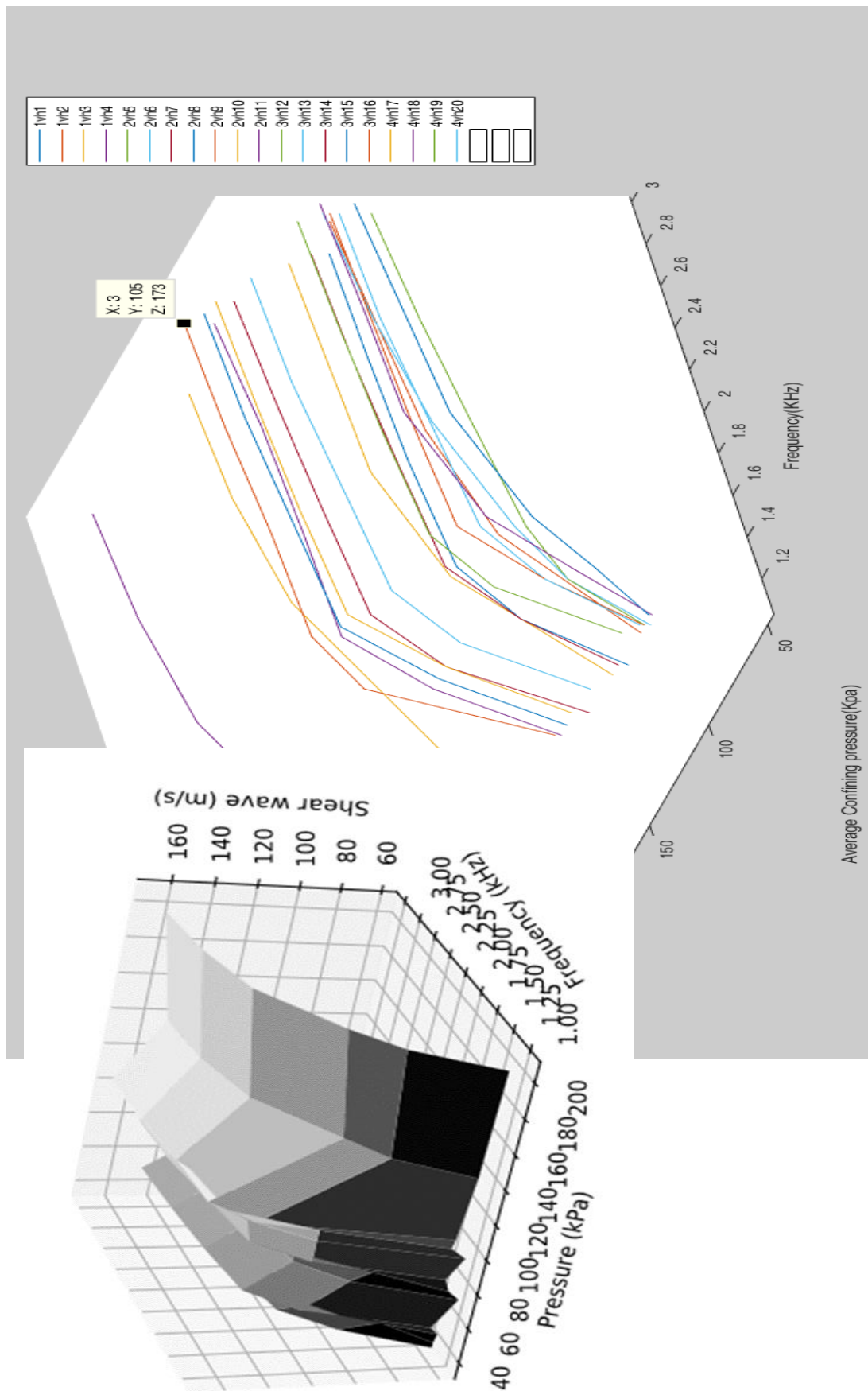
Figure 9.1: The increment of applied frequency and Vs, shear wave velocity at various stress levels during consolidation process

9.3 Near field effect

After the installation of the specimen, the measurement was performed under unconfined condition using a sinusoidal pulse waveform. At the next stage, the sample was consolidated at different confining pressure. During consolidation, the wave was being transmitted every 10 seconds. Applied input frequency plays a crucial role to obtain an exact estimate of shear wave velocity. For this purpose, frequency should be increased with consolidation time depending on the stiffness of the soil as mentioned before. The accurate selection of input wave frequency appears to be essential to avoid errors associated with the bender element test, such as near field effects, wave dispersion, boundary reflection and etc. At the beginning of the test, the receiver is vibrating with a lower frequency depending on the stiffness of the soil. For this purpose, the frequency of the input signal should be low to imitate the movement of the receiver bender element. It would be, therefore, challenging the appropriate selection of input signal frequency, especially under unconfined conditions. The magnitude of approximately 1KHz input frequency deemed to be sufficiently low to adapt the movement of the receiver and reduce the influence of the near-filed effect simultaneously. On the whole, reduction of the number of wavelengths between transmitter and receiver masks the received S-wave at the receiver bender in the time domain, leading to the overestimation of shear wave velocity which is called the near-field effect. Arroyo et al. (2003) believed that the near-field effect exaggerates shear wave velocity measurement between 10-15% when using a single sin-shape pulse.

This phenomenon can also be observed in the initial downward defection of the received signal (Jovicic et al., 1996). The near- field effect has been investigated at a special case for 2vh8 test where the reduction of near-field effect occurred by using frequency equal to 2kHz (Figure 9.3). In the meantime, not any noticeable change in V_s measurement was observed when applying the frequency of input signal higher than 2KHz in this particular case. Some researchers, however, suggested that the near-filed effect is likely to disappear when d/λ greater than 2. Arulnathan et al. (1998), however, believed that in the case of d/λ greater than 1 the near-field effect tends to decay. It can be observed in Figure 9.2 the near-field effect causes just a 5% increase in shear wave velocity to 164m/s from 156m/s. Where the interfering effect of P-wave contributes to an initial higher bump in the received signal, leading to overestimation of measured shear wave velocity. Finally, the near-field effect faded away with d/λ higher than 1.2 when approaching the end of consolidation in Figure 9.3. It is, therefore, concluded the near-filed effect cannot significantly account for inaccuracy and scatter related to bender

element testing under confined conditions when approaching the end of consolidation as the wavelength decline.
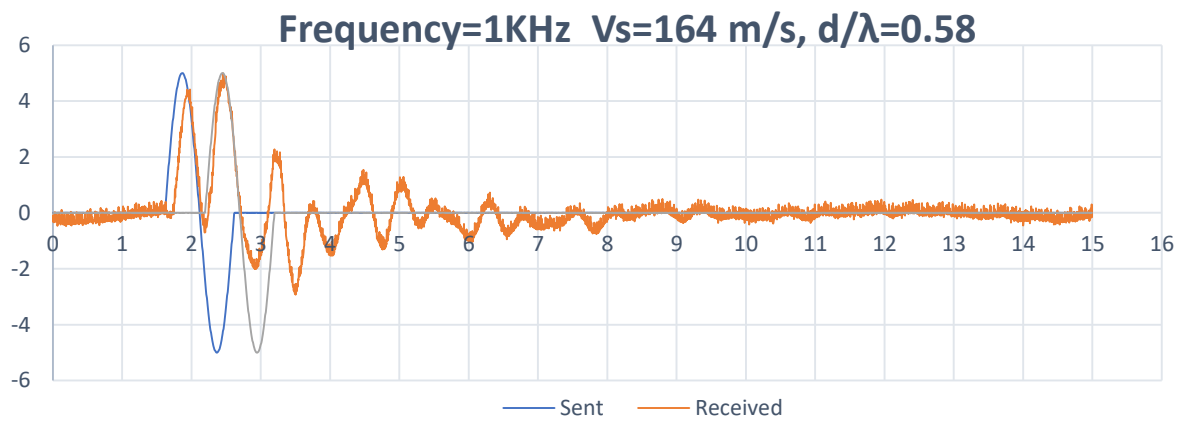
Figure 9.2: Near field effect at f=1 kHz Vs=164 m/s
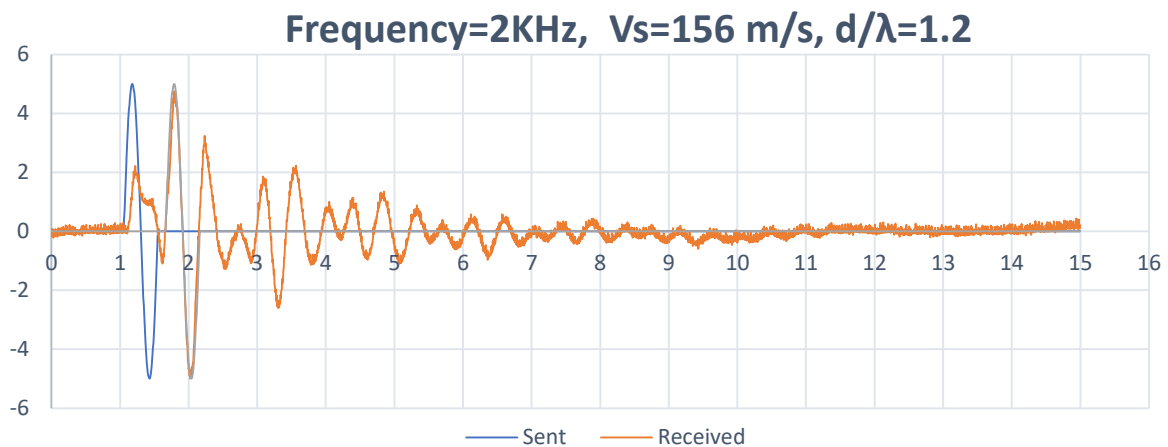
Figure 9.3: Disappearance of the near field effect at f=2 kHz Vs=156 m/s

9.4 Development of G$_{max}$ during K0 Consolidation

The five block-samples, including four mini-block and one big-block, were used for bender element test within k0 consolidation. All the fresh samples (three out of four mini-blocks) were tested immediately a couple of days after the extraction, except 4vh21 which was stored for 3 months with the aim of evaluation of aging on G$_{max}$ degradation. The horizontal stress component could be obtained from the in situ dilatometer measurements. The evolution of G$_{max}$ with the growth of effective consolidation stress by performing bender element test incorporated with the triaxial test can be observed in Table 9.2. The shear wave velocity variation versus time is plotted in Figure (9.4) until Figure (9.6), and the measurement was carried out at three following stages:

- ✓ Unconfined condition
- ✓ At the end of primary consolidation (EOPC)
- ✓ After 24 hours from the beginning of consolidation

Both the Expelled water (cm3) and Shear wave velocity (m/s) were measured during the test. Since the measurement of G$_{max}$ at a small strain range, the value of axial strain was negligible, but its effect on travel distance was taken into account. The interpretation of results reveals the maximum increase in shear wave velocity occurred during primary consolidation, where the sample experienced maximum water expulsion and a corresponding decreasing trend in the void ratio change. Reduction of porosity while keeping clay particle structurally integrated is a key factor to prevent sample disturbance at this stage. This increasing trend of shear wave velocity can also be seen after the end of primary consolidation but at a slower rate. This phenomenon is believed to be as a result of the displacement of clay particles into stable conditions depending on inter-particle physical and electrochemical force (Mitchell, 2005). The samples from greater depths showed higher shear wave velocity variation at the starting point when just approximately 10Kpa consolidation pressure was imposed for flushing filter. This would be indicative of the reverse relationship between void ratio and G$_{max}$ since the samples with lower void ratio from greater depth have more tendency to regain their initial shear modulus when even subjected to the low-stress level. The comparison between big-block and mini-block (4) taken from approximately the same depth reveals less variation of G$_{max}$ for most specimens from big-block reflecting most likely higher potential residual effective stress

in big-block which is more evident at low confining pressure. What is more, mini-block (2) fresh samples from the surface exhibited higher convergence of value after 24-hour consolidation which will be characterized more precisely in the following chapter.

Table 9.2: Illustration of performed tests on block sample using bender element

Test no	Sample	Depth(m)	Date of sampling	K0	Vs(m/s) Unconfined condition	Confining pressure(Kpa)	Vs(m/s)at the end of primary consolidation	Gmax(Mpa) at the end of primary consolidation	Vs(m/s)after24-hour consolidation	Gmax(Mpa)after 24-hour consolidation
1vh1	Miniblock(1) Old sample	7.5	19.06.2018	0,6	62	45	129	30	130	31
1vh2				0,72	60	54	133	32	136	34
1vh3				1	61	75	137	34	143	37
1hh4				0,6	63	45	143	37	145	38
2vh5	Bigblock Old sample	12.8	30.01.2019	0,46	65	54	146	39	150	41
2vh6				0,7	64	82	152	42	156	44
2vh7				0,8	57	94	152	42	157	45
2vh8				0,85	65	100	164	49	167	51
2vh9				0,9	64	105	169	52	173	54
2hv10				0,8	66	94	162	48	165	50
2hv11				0,9	65	105	157	45	160	47
3vh12	Miniblock(2) Fresh sample	6,8	24.02.2020	0,6	62	42	131	31	133	32
3vh13				0,73	61	50	128	30	134	33
3vh14				1	60	70	131	31	136	34
3hv15				1	55	70	123	28	128	30
3hv16				0,73	59	50	134	33	138	35
4vh17	Miniblock(3) Fresh sample	6,5	24.02.2020		61	140	150	41	153	43
4vh18					60	200	159	46	164	49
4vh19				0,74	60	50	114	24	120	26
4hh20				0,74	62	50	134	33	141	36
4vh21	Miniblock(3) test 3 months after sampling	6,5	24.02.2020		56	140	148	40	151	41
5vh22	Miniblock(4) Fresh sample	13,2	29.05.2020	0,7	57	90	140	36	147	39
5vh23				0,4	57	50	140	36	145	38
5hh(1)24				0,7	59	90	159	46	167	51
5hh(2)25				0,7	59	90	169	52	173	54

Figure 9.4: Shear wave velocity (top) and expelled water (bottom) measurement during isotropic consolidation and a sufficient period of creep for Big-block

Figure 9.5: Shear wave velocity (top) and expelled water (bottom) measurement during isotropic consolidation and a sufficient period of creep for Mini-block 2

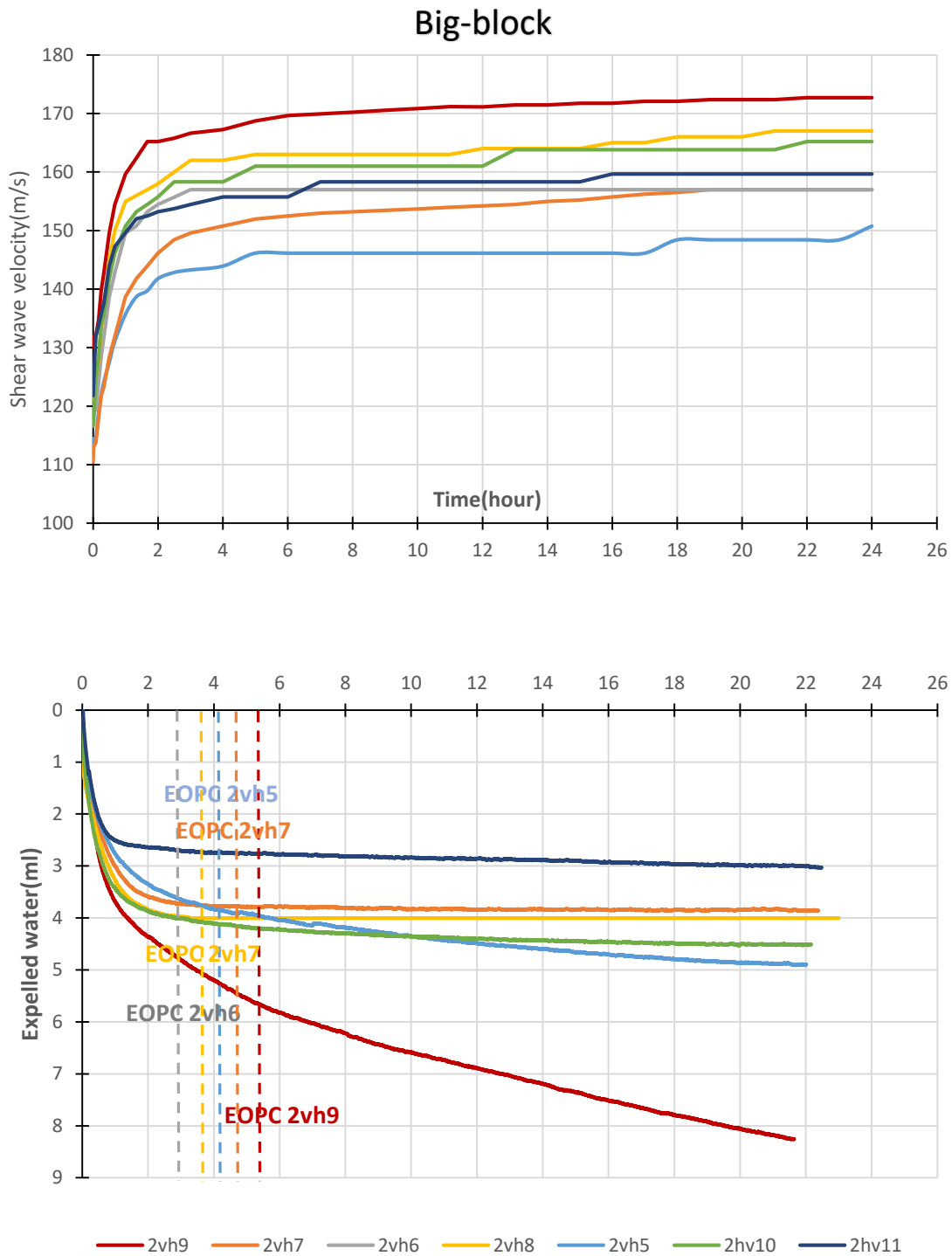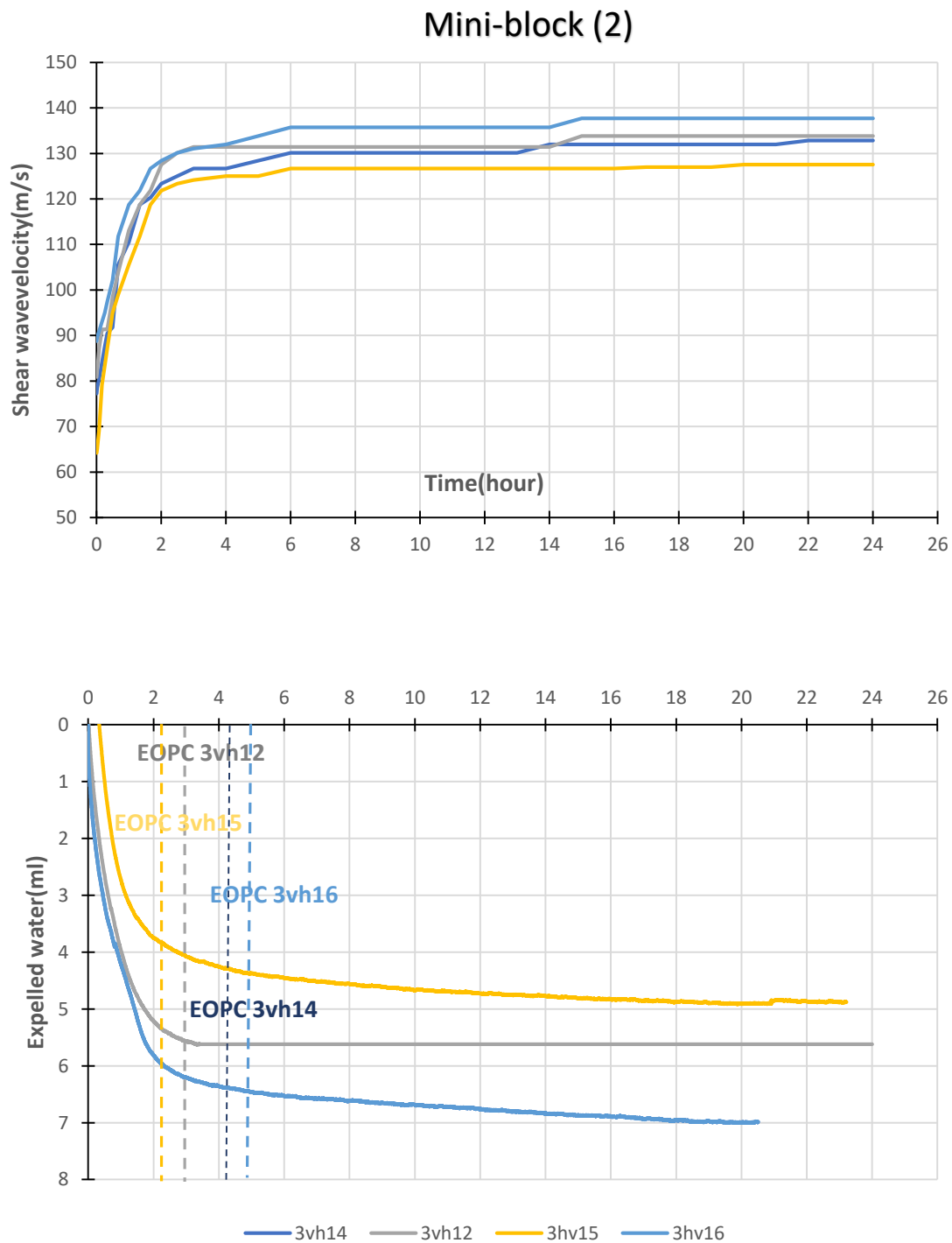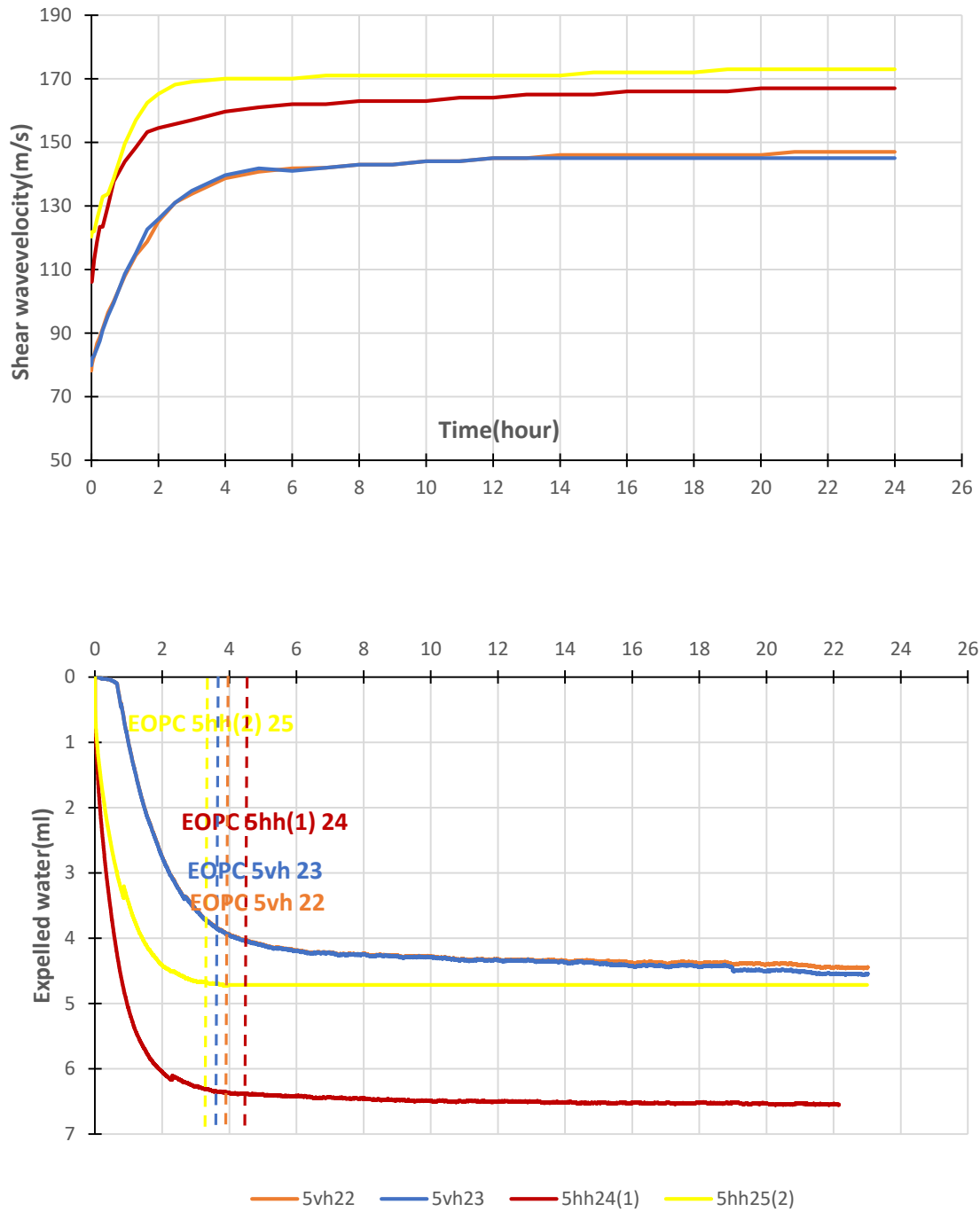**Figure 9.6: Shear wave velocity (top) and expelled water (bottom) measurement during isotropic consolidation and a sufficient period of creep for Mini-block 4**

9.5 Sample Quality Assessment

It is well understood that the reliability of the results is strongly dependent on sample quality. Sample quality evaluation was carried out based on two procedures described in section 5.2 with OCR above 2 for the top 10 meters and 1.5-2 for between 10 and 20-meter depth. The assessment criteria based on methods indicated by (Landon et al, 2007) and (Donohue et al, 2010) could not be indicative since shear-wave velocity-assessment should be carried out immediately after extraction prior to the dissipation of residual effective stress begin to occur. However, methods based on expelled water at the end of primary consolidation and void ratio variation are employed for the assessment of sample quality (Table 9.3). Opened block samples seem to be more prone to chemical, biological alteration. Therefore, it is essential to test the specimen immediately after opening the sample to avoid plausible sample disturbance. It is of crucial importance to avoid leaving sample in room temperature. On the whole, all the specimens consolidated under isotropic confining pressure presented a good quality (Figure9.7 until Figure 9.8). However, specimen 1vh3 does not fulfill the void ratio requirement.

Table 9.3: Sample quality assessment based on volumetric strain and void ratio change

Test no	Sample	Depth(m)	Date	OCR	Confining pressure(Kpa)	εvol %	Quality	Δe/e0	Quality
1vh1	Miniblock(1)	7.5	19.06.2018	(2-3)	45	(-)		(-)	(-)
1vh2				(2-3)	54	0,8	Perfect	0,014	Very good
1vh3				(2-3)	75	2,84	Acceptable	0,050	Poor
1hh4				(2-3)	45	(-)		(-)	(-)
2vh5	Bigblock	12.8	30.01.2019	(1,5-2)	54	1,64	Acceptable	0,030	Very good
2vh6				(1,5-2)	82	1,74	Acceptable	0,032	Very good
2vh7				(1,5-2)	94	1,7	Acceptable	0,031	Very good
2vh8				(1,5-2)	100	1,75	Acceptable	0,032	Very good
2vh9				(1,5-2)	105	2,13	Acceptable	0,039	Very good
2hv10				(1,5-2)	94	1,7	Acceptable	0,031	Very good
2hv11				(1,5-2)	105	1,2	Perfect	0,022	Very good
3vh12	Miniblock(2)	6.8	24.02.2020	(2-3)	42	2,74	Acceptable	0,048	Good to Fair
3vh13				(2-3)	50	(-)		(-)	(-)
3vh14				(2-3)	70	2,72	Acceptable	0,048	Good to Fair
3hv15				(2-3)	70	1,77	Acceptable	0,031	Good to Fair
3hv16				(2-3)	50	2,72	Acceptable	0,048	Good to Fair
4vh17	Miniblock(3)	6.5	24.02.2020	(2-3)	140	(-)		(-)	(-)
4vh18				(2-3)	200	(-)		(-)	(-)
4vh19				(2-3)	50	1,96	Acceptable	0,035	Good to Fair
4hh20				(2-3)	50	2,5	Acceptable	0,044	Good to Fair
4vh21				(2-3)	140	(-)		(-)	(-)
5vh22	Miniblock(4)	13.2	29.05.2020	(1,5-2)	90	1,92	Acceptable	0,035	Very good
5vh23				(1,5-2)	50	1,92	Acceptable	0,035	Very good
5hh24(1)				(1,5-2)	90	2,84	Acceptable	0,052	Good to Fair
5hh25(2)				(1,5-2)	90	2,05	Acceptable	0,038	Very good

2<OCR<3   6-10 m Depth
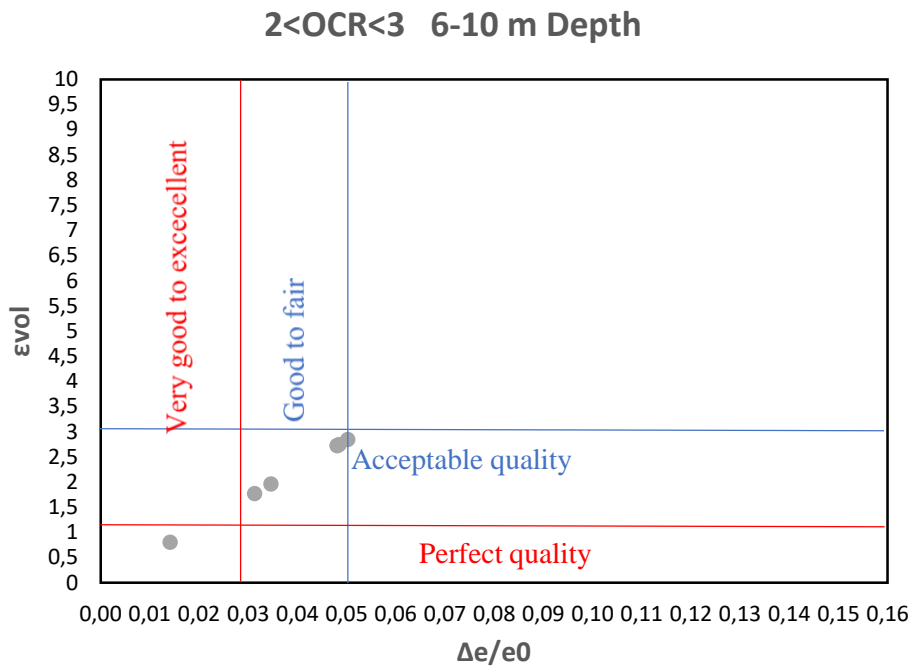
Figure 9.7: Sample quality evaluation for sample taken from depth between 6 and 10 meter

1.5<OCR<2   10-20 m Depth
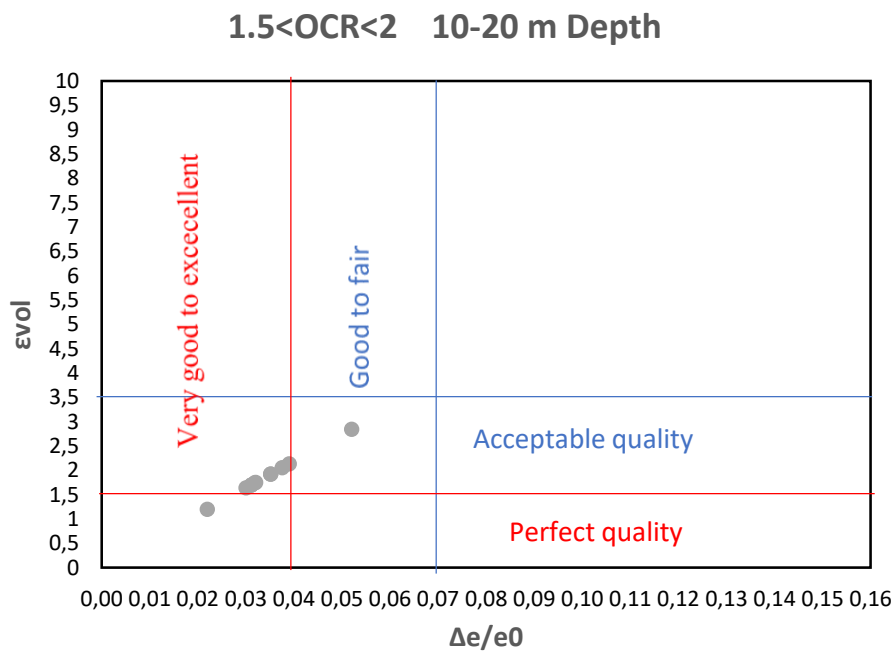
Figure 9.8: Sample quality evaluation for sample taken from depth between 10 and 20 meter

Chapter 10

Discussion

In this chapter, the main result will be discussed. The contributing factors to G_{max} value will be illustrated, and the comparison between field and lab results will be drawn. Anisotropy study will be carried out in the following.

10.1 The effect of average confining pressure on shear wave velocity and G_{max}

The investigation of the influence of isotropic confining pressure on shear wave velocity has been carried out using both big-block and mini-block samples. The sample characteristics and test conditions are listed in Table 9.2. The samples were consolidated isotropically under average confining pressure $p' = \frac{\sigma'_v + 2\sigma'_h}{3} = (\frac{1+2k_0}{3})\sigma'_v$ as target stress level at various K_0 value. The comparison between $V_{s(vh)}$, $V_{s(hv)}$, $V_{s(hh)}$ and corresponding maximum shear modulus obtained after 24-hour consolidation from lab results with the recommended equation 2.5 presented by L'Heureux et al., (2013) and defined parameters for Norwegian clay with low plasticity was drawn (Figure 10.1 until 10.8). Parameters were assumed to be in the range of $F(e)=\frac{1}{e^{1.3}}$, S=500-700 and n=0.25, followed by normalizing with F(e) since the samples were taken from different depths, and provide a framework for sample quality assessment as well. It was thought there is a good correlation between test results and that inferred from the equation. Most of the values fall into range defined by the empirical equation, most notably after normalizing with F(e). The stress-dependency of small-strain shear modulus observed, indicating a power regression of approximately 0,5 for G_{max} versus average confining pressure which is consistent with Figure 2.5 indicated by Viggiani and Attkinson (2005) for low plasticity sensitive clay, and the value of m between 0.5 and 0.6 as confirmed by many other researchers. It would seem reasonable that the rate of the increasing trend for G_{max} decreases as mean effective stress increases since the soil becomes stiffer gradually at higher consolidation stress. Meanwhile, a lower rate of increase in shear wave velocity with mean effective stress and less dispersion of results obtained could be indicative of high-quality samples as a mild increase in shear wave velocity with an increase of consolidation stress can be observed for fresh samples testing a couple of days after the extraction.

The big-block exhibited the highest shear wave velocity and corresponding G_{max} in all cases, hitting the peak of $V_{s(vh)}$ equal to 173 m/s at 105 Kpa consolidation stress, indicative of representative and reliable sample. The mini-block (3) with higher OCR, even though, reaches a peak of 164 m/s when imposing approximately twice consolidation stress equal to 200 Kpa (Figure 10.1).

To investigate the effect of long storage time on shear wave velocity this study also involved the test performance on both the mini-block (1) as old and mini-block (2) as a fresh sample with a few days of storage time while both of them were taken from approximately the same depth and equal OCR value. As can be seen in Figure 10.1 the fresh sample mini-block (2) presented less scatter of values and higher consistency of results with changing K0 values at corresponding average confining pressures. The investigation followed in test 4vh21 where the negligible difference in shear wave velocity measurement observed between the specimens after a couple of days storage (4vh17) and that of tested after 3 months while both specimens trimmed from the same mini-block (3). It was, therefore, concluded short-term storage under appropriate conditions does not make any substantial difference in shear wave velocity measurement.

It is well-known that the presence of a silt layer, the identity of the underlying layer, fissures and material with high permeability, inhomogeneity and detrimental factors associated with sampling practice such as extraction, transportation, and storage may affect sample quality, may account for the high amount of loss of RES and moisture in addition to the destruction of soil bonding and mechanical damage. In this respect, the results from the fresh sample illustrate a large amount of suction dissipation after only three days of storage since there seems not to be a significant discrepancy between fresh and old mini-block specimens shear wave velocity value under unconfined conditions.

Moreover, big-block represented slightly higher shear wave velocity under unconfined conditions when compared to mini-block, indicating big-block can maintain more of its initial structure particle bonding and potential RES after sampling process and during the consolidation process.

The orientation of the bedding plane with respect to the bender element contributes significantly to various G_{hh} and G_{hv} values. The fresh mini-block (4) presented the value of G_{hh} (2) when polarization parallel to the bedding plane and the lower G_{hh} (1) occurred due to the inclined wave propagation regarding the bedding plane (Figure 10.5 until 10.8).

Figure 10.1: Variation of vertical shear wave velocity after 24-hour consolidation with isotropic confining pressure
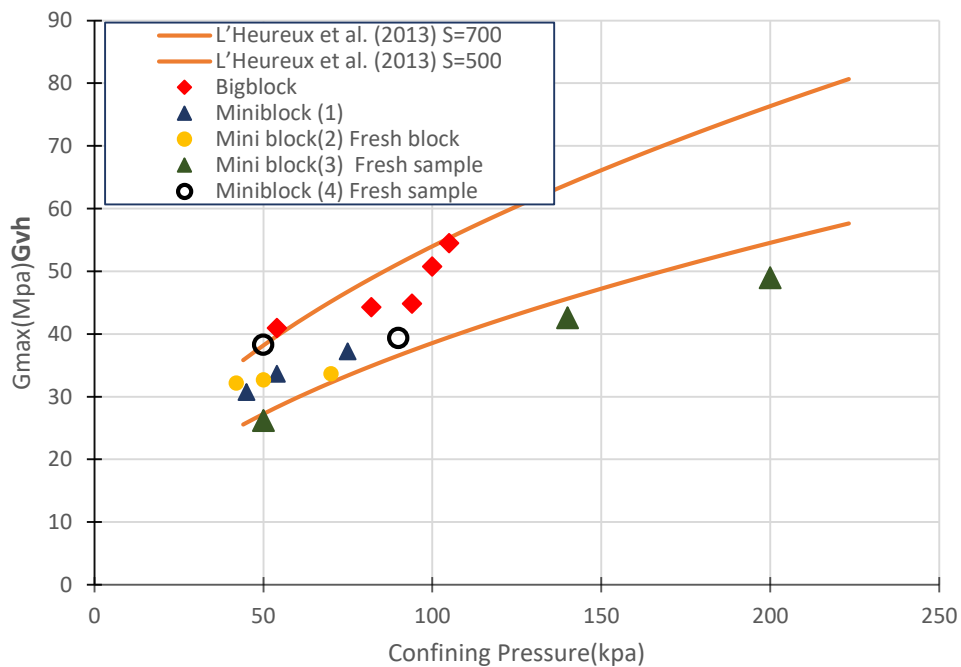
Figure 10.2: Variation of vertical maximum shear modulus after 24-hour consolidation with isotropic confining pressure
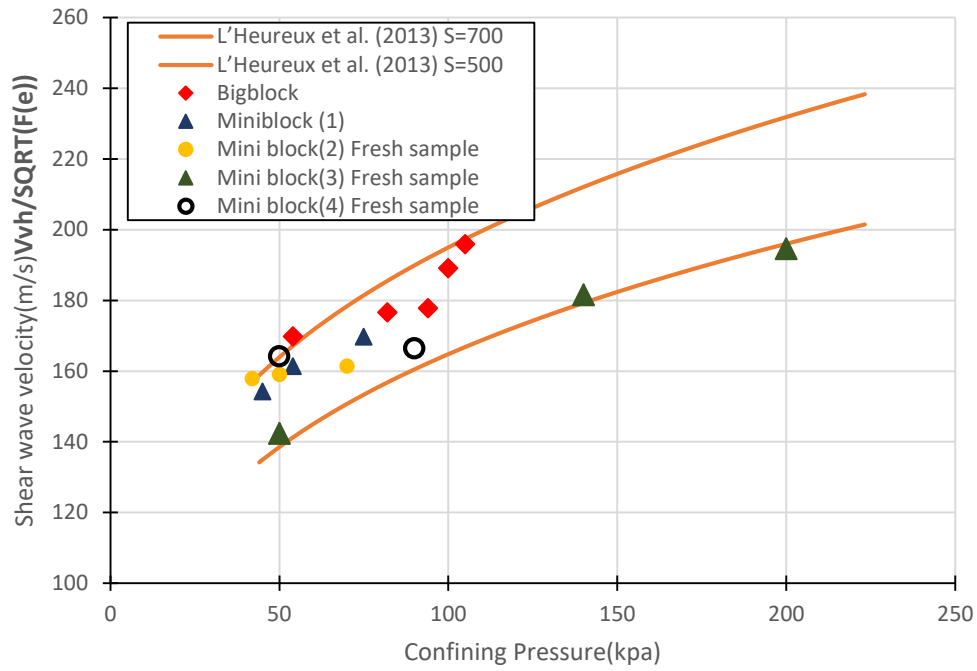
Figure 10.3: Variation of normalized vertical shear wave velocity after 24-hour consolidation with isotropic confining pressure
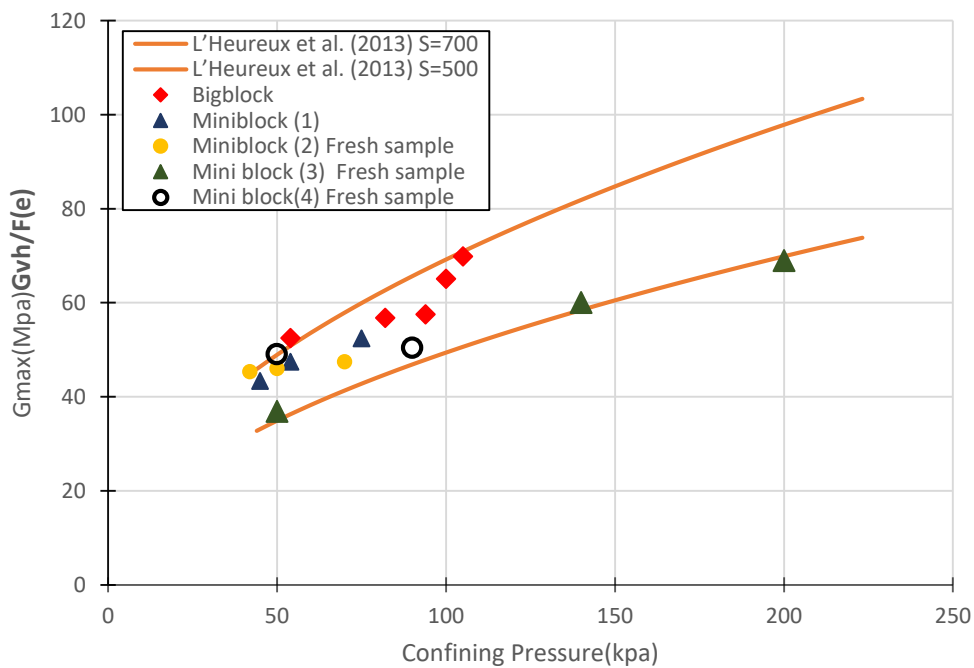
Figure 10.4: Variation of normalized vertical maximum shear modulus after 24-hour consolidation with isotropic confining pressure
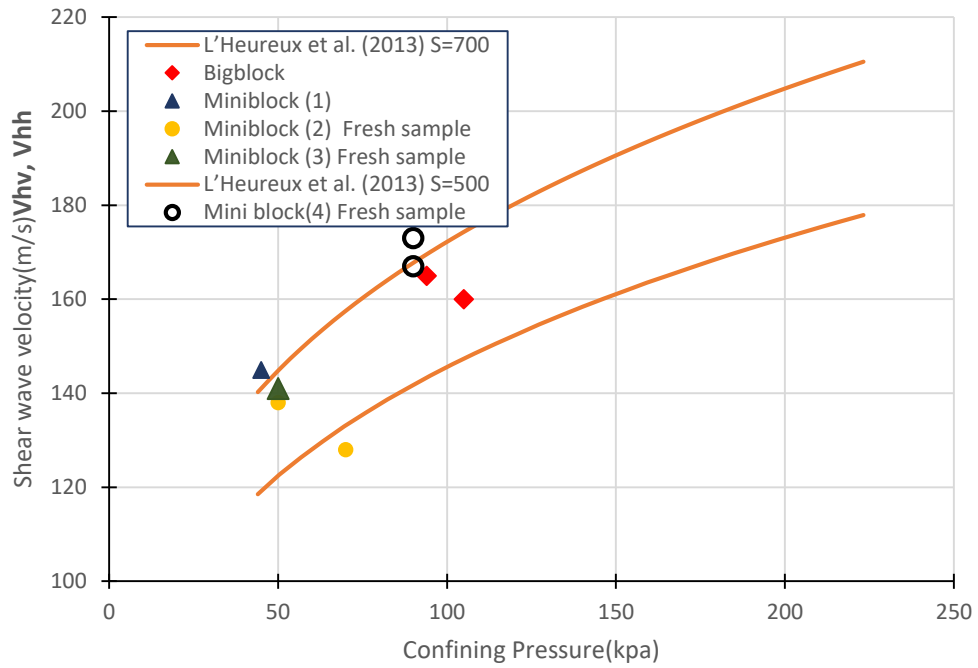
Figure 10.5: Variation of horizontal shear wave velocity after 24-hour consolidation with isotropic confining pressure
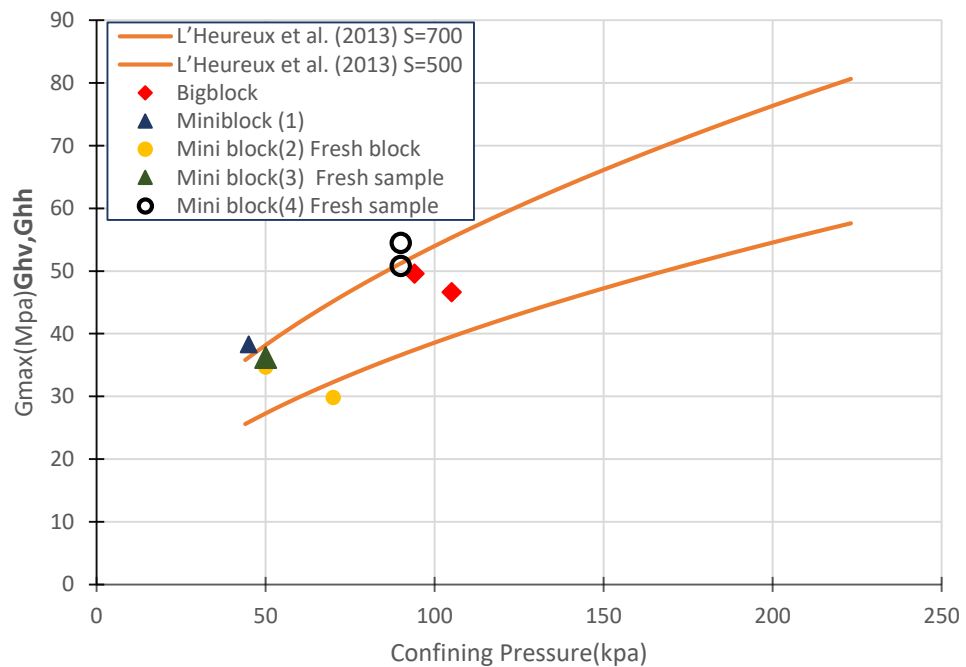
Figure 10.6: Variation of horizontal maximum shear modulus after 24-hour consolidation with isotropic confining pressure
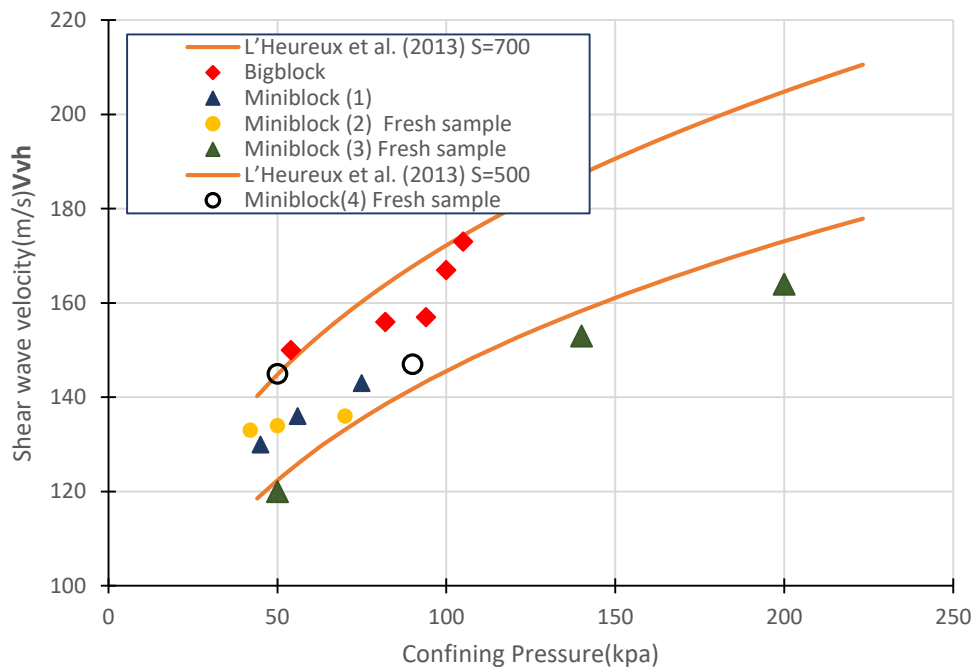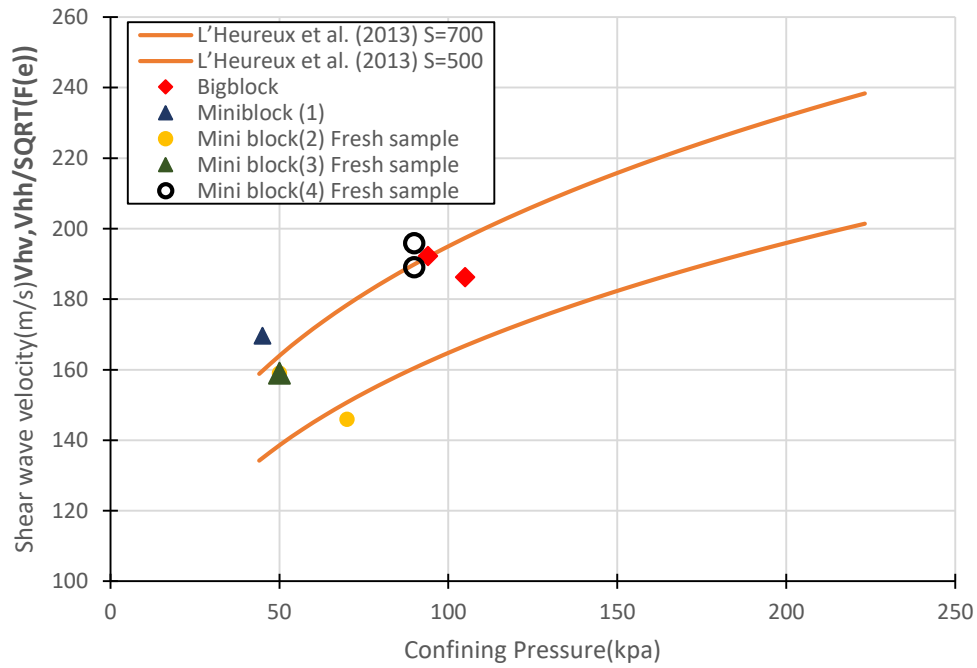
Figure 10.7: Variation of normalized horizontal shear wave velocity after 24-hour consolidation with isotropic confining pressure
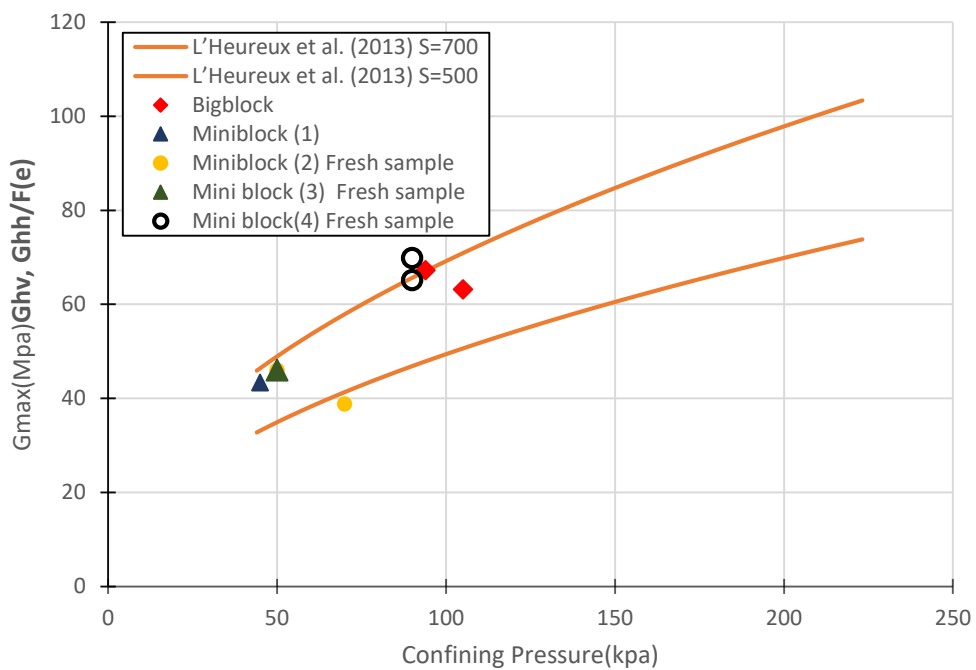
Figure 10.8: Variation of normalized horizontal maximum shear modulus after 24-hour consolidation with isotropic confining pressure

10.2 Variation of G_{max} with depth and In-situ measurement

The investigation of the variation of V_s and G_{max} with depth performed and the interpretation revealed that there seems to be an acceptable correlation between bender element results and empirical equation 2.7 indicated by L'Heureux et al. (2017) (Figure 10.9). The bender element results utilizing mini-block and big-block exhibit an increasing trend for V_s with depth. It is worth mentioning that the results from big-block utilized for V_s at greater depth when subjected to corresponding mean effective stress in the lab. Moreover, Ferreira et al. (2011) employed the ratio between lab and field shear wave velocity as an indicator of sample quality assessment. Where the sample with ratio $\frac{V_{Lab}}{V_{Field}}$ between 0.6 and 0.8 can be recognized as good to excellent quality. Based on this evaluation system as can be seen in Figure 10.9 most of the samples can be classified as good to excellent quality, indicating approximately $0.6 < \frac{V_{Lab}}{V_{Field}} < 0.75$. Note that this ratio between field and lab for G_{max} is anticipated to be higher (Figure 10.9, b).

(a)   (b)
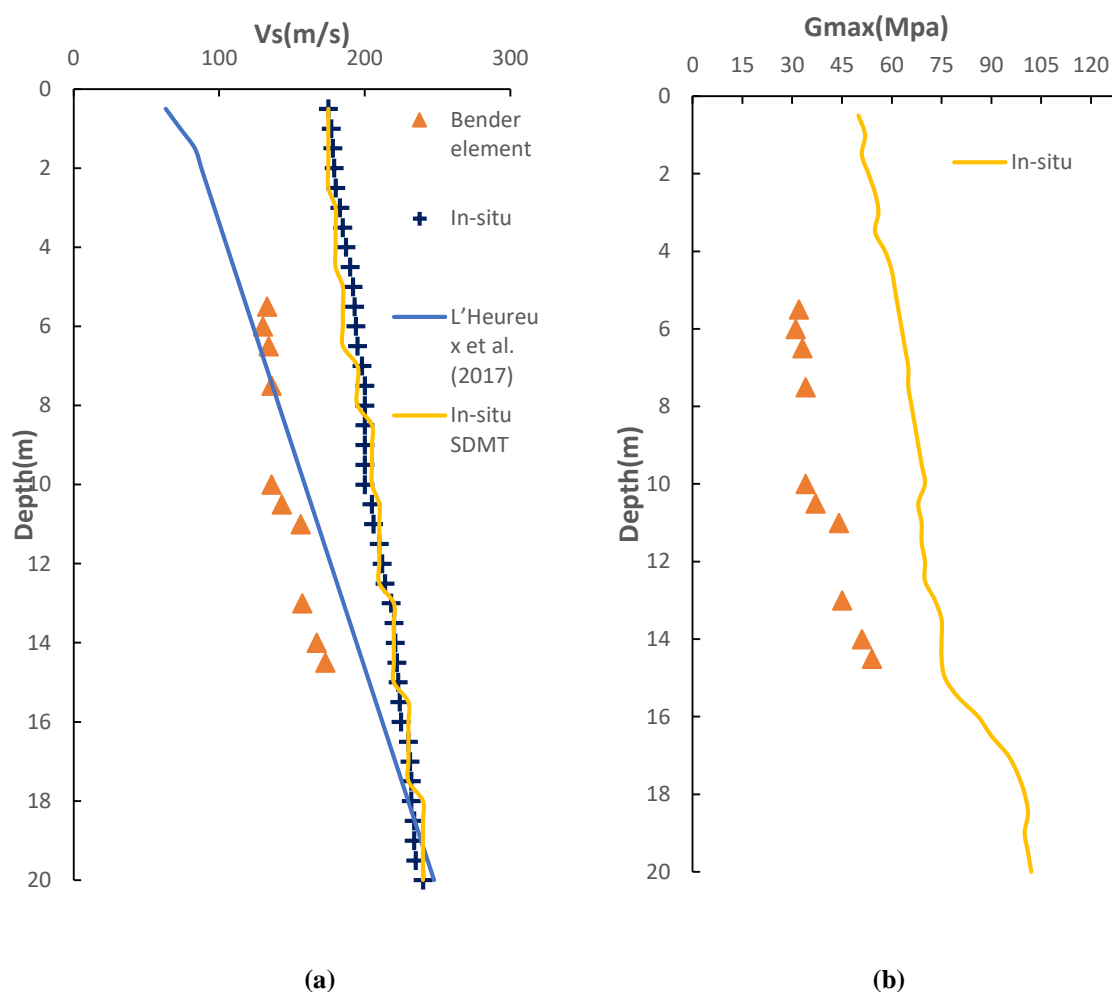
Figure 10.9: (a)Variation of shear wave velocity, Vs (b)and maximum shear modulus, G_{max} with depth

10.3 The effect of water content on maximum shear modulus (G_{max})

It is well recognized that the contribution of pore volume filled with water to shear wave velocity and corresponding G_{max} is undeniable. Maximum shear modulus at small strain (G_{max}) is expected to decline with increasing water content while keeping other contributing parameters constant (Figure 10.10). The values are plotted and lower value of G_{max} at surface level with higher water content than samples taken from depth was observed. Hence, the fresh samples from surface tended to have a lower value of G_{max} between 30 and 35 Mpa with 46% water content, and samples with 43% water content exhibited approximately an average value of 50 Mpa of G_{max}. In principle, in Norwegian practice normalized G_{max} with regard to the sum of average confining pressure and attraction will be usually taken into account (Janbu, 1985). When to evaluate the influence of water content on G_{max}.

$$g_{max} = \frac{G_{max}}{\sigma'_m + a} \tag{10.1}$$
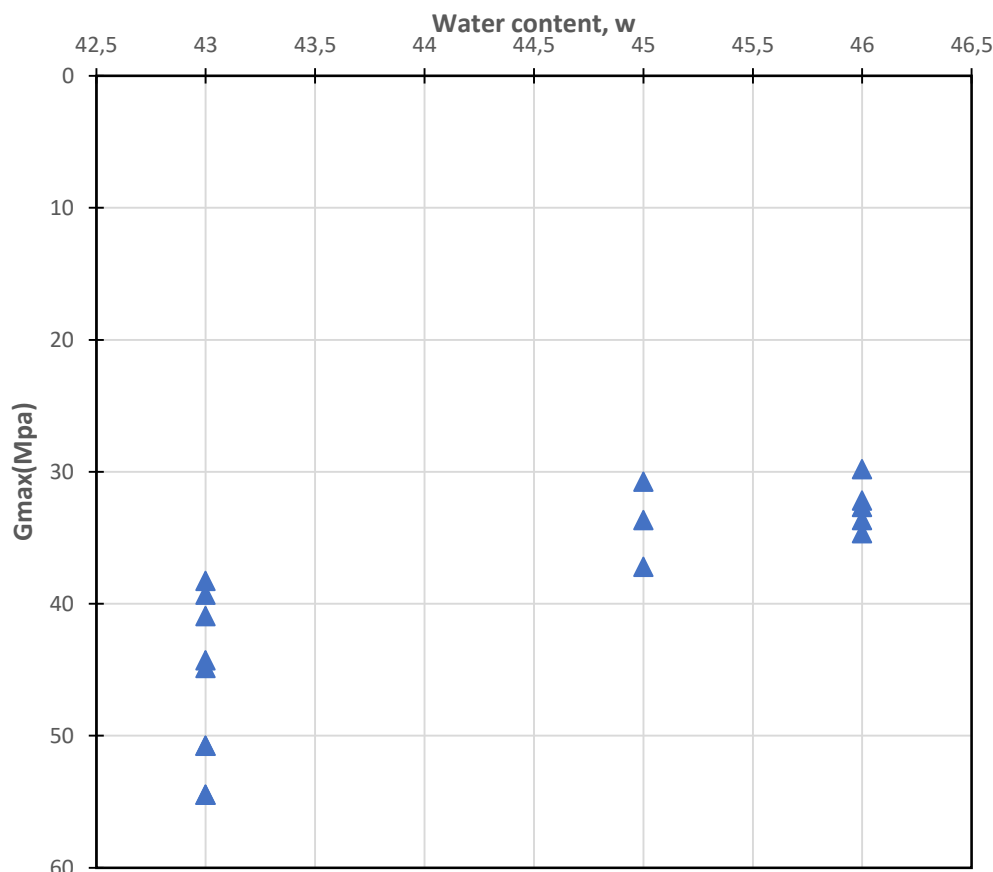
Figure 10.10: Variation of Maximum shear modulus, Gmax after 24-hour consolidation with water content, w

10.4 Plasticity index with respect to G_{max}

Figure 10.11 characterizes the variation of the plasticity index with G_{max}, and the increasing trend for G_{max} with decreasing plasticity was obtained. It is well recognized that plasticity increases G_{max} due to an increase in friction at contact point particle for coarse-grained material, leading to longer linear elastic part, as inter-particle contact force, roughness and friction are of profound effect when the determination of G_{max} for granular material. The effect of plasticity on G_{max} for fine-grained material like clay cannot be thoroughly interpreted with minimal data. Hardin (1978) stated that the influence of the plasticity index on G_{max} is highly dependent on OCR. However, other researches believed that the effect of the plasticity index on G_{max} would not seem to be verified confidently. Therefore, there would not seem to be a decisive conclusion regarding the effect of plasticity on G_{max} for clay.
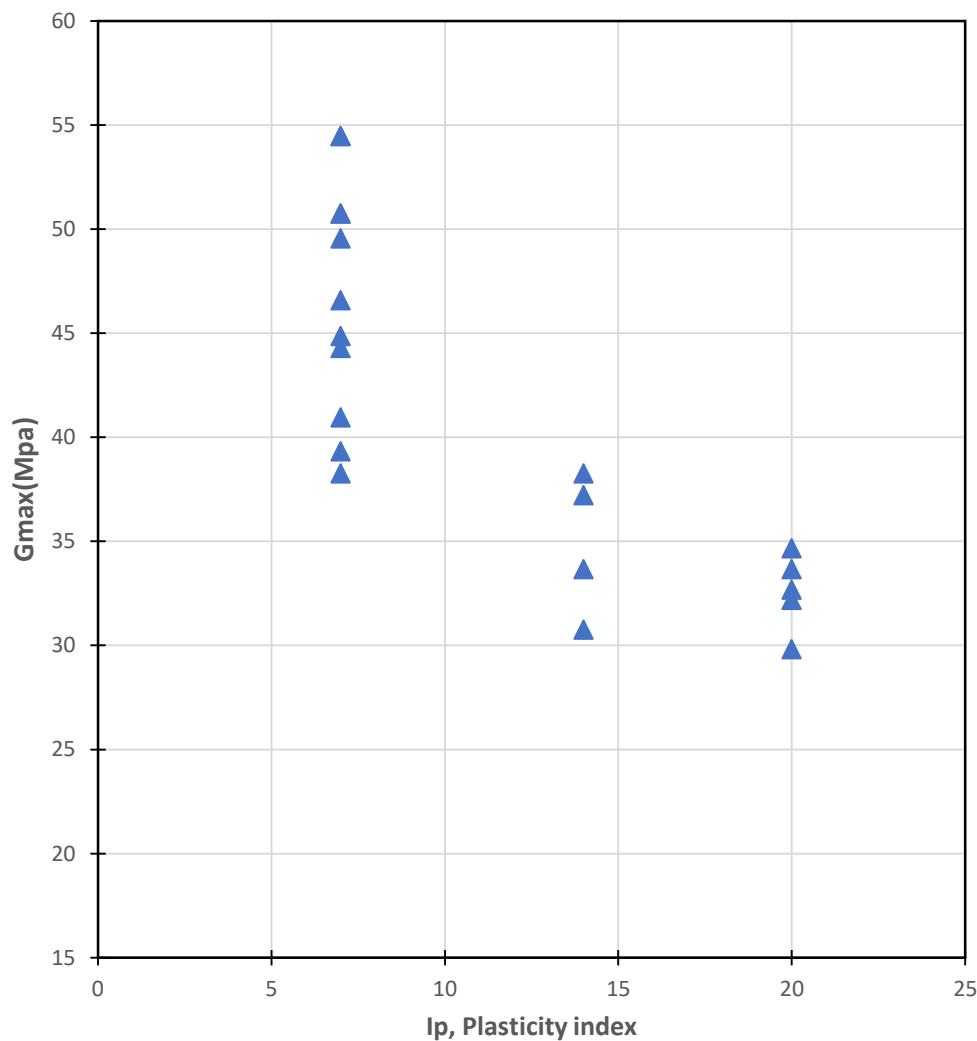
Figure 10.11: Variation of Maximum shear modulus, Gmax after 24-hour consolidation with Plasticity index, Ip

10.5 Comparison of the field and lab values of G_{max}

It would seem interesting to compare the discrepancy of the G_{max} value acquired from the field using Flotten data from L'Heureux et al. (2019) and the bender element indicated by the vertically-cut sample. The results revealed that approximately 33% increase of field measurement, since values falling above the line (Figure 10.12). There exist a large number of reasons which may account for this inconsistency of result. Note that soil under anisotropic stress conditions in the field is being consolidated under isotropic confining pressure (Maja, 2019). Moreover, unloading which occurs after extraction causes both substantial stress relief and loss of inter-particle bonding which leads to intricate retrieval process of the sample when reaching its in-situ stress condition. Cementation, creep, sample degradation, uncertainties associated with lab testing and frequency effect seem to be other factors that may enhance poor agreement between G_{max} from field and laboratory test. Nishimura et al. (2005), however, stated that the effect of sample disturbance, including transportation, storage, and manipulation during preparation does not seem to be significant. Moreover, the below hydrostatic condition of in-situ pore pressure based on the yearly average should not be neglected as one of the major reasons behind the higher value of field G_{max} as mentioned in chapter 7 (Maja, 2019).
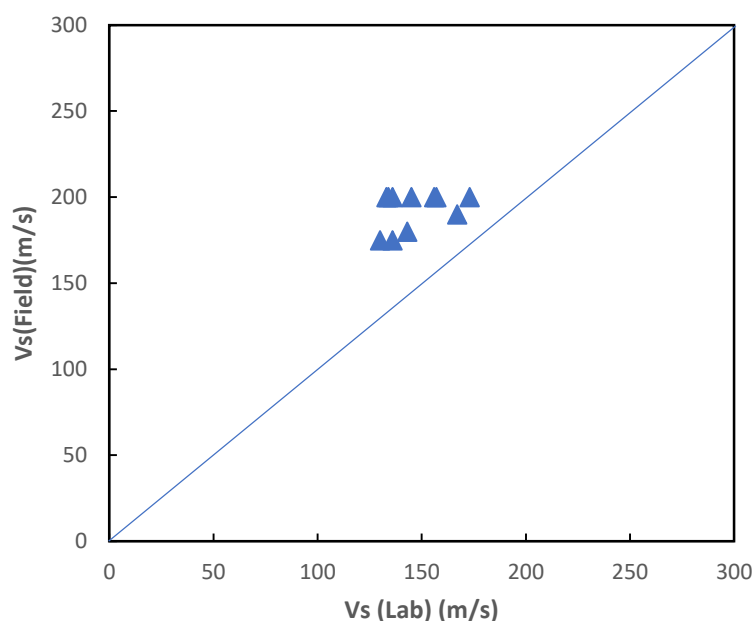
Figure 10.12: Comparison between shear wave velocity after 24-hour consolidation from Bender element test and field measurement

10.6 G~max~ In terms of aging Effect

NG value defined as a normalized shear modulus increase with time, can be employed to predict the increasing trend of G_{max} after primary consolidation caused by creep. To obtain an approximate estimate of G_{max} after primary consolidation (EOPC), equation (2.11) by Kokusho et al. (1982) can be utilized. The results presented in Table 10.1, indicate the higher development of G_{max} caused by creep is likely to occur for the sample with higher plasticity. As can be seen in Table 2.11 NG value does not seem to be significant for low-plasticity clay. Kim et al. (2014) suggested the below equation for G_{max} value after consolidation in addition to a period of creep.

$$G_{consolidation+creep} = G_{consolidation} * \left(1 + N_G \log\left(\frac{t}{t_{eop}}\right)\right) \tag{10.1}$$

where t_{eop} is a reference time indicating end-of-primary consolidation, G_{con} is the maximum shear modulus caused by primary consolidation, and t is the corresponding significant time before t_{eop} associated with ΔG.

Table 10.1: The effect of creep on Gmax

Sample no	Miniblock(1)	Bigblock	Miniblock(2) Fresh	Miniblock(3) Fresh	Miniblock(4) Fresh
NG	0,10	0,07	0,12	0,12	0,07
G0(after Consolidation and Creep)	1.1G0	1.07G0	1.12G0	1.12G0	1.07G0

The discrepancy between G_{max} after 24-hour consolidation and end of primary consolidation found to be approximately an average value of 5% for both big-block and mini-block samples. The results in Table 10.1 is observed to be slightly higher than the values inferred from the bender element. The longer consolidation time is expected to compensate somewhat for this discrepancy. G_{max} value after primary consolidation keeps its increasing trend gradually at a lower rate until reaching the peak at a roughly stable magnitude. Kim et al. (2014) suggested that the NG is not a constant value, as it tended to decrease with time, indicating the hypothesis of attributing discrepancy between filed and lab value to the aging process needs to be treated cautiously. There would be a large number of factors that may account for this discrepancy as mentioned before.

10.7 Influence of void ratio on G~max~

The void ratio is undoubtedly the most influential parameter which affects G_{max} substantially. Based on the comparison between two functions, there seems to be good agreement between empirical Equation 2.5 by Donohue and Long (2010) and L'Heureux et al. (2013) taking n=0,25, $F(e) = 1/e^{1.3}$, and test results. $F(e) = 1/e^{1.3}$ is meant to be the best void ratio function fit for Norwegian sensitive clay in Figure 10.13. Investigation of the effect of void ratio variation on G_{max} was carried out and it was observed with decreasing void ratio (e), G_{max} increases depending on the magnitude of average confining pressure. It was found at the mean effective stress of 50 Kpa, when the void ratio decreases from 1.3 to 1.2, G_{max} experienced an increase of approximately 5Mpa, from 35Mpa to 40Mpa. Note that the rate of G_{max} variation is higher for the region with lower void ratio and a high amount of average effective stress simultaneously. The increasing trend, however, seems to be more moderate for F(e)=1/e^1.3 than $F(e) = \frac{(2.97-e)^2}{1+e}$ function. The blue and orange marks showing G_{max} value for 50Kpa and 100Kpa consolidation stress respectively. The green marks representing G_{max} value for 75Kpa average confining pressure which falls between 50Kpa and 100 Kpa consolidation pressure. Thus, the results represent a strong dependency of the G_{max} with respect to void ratio variation.
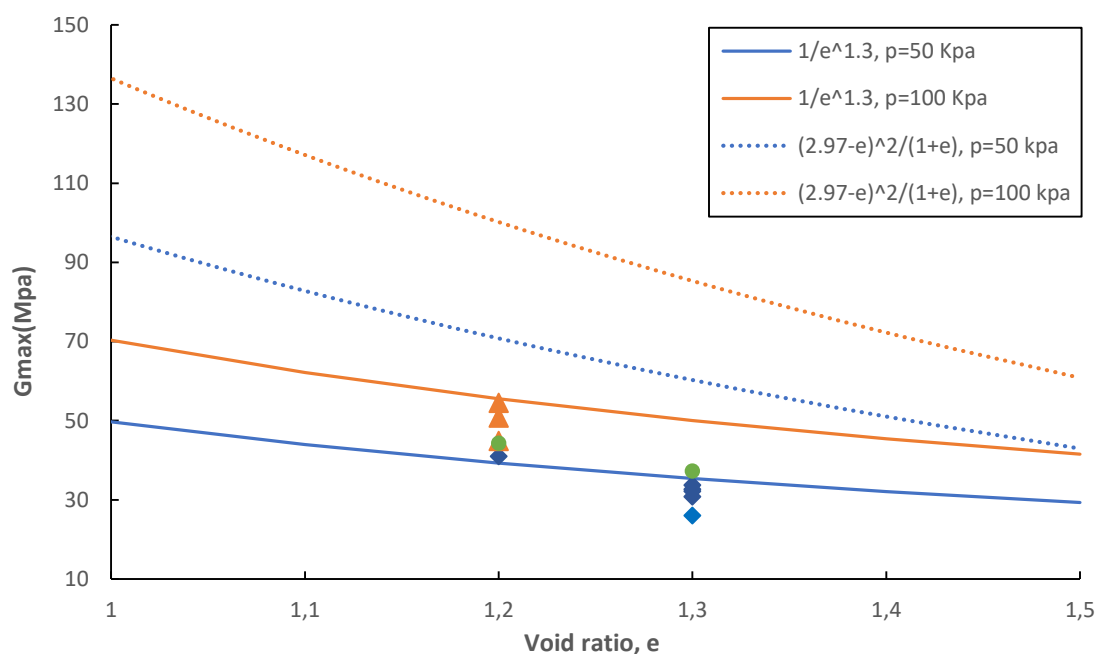
Figure 10.13: Illustration of variation of Gmax after 24-hour consolidation with void ratio(e) at corresponding consolidation stress

10.8 Small-Strain Stiffness Anisotropy

The analytical study of stiffness anisotropy of clay is of vital significance in many engineering geotechnical aspects. The detrimental effect of inherent anisotropy on wall deflection in deep excavation and settlement in tunneling, for example, are particularly two salient examples of these which make it necessary to examine anisotropy behavior of Norwegian quick clay more accurately. For this purpose, the thin and platy morphology of clay should be taken into consideration when resulting from the vertical depositional process. Tonje et al. (2019) denoted that clay minerals in the marine conditions are of flocculated particles open structure similar to the plate, a large number of voids filled with water, and high electrochemical activity with the existence of horizontal bedding plane. Layering characteristics of clay mineral undoubtedly play a crucial contribution to the anisotropy behavior of clay. In this way, Bao et al. (2018) found that the orientation of the bedding plane has a profound effect on G_{max} evaluation and the corresponding degree of stiffness anisotropy along with hydraulically-induced anisotropy.
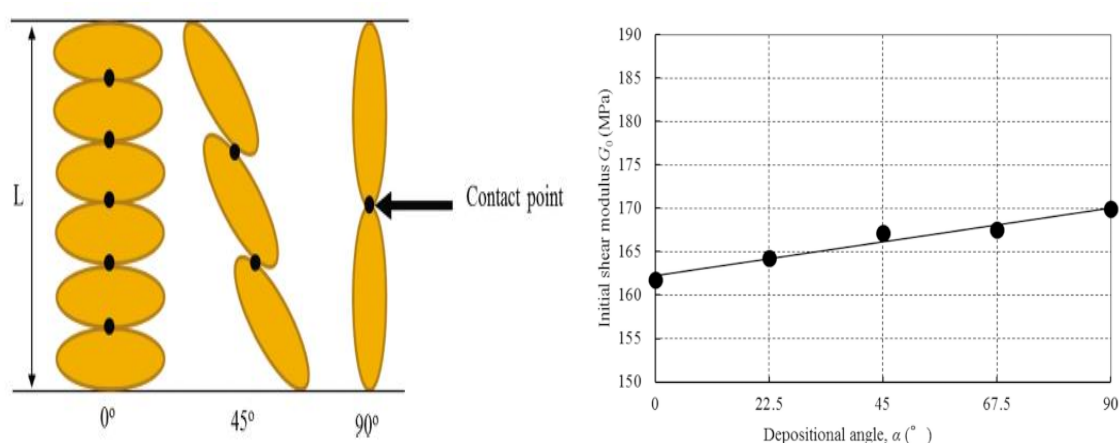
Figure 10.14: Effect of depositional angle on Gmax (Bao et al., 2018)

As can be seen in Figure 10.14 G_{max} increases with increasing depositional angle which indicates G_{max} would be higher in the horizontal direction than vertical one caused by reduction of inter-particle contact point acting as a discontinuity surface. Meanwhile, the rate of water expulsion is expected to be higher when the depositional angle is equal to 90 degrees.

Furthermore, the variation of consolidation pressure with fabric anisotropy is a matter of kind of soil. Thus, inherent anisotropy is well-known to be also highly dependent on particle orientation and aspect ratio during the depositional process (Wang et al., 2007), while stress-induced anisotropy corresponds to in-situ stress state, K_0 value, and particle contact force

(Landon et al., 2007). The ratio of horizontal and vertical G_{max} can be represented as stiffness anisotropy at specific stress conditions.

$$\frac{G_{hh}}{G_{vh}} = \frac{S_{hh}F(e)(OCR)^K P_a^{(1-2nh)}(\sigma_h')^{2nh}}{S_{vh}F(e)(OCR)^K P_a^{(1-nv-nh)}(\sigma_v')^{nv}(\sigma_h')^{nh}} \tag{10.2}$$

Where the double subscript indicates the direction of wave propagation followed by the direction of wave polarization, S is a material stiffness constant in the vertical (S_{vh}) or horizontal (S_{hh}) directions, F(e) is an empirical void ratio function, OCR is over-consolidation ratio, k is an empirical constant proportional to clay plasticity index, p_r is a reference stress (1 atm) nv and nh are vertical and horizontal empirical stress exponents, and σ_v' and σ_h' are effective stresses in the vertical and horizontal directions. When changing from in-situ anisotropic stress condition to isotropic consolidation of sample with the same confining pressure at different orientations, the ratio of can be expressed as:

$$\frac{G_{hh}}{G_{vh}} = \frac{S_{hh}}{S_{vh}} \tag{10.3}$$

This ratio referred to as Stress-dependent inherent anisotropy which takes the effect of inherent anisotropy when applying the same stress condition concerning sample orientation. Needless to say, measurement of G_{max} values in the lab is believed to be affected by the loss of residual effective stress (pore water suction) caused by sampling practice or a period of storage time regardless of other contributing factors when replacing stress conditions with residual effective stress. Landon et al. (2007) applied this factor by representing the below equation.

$$\frac{G_{hh}}{G_{vh}} = \frac{S_{hh}F(e)p_r^{0.5}(\sigma_r')^{0.5}}{S_{vh}F(e)P_r^{0.5}(\sigma_r')^{0.5}} \tag{10.4}$$

Where σ_r' is isotropic residual effective stress. This ratio is known as suction-induced anisotropy, since the dissipation of residual effective stress does not occur at a constant rate, and uniformly after extraction. For the samples with identical residual effective stress the inherent anisotropy ratio appears as below equation:

$$\frac{G_{hh}}{G_{vh}} = \frac{S_{hh}}{S_{vh}} \tag{10.5}$$

This ratio can be recognized as suction-dependent inherent anisotropy which would seem independent of suction when it comes to identical residual effective stress. Even though stress term has canceled out in this equation, but Li (2003) and Mui (2005) expressed that anisotropy

increases while inducing isotropic suction to the sample. This increasing trend, however, is not believed to be significant at suction higher than the air-entry value for unsaturated soil (Ng et al., 2008). In principle, the suction dependent inherent anisotropy might be the most likely cause of the discrepancy between the degree of fabric anisotropy from experimental testing and in-situ measurement.

In this research, the anisotropy investigation has been carried out using corresponding K0 value which can be inferred from the dilatometer in-situ test but subjecting to the isotropic confining pressure to obtain the more realistic value of anisotropy ratio. Due to limitations in the number of the horizontal specimen, it was not possible to assess anisotropy at numerous consolidation pressures.

<div align="center">(a)   (b)</div>
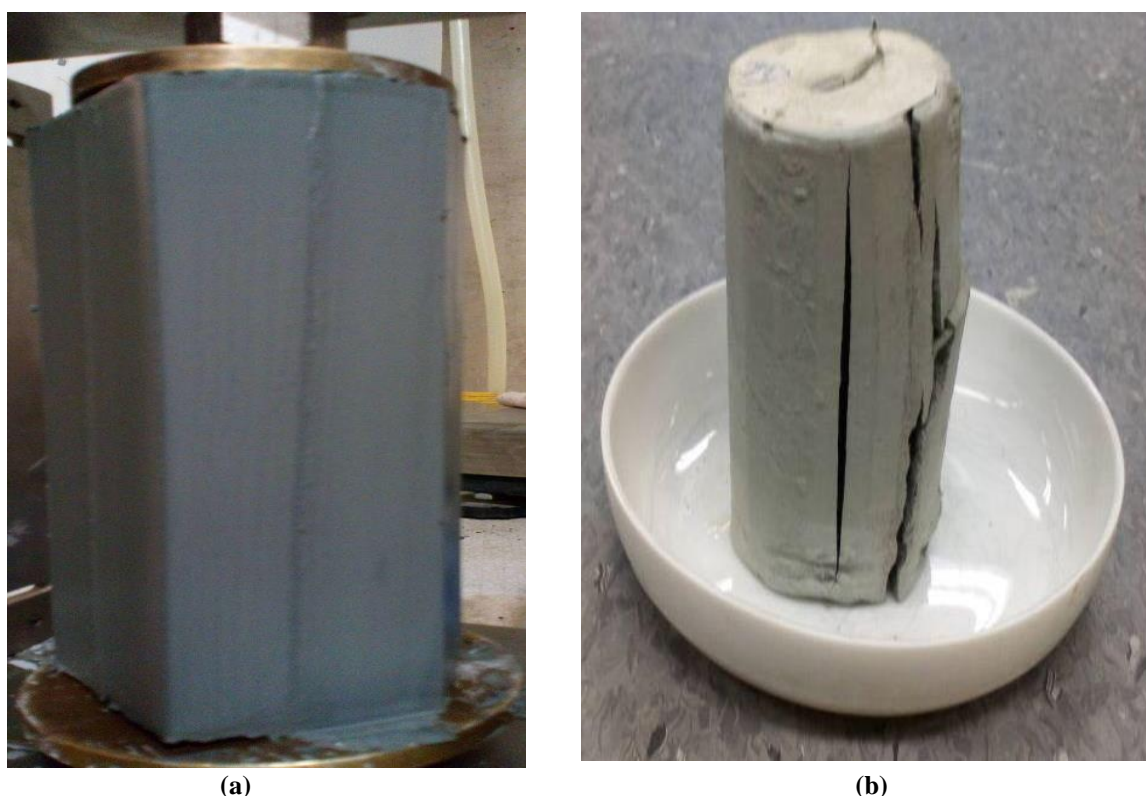
Figure 10.15: (a): Orientation of bedding plane for horizontally-cut specimen during trimming specimen (b): Exposure of any possible fissures or small-scale discontinuities caused by BE oscillation during consolidation after drying

Anisotropy investigation for the sample from a great depth or when applying high confining pressure calls for having alternative bender elements at horizontal orientation mid-height of the sample. Due to issues related to the bedding plane causing moving along the bedding plane which mainly emerges from the weak electrostatic bond between layers than within the layers,

and consequently samples disturbance or failure might occur as can be seen in Figure 10.15 for the horizontally-cut specimen. The influence of the bedding plane and particle shape anisotropy formed during the depositional process can explain the failure mode of the specimen subjected to bender element oscillation parallel to the bedding plane. The anisotropy behavior of clay can also be perceived in micro and macro-structure properties of clay, including chemical composition, particle bond at a different orientation, lamination, varved clay, pore geometry in addition to unknown geological effects, cementation and creep among others. In principle, the variation of silt content with depth reduces accuracy in the determination of anisotropy ratio, since it affects hydraulic conductivity, suction-induced anisotropy, grain contact force. The cross-anisotropy characteristics of clay have been investigated in Figure 10.16. It was found this property cannot be thoroughly supported by lab testing. The average value, however, seems to verify somewhat these features for both fresh and old samples.
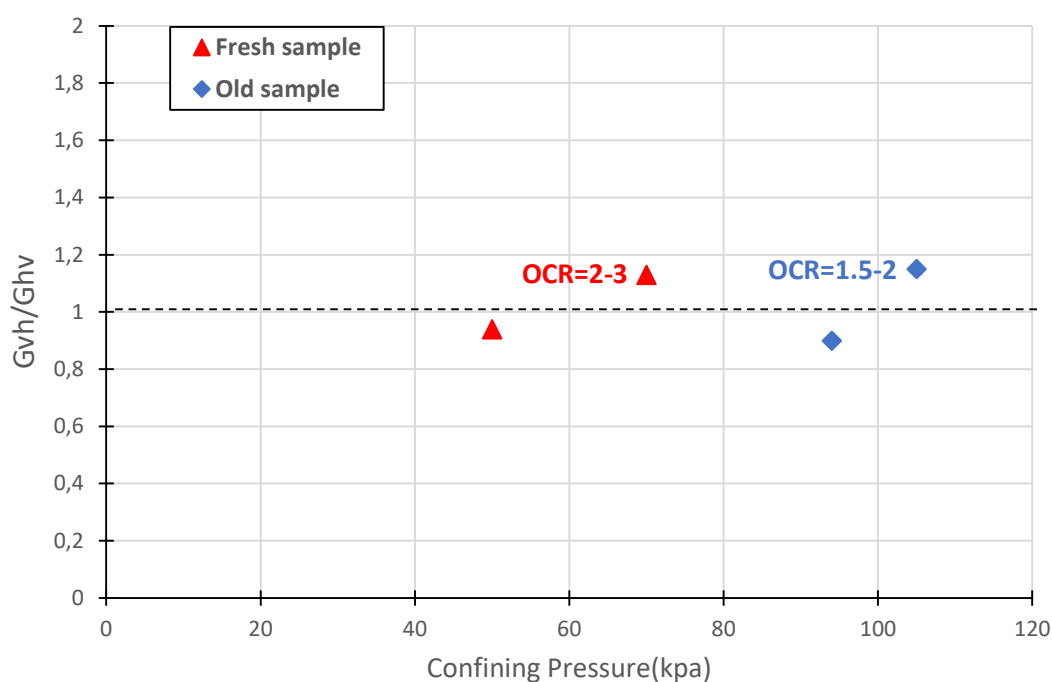
Figure 10.16: Illustration of cross-anisotropy ratio (EOPC) with isotropic confining pressure

The degree of fabric-induced anisotropy is meant to be controlled by soil particle configuration, orientation, morphology, and bonding established by induced stress or suction. It is anticipated that the degree of fabric-induced anisotropy increases with increasing average confining pressure until it contributes to grain contact bonding, along with a higher rate of void ratio reduction (Figure 10.17).

Moreover, fabric-induced anisotropy was observed to be higher (1.38) for fresh sample compared to old sample (1.22) from surface level (Figure 10.18 and 10.19) which might be attributed to its capability to regain its initial particle arrangement state during the retrieval consolidation process possibly caused by higher over-consolidation ratio. The existence of higher potential suction would be another reason for the higher anisotropy ratio for the fresh sample in some cases. Conversely, the lower value of fabric-induced anisotropy for the old sample might be due to the reduction of OCR, loss of mechanical properties, and RES caused by long storage time. Needless to say, the amount of data is substantially minimal to obtain a more reliable estimate. Given clay mineral, Hori et al. (2006) found that fabric-induced anisotropy ratio increases with increasing clay content and mineral.
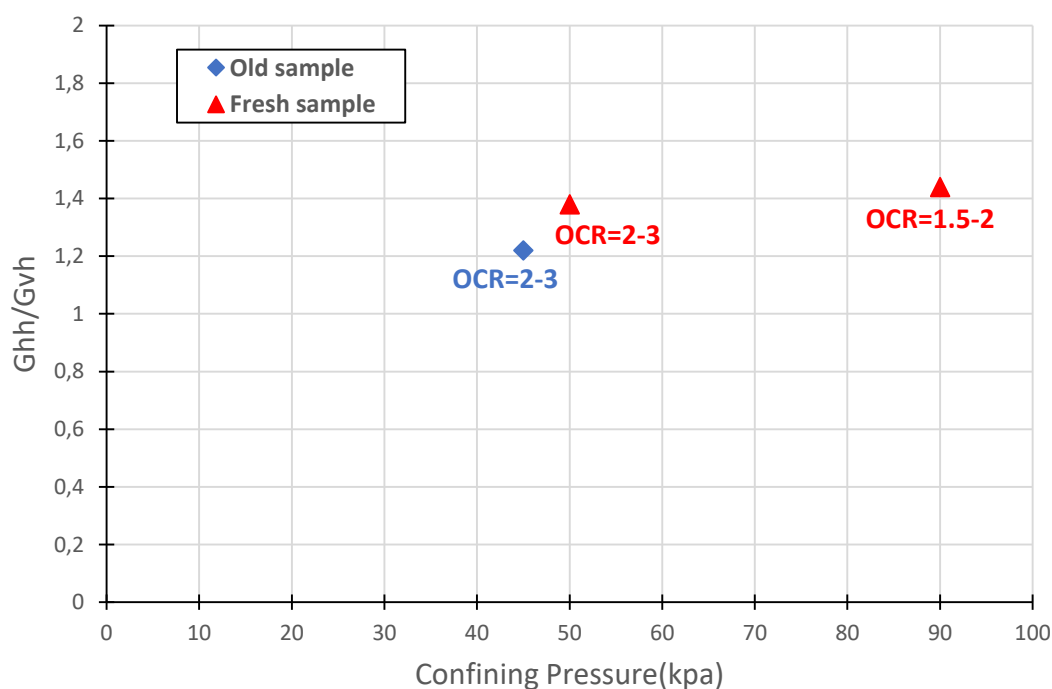
Figure 10.17: Illustration of fabric anisotropy ratio (EOPC) with isotropic confining pressure
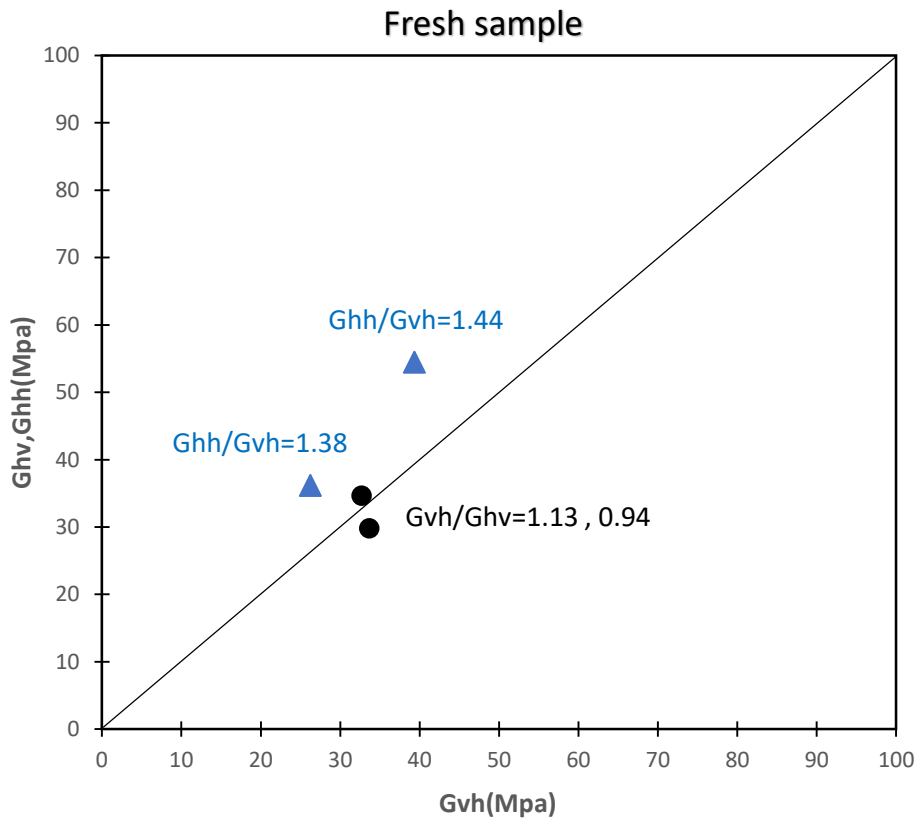
Figure 10.18: Relation of Gvh, Ghv and Ghh (EOPC) for Fresh sample
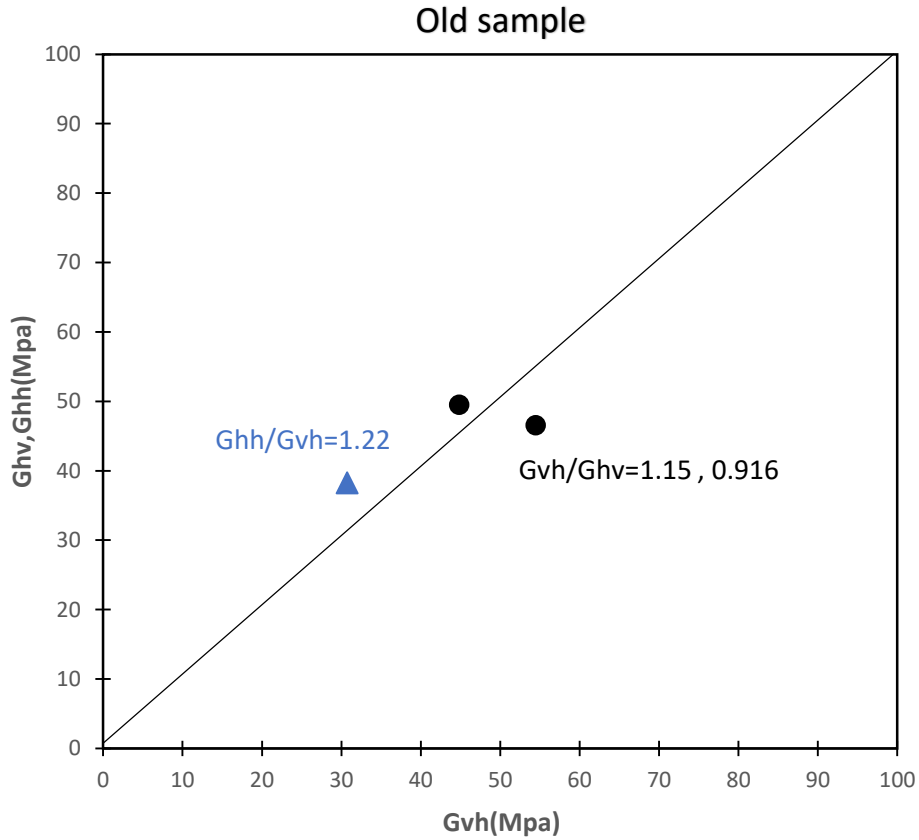
Figure 10.19: Relation of Gvh, Ghv and Ghh (EOPC) for Old sample

10.9 Comparison of G_{max} with Previous Relevant Study

In this section, the comparison between the results at the end of primary consolidation (EOPC) from the previously conducted bender element testing for Norwegian quick clay from Flotten NGTS by Beeston (2018) and Maja (2019) with those inferred in this study (EOPC) have been carried out (Figure 10.20 until 10.22). There is a good correlation between results from Maja (2019) and Beeston (2018). Likewise, the discrepancy would seem to be noticeable at low confining pressure between values from this study and previous laboratory exercise, and in particular, for big-block. This might be due to the fact that low confining pressure is more sensitive to sample quality. The results from mini-block samples, however, approach relatively at high mean effective stress. The soil degree of variability, quality of applied samples, test setup, and more importantly applied input frequency might be the most plausible causes of this inconsistency of results. Note that conventional sample quality assessment based on water expulsion and void ratio change may not provide a comprehensive basis for the micro-structural disturbance in many cases. Moreover, in-situ anisotropic stress conditions do not correspond to the lab isotropically-consolidated samples accurately which means that measured water expulsion might not be reliable and accurate in this method (Maja, 2019). The various K0 value applied in this research can also contribute to higher shear wave velocity and associated stiffness at the small-strain range.
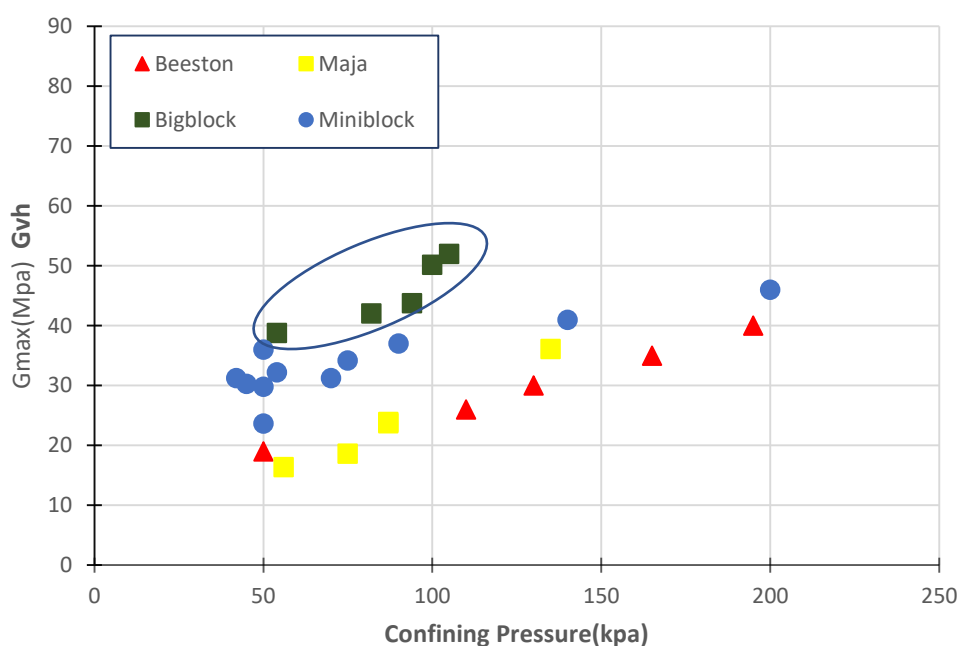
Figure 10.20: Comparison of Gvh, vertical maximum shear modulus (EOPC) with previous measured laboratory values for Flotten NGTS quick Clay
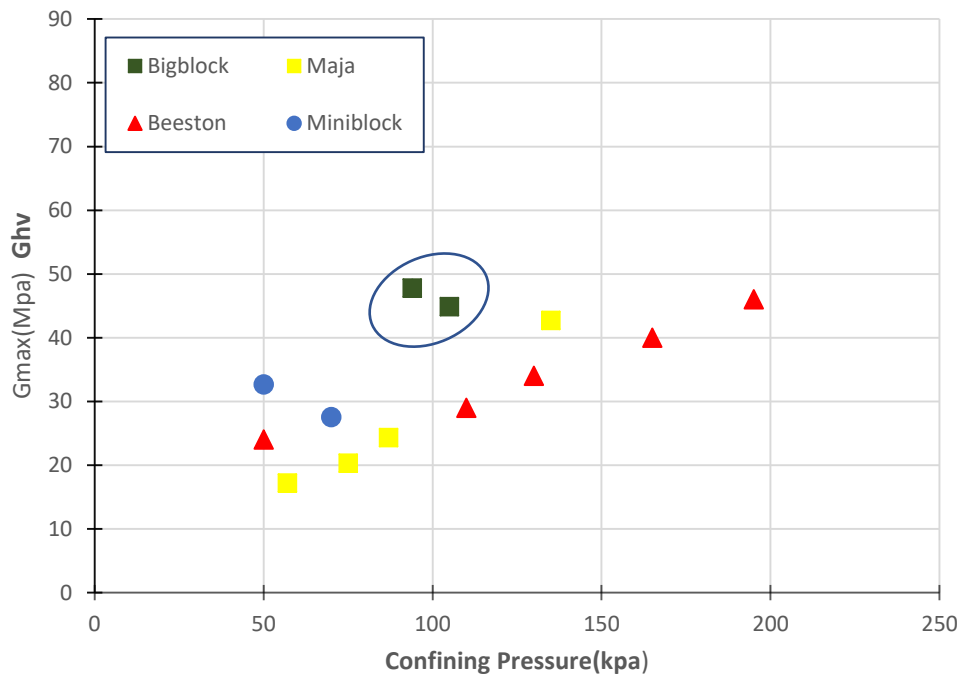
Figure 10.21: Comparison of Ghv, horizontal maximum shear modulus (EOPC) with previous measured laboratory values for Flotten NGTS quick Clay
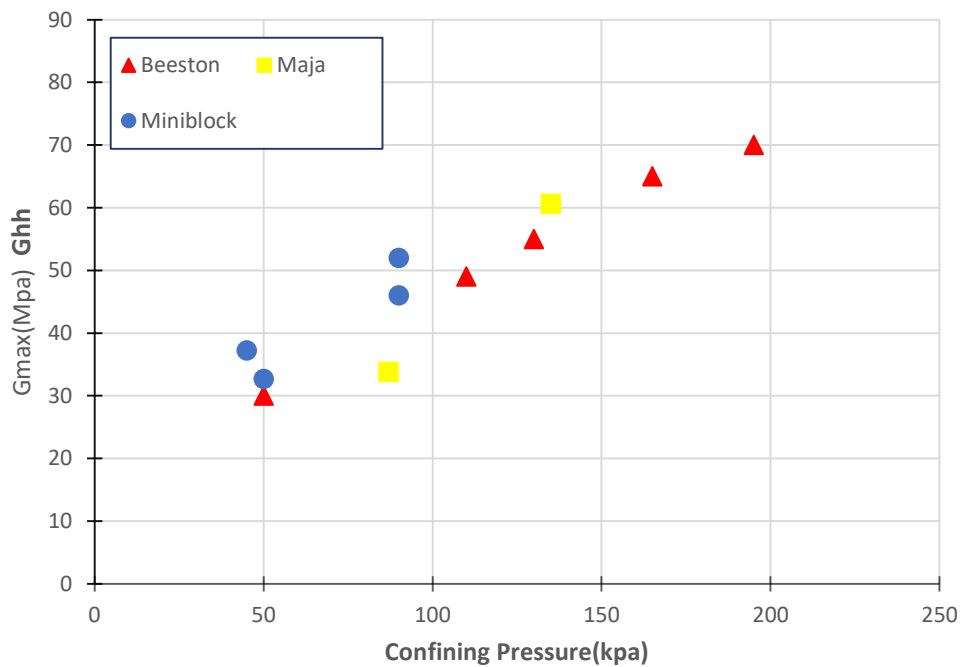
Figure 10.22: Comparison of Ghh, horizontal maximum shear modulus (EOPC) with previous measured laboratory values for Flotten NGTS quick Clay
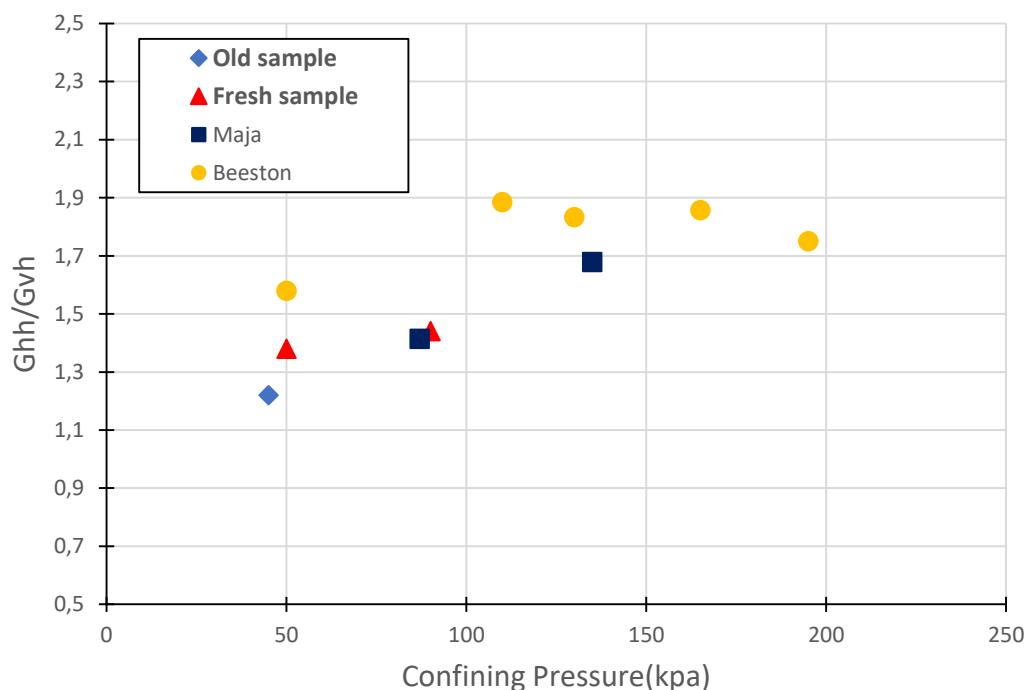
Figure 10.23: Comparison of measured Inherent anisotropy (EOPC) with previous measured laboratory values for Flotten NGTS quick Clay

The investigation was followed by comparing the measured degree of fabric anisotropy (Figure 10.23) obtained by other researchers. The inherent stiffness anisotropy ratios at small-strain ranged between 1.22 and 1.88 which is deemed to be significant for Norwegian quick clay. The experimental results from Beeston (2018), however, seem to overestimate more or less the degree of fabric-anisotropy. As can be seen, the degree of inherent anisotropy is closely dependent on stress level, representing the increasing trend with raising consolidation stress at the corresponding depth. In addition, the OCR is thought to affect the stiffness anisotropy at small-strain. Large scatter was found for samples taken from surface level subjected to low consolidation stress. This can be described by the higher OCR for the fresh sample taken from surface level and old samples experiencing high potential OCR reduction. This phenomenon undoubtedly characterizes the devastating effect of long storage on the mechanical properties of clay as a whole, including the reduction of OCR, loss of structure, stiffness, and RES (Amundsen et al., 2016).

Chapter 11

Summary and recommendations for further work

11.1 Conclusion

The main emphasis of this research was on laboratory investigation of the small-strain shear modulus of the Flotten clay at a Norwegian geotechnical test site near Tiller, Trondheim. Besides, incorporation of anisotropy behavior of clay into numerical modeling can improve the accuracy of the result and make it more realistic. For this purpose, the presence of stiffness anisotropy, including fabric or stress-induced anisotropy was intended to be addressed as well. It would seem interesting to evaluate the effect of size of block-sample and storage time on G_{max} and stiffness anisotropy to correspond to the quality of the sample, how it is possible to evaluate the extent of sample degradation using shear wave velocity measurement, to overcome this issue and minimize the disturbing effect.

The bender element test was performed using mini-block, big-block for both fresh and old samples at the different orientations of samples. The measurement was carried out under unconfined and during 24-hour consolidation. Index parameters were also determined for each block sample to correlate with G_{max}, and quantify parameters influencing G_{max}. While the results fit well with the void ratio as the most dominating index parameter at corresponding stress level. The contribution of water content, plasticity index, stress state, was also entirely investigated. The comparison between field and lab results was drawn, and the main causes of discrepancy was identified.

The samples taken from the greater depth with lower void ratio, experienced a higher increasing trend of G_{max} and corresponding stiffness during primary consolidation when subjected to high-stress level. This might be the reason why samples from greater depth would not be representative and reliable in many cases since they are more sensitive to sample disturbance during the retrieval consolidation process.

Sample quality assessment was carried out in this study based on the two techniques, such as change in volumetric strain indicated by Andresen et al. (1979), change in the void ratio indicated by Lunne et al. (2006) and it was concluded most of the samples exhibited acceptable good quality.

There is a high degree of uncertainty to evaluate the effect of type of sample on the soil mechanical properties, and sample quality as a whole. For this purpose, the relationship between G_{max} and average confining pressure was examined for a different kind of sample at various stress levels. Normalizing G_{max} with $F(e)$ function also enabled to assess sample quality properly. It was, therefore, concluded that the shear wave velocity increases at a decreasing rate, as the soil becomes densified. The big-block represented higher shear wave velocity (150m/s≤$V_{s(vh)}$≤173m/s), while the fresh mini-block from surface defined as a carefully extracted, transported stored under appropriate conditions, and tested a couple of days after the extraction, experienced a moderate non-linear increase of G_{max} in terms of increasing mean effective stress (120 m/s≤$V_{s(vh)}$ ≤164 m/s). While both of the samples reached the maximum value of $V_{s(vh)}$ approximately 195 m/s after normalizing with $\sqrt{F(e)}$, the low rate of increase in $V_{s(vh)}$ with various mean confining pressure for big-block would be representative of the high-quality sample resulting from stronger inter-particle bonding, and its original fabric and structure.

In terms of the effect of aging on G_{max} degradation, the results from two mini-block samples taken from approximately the same depth also directly compared to evaluate the effect of long-term storage on shear wave velocity, and corresponding G_{max}. The higher scatter of results was acquired for mini-block with long storage time (more than one year). However, no substantial degradation of G_{max} observed for specimens trimmed from the same mini-block tested after a couple of days and that of tested approximately after three months of storage under suitable conditions. Thus, the fulfillment of storage standards and procedures, involving humidity, temperature, wrapping, and sealing conditions will certainty prevent degradation of G_{max} to a great extent caused by short-term aging.

It is well-recognized Tiller-Flotten quick clay is inherently anisotropic ranged roughly between 1.22 and 1.44, and stress-dependent, increasing trend with increasing stress level, which can be attributed to the arrangement of clay particles to multi-aggregated model (Wang et al., 2007). In other words, the degree of fabric-anisotropy increases during the consolidation process prior to reaching a relatively stable level. The presence of small-scale inhomogeneity (varved clay, silt content) may account for a high degree of variability and uncertainty in this case which sheds light on different layering characteristics with respect to specimen orientation. In general, various clay content, mineral and laminations, and bedding plane orientation seem to be one of the most plausible causes of the inherent anisotropy behavior of Tiller-Flotten quick clay.

The degree of fabric-anisotropy was found to be higher for the fresh sample than the aged sample with long storage time, while both taken from the same depth and in-situ stress level. This can be most primarily described by anisotropy structure of low-plasticity marine clay with high OCR caused by proper alignment of plate-like clay particles. The discrepancy of the degree of fabric-anisotropy between aged and fresh samples is believed to be related to the reduction of OCR, destruction of soil mechanical properties caused by long storage time for the old mini-block sample which is likely to be pronounced by potential chemical alteration or loss of RES.

The cross-anisotropy characteristic of the quick clay would not seem to be supported in the lab testing. The average value of the test results, however, verify this property of Flotten clay to a great extent. Besides, Pennington et al. (1997) indicated that V_{hv} would be greater than V_{vh} since the hv wave traveling along with the bottom stiffer layer, while V_{vh} passes through different layers. Apart from the existence of inhomogeneity in clay, nevertheless, Tiller-Flotten quick clay is of varved and laminated structure with a variation of water content and stiffness as a whole at different layers which contributes to shear wave velocity and therefore in some cases, the value of V_{hv} might be higher than V_{vh} based on the test results. What is more, the orientation of the bedding plane formed during the depositional process with regard to the bender element plays a crucial role in the cross-anisotropy determination. In principle, the cross-anisotropy characteristics of clay should be taken into meticulous consideration.

Not surprisingly, the appropriate adjustment of the orientation of the bedding plane concerning the bender element is of crucial significance when it comes to finding an accurate value of G_{hv}, G_{hh}, and consequently the degree of anisotropy, reflecting the contribution of depositional angle to the degree of stiffness anisotropy.

Quality of received signal plays a vital role to obtain a satisfactory result of challenging travel time and corresponding shear wave velocity. Appropriate detection of input frequency and input signal amplitude to avoid unwanted noise seems to be essential. Moreover, the overestimation caused by near-field does not seem to be substantial at the end of consolidation. The near-field effect, however, tended to decay when d/λ higher than approximately 1.2 when approaching the end of consolidation, with the reduction of wavelength between transmitter and receiver bender element. More importantly, as the soil became densified during the test, the frequency of the input signal was set to increase to adapt to the resonance frequency of the bender element to obtain a reliable measurement of G_{max} as well as to reduce near-field effect

simultaneously. In this research, the application of input frequency higher than 3KHz would not seem to be necessary.

Previously conducted bender element testing represents relatively lower values, particularly at low confining pressure. This might be most primarily due to soil variability, different applied frequency of input signal, sample quality, test errors, and various K0 values which may account for a high degree of uncertainty, especially at the low-stress level.

11.2 Further work

Indeed, it is obvious that advanced bender element apparatus is required to eliminate errors and the degree of uncertainty associated with this test and to improve the quality of the received signal as well. Furthermore, the development of signal processing and data interpretation would make the test 's results more reliable. It is well-known that sample disturbance, sampling procedures are devastating effects regarding the bender element test. It is crucial to realize how to minimize the effect of the sampling process on test results.

Since both Clay content and mineralogical composition are the most important parameters which significantly contribute to the clay degree of anisotropy it is suggested to take the effect of clay s' content characteristics into meticulous consideration. The numerical modeling of the depositional process with the variation of soil layering, grain size, shape, orientation in addition to clay content, and mineral can quantify parameters that have a profound effect on clay stiffness and anisotropy at the small strain.

It is preferable to perform an anisotropy study by the bender element at mid-height, top, and bottom of the specimen simultaneously than taking a horizontal specimen from block sample which makes interpretation more realistic, and to adapt the consolidation stress to in-situ stress conditions more importantly. It is mainly due to the bedding plane or lamination, discontinuity surface will be placed at the long dimension of the sample when cutting specimen horizontally, which results in a likely movement along these surfaces, and in consequence adversely affects the soil behavior during the retrieval consolidation process, back to its in-situ stress condition. There will be an also higher possibility of sample disturbance, fissure and fracture, and potential damage when imposing high-stress levels along the bedding plane which is likely to

be pronounced by the oscillation of the bender element parallel with orientation of bedding plane.

The study of anisotropy and cross-anisotropy concept of quick-clay is highly dependent on parameters that are substantially susceptible to disturbance, and even with taking all contributing factors into account, it would seem reasonably challenging to obtain value representative of field anisotropy. Higher accuracy of this investigation calls for state-of-the-art either lab or field equipment and technique.

Complementary promising sample quality assessment criteria are required to obtain a deep insight into soil alteration, loss of structure during sampling, including the image or microstructural analysis. Moreover, the evaluation of likely chemical and biological change of the sample should not be neglected.

It is worthwhile to measure shear wave velocity at all stages of sampling from extraction until testing in the lab to recognize factors influencing sample quality and stages at which the largest sample disturbance occurs more precisely and reliably.

References

Amundsen, H. A., Thakur, V., & Emdal, A. (2016). Sample disturbances in block samples on low plastic soft clays. Proceedings of the 17th Nordic Geotechnical Meeting. Reykjavik.

Amundsen, H. A., Jønland. J, Emdal, A, & Thakur, V. (2017). An attempt to monitor pore pressure changes in a block sample during and after sampling. Géotechnique Letters 7

Anderson, D. G., & Stokoe, K. H. (1978). Shear Modulus: A Time-Dependent Soil Property. Dynamic Geotechnical Testing, 66-90. doi:10.1520/STP35672S

Andresen, A., & Kolstad, P. (1979). The NGI 54 mm samplers for undisturbed sampling of clays and representative sampling of coarser materials. Proceedings of the International Symposium on Soil Sampling.

Arroyo, M., Muir Wood, D., & Greening, P. D. (2003). Source near-field effects and pulse tests in soil samples. Géotechnique, 53(3), 337-345. doi:10.1680/geot.2003.53.3.337

Arulnathan, R., Boulanger, R. W., & Riemer, M. F. (1998). Analysis of Bender Element Tests. Geotechnical Testing Journal, 21(2), 120-131. doi:10.1520/GTJ10750J

ASTM. (2014). Standard test methods for cross-hole seismic testing. ASTM D4428/D4428M-14, West Conshohocken, PA.

ASTM. (2014). Standard test methods for down-hole seismic testing. ASTM D7400-14, West Conshohocken, PA.

Bao Ngoc Le, Hirofumi Toyota, and Susumu Takada. Detection of Elastic Region Varied by Inherent Anisotropy of Reconstituted Toyoura Sand (2018). Engineering Geology and Geological Engineering for Sustainable. DOI 10.1007/978-3-319-61648-3_5

Beeston, A. (2018). A study of the Dynamic Properties of Quick Clay from Flotten NGTS. Master's thesis, NTNU, Trondheim, Norway.

Benz, T. (2007). Small-strain stiffness of soils and its numerical consequences. Univ. Stuttgart, Inst. f. Geotechnik.

Benz, T., Schwab, R., & Vermeer, P. (2009). Small-strain stiffness in geotechnical analyses. Bautechnik Special issue - Geotechnical Engineering, 16-27. doi:10.1002/bate.200910038

Berre, T., & Bjerrum, L. (1973). Shear strength of normally consolidated clays. Proc. 8th ICSMFE, (ss. 39-49). Moscow.

Biot MA, Theory of propagation of elastic waves in a fluid-saturated porous solid. Low frequency range. J Acoust Soc Am1956;28(2):168–78.

Biot MA, Theory of propagation of elastic waves in a fluid-saturated porous solid. Higher frequency range. J Acoust Soc Am1956;28(2):179-91.

Blewett, J., Blewett, I. J., & Woodward, P. K. (2000). Phase and amplitude responses associated with the measurement of shear-wave velocity in sand by bender elements. Canadian Geotechnical Journal, 37(6), 1348-1357. doi:10.1139/t00-047

Brignoli, E. G., Gotti, M., & Stokoe, K. H. (1996). Measurement of Shear Waves in Laboratory Specimens by Means of Piezoelectric Transducers. Geotechnical Testing Journal, 19(4), 384-397.

Brosse. A_, Hosseini. Kamal. R , JARDINE.R.J & M. R. COOP. (2017). The shear stiffness characteristics of four Eocene-to-Jurassic UK stiff clays. Géotechnique 67, No. 3, 242–259.

Camacho-Tauta, J. F., Alvarez, J. D., & Reyes-Ortiz, O. (2012). A procedure to calibrate and perform the bender element test. Dyna, 79(176), 10-18.

Campanella, R.G., Robertson, P.K., and Gillespie, D. (1986). Seismic cone penetration test. Use of in situ tests in geotechnical engineering, Proceedings, In Situ '86, ASCE. Geotechnical Specialty Publication No. 6, Samuel P. Clemence (ed.), Balcksburg, VA, June, pp. 116-130.

Cercato, M. (2009). Addressing non-uniqueness in linearized multichannel surface wave inversion. Geophys. Prospect., 57(1), 27–47.

Chan chee-Ming (2010). Bender Element Test in Soil Specimens: Identifying the Shear Wave Arrival Time. Universiti Tun Hussein Onn, Malaysia.

Clayton, C. (2011). "Stiffness at small strain: research and practice." Géotechnique, 61(1), pp.5-37.

Clayton, C., Theron, M. and Best, A. (2004). The measurement of vertical shear-wave velocity using side-mounted bender elements in the triaxial apparatus. Géotechnique, 54(7), pp. 495-498.

Clayton, C., Mathews, M.C. and Simons. N.E. (1995). "Site Investigation." 2nd Edition, Department of Civil Engineering, University of Surrey.

Comina, C., Foti, S. Musso, G. and Romero, E. (2008). EIT Oedometer: An advanced cell to monitor spatial and time variability in soil with electrical and seismic measurements. Geotechnical Testing Journal, 31(5): pp. 1-9.

Connolly, T. and Kuwano, J. (1999). Shear stiffness anisotropy measured by multidirectional bender element transducers. Pre-failure Deformation Characteristics of Geomaterials: Proc, of 2nd International Symposium on Pre-Failure Deformation Characteristics of Geomaterials: Torino 99: Torino, Italy 28-30 September, 1999, Vol. 1: 205 CRC Press

D.C.F.Lo Presti and M.Jamiolkowski (1998). Discussion: Estimate of elastic shear modulus in Holocene soil deposits. Soil and Foundations, 38(263-265)

Donohue, S., & Long, M. (2010). Assessment of sample quality in soft clay using shear wave velocity and suction measurements. Géotechnique, 883-889. doi:10.1680/geot.8.T.007.3741

Dyvik, R., & Madshus, C. (1985). Lab measurements of Gmax using bender elements. ASCE Annual Convention on Advances in the Art of Testing Soils under Cyclic Conditions, (ss. 186-196). Detroit, Michigan.

Emdal, A., Gylland, A., Amundsen, H. A., & Long, M. (2016). Mini-block sampler. Canadian Geotechnical Journal, 53(8), 1235-1245. doi:10.1139/cgj-2015-0628 GDS. (u.d.). Bender element technical specification.

Ferreira, C. M. d. F. (2009). The use of seismic wave velocities in the measurement of stiffness of a residual soil. Porto: [s. n.].

Ferreira, C. V. d. F., A. and Santos, J.A. (2007). Comparison of simultaneous bender elements and resonant column tests on Porto residual soil, Soil Stress-Strain Behavior: Measurement, Modeling and Analysis." A Collection of Papers of the Geotechnical Symposium in Rome, 2006, Ling, Callisto, Leshchinsky & Koseki (Eds.):535.

Ferreira C, Viana da Fonseca A, Nash D (2011) Shear wave velocities for sample quality assessment on a residual soil. Soils Found 51(4):683–692 (Special Issue on ''Deformation Characteristics of Geomaterials'', Elsevier)

Fonseca, A.V., Ferreira, C., Fahey, M. (2009). A framework interpreting bender element tests, combining time-domain and frequency-domain methods. Geotechnical Testing Journal, 32(2),

Gasparre, A. (2005). Advanced laboratory characterization of London Clay. PhD thesis, Imperial College London, London, UK.

References

Gasparre, A., Nishimura, S., Coop, M. R. & Jardine, R. J. (2007a). The influence of structure on the behaviour of London Clay. Géotechnique 57, No. 1, 19–31. 2007.57.1.19.

Gasparre, A., Nishimura, S., Anh-Minh, N., Coop, M. R. & Jardine, R. J. (2007b). The stiffness of natural London Clay. Géotechnique 57, No. 1, 33–47,. 2007.57.1.33.

Gasparre, A., Hight, D. W., Coop, M. R. & Jardine, R. J. (2014). The laboratory measurement and interpretation of the small strain stiffness of stiff clays. Géotechnique 64, No. 12, 942–953

Graham, J., & Houlsby, G. T. (1983). Anisotropic elasticity of a natural clay. Géotechnique, 33(2), 165-180. doi:10.1680/geot.1983.33.2.165

Gylland, A., Long, M., Emdal, A., & Sandven, R. (2013). Characterisation and engineering properties of Tiller clay. Engineering Geology, 164, 86-100. doi:10.1016/j.enggeo.2013.06.008

Hardin, B. O. (1978). Nature of stress-strain behaviour for soils. Proceedings of the ASCE Geotechnical Engineering Division Specialty Conference, 1, ss. 3-90. Pasadena, California.

Hardin, B. O., & Richart, F. E. (1963). Elastic wave velocities in granular soils. Journal of Soil Mechanics and Foundations Division, 89(1), 33-66.

Hardin, B.O. and Blandford, G.E., (1989). "Elasticity of Particulate Material." J. Geotech. Eng. Div., ASCE, 115(6), 788-805.

Hasan, A. M. (2016). Small strain elastic behaviour of unsaturated soil investigated by bender/extender element testing. Ph.D.thesis. University of Glasgow.

Hoar, R. J., and Stokoe, K. H. (1978). Generation and measurement of shear waves in situ. Dynamic geotechnical testing, ASTM, Philadelphia, 3–29.

Hori, T., Yamashita, S., & Suzuki, T. (2006). Anisotropy of elastic moduli at small strain of sand and clays by bender element test. Proceedings of the International Symposium on Geomechanics and Geotechnics of Particulate Media. Ube, Japan.

ISO. (2014a). Geotechnical investigation and testing - Laboratory testing of soil - Part 1: Determination of water content. Switzerland: International Organization for Standardization.

ISO. (2014b). Geotechnical investigation and testing — Laboratory testing of soil — Part 2: Determination of bulk density. Switzerland: International Organization for Standardization.

ISO. (2015). Geotechnical investigation and testing — Laboratory testing of soil — Part 3: Determination of particle density. Switzerland: International Organization for Standardization.

ISO. (2016). Geotechnical investigation and testing — Laboratory testing of soil — Part 4: Determination of particle size distribution. Switzerland: International Organization for Standardization.

ISO. (2017). Geotechnical investigation and testing — Laboratory testing of soil — Part 6: Fall cone test. Switzerland: International Organization for Standardization.

ISO. (2018a). Geotechnical investigation and testing — Laboratory testing of soil — Part 9: Consolidated triaxial compression tests on water saturated soils. Switzerland: International Organization for Standardization.

ISO. (2018b). Geotechnical investigation and testing — Laboratory testing of soil — Part 12: Determination of liquid and plastic limits. Switzerland: International Organization for Standardization.

Jamiolkowski, M., Ladd, C. C., Germaine, J. T., & Lancelotta, R. (1985). New developments in field and laboratory testing of soils. Proc. 11th ICSMGE, (ss. 57-153). San Francisco.

Jamiolkowski, M., Lancellotta, R., & Lo Presti, D. C. (1995). Remarks on the stiffness at small strains of six Italian clays. Pre-failure Deformation of Geomaterials , (ss. 817-836). Balkema.

References

Janbu, N. (1985). "Soil models in offshore engineering: The 25th Rankine lecture." Géotechnique, 35(3), 241–281.

J.biarez and P.Y.Hicher. (1994). Elemantary Mechanics of Soil Behaviour. Balkema

Jovicic, V., & Coop, M. R. (1998). The Measurement of Stiffness Anisotropy in Clays with Bender Element Tests in the Triaxial Apparatus. Geotechnical Testing Journal, 21(1), 3-10. doi:10.1520/GTJ10419J

Jovicic, V., Coop, M. R., & Simic, M. (1996). Objective criteria for determining Gmax from bender element tests. Géotechnique, 46(2), 357-362. doi:10.1680/geot.1996.46.2.357

Kartverket. (2019). Available at: http://norgeskart.no (Accessed: May 2019).

Kawaguchi, T., Mitachi, T., & Shibuya, S. (2001). Evaluation of shear wave travel time in laboratory bender element test. Proceedings of the International Conference on Soil Mechanics and Geotechnical Engineering., (ss. 155-158).

Kim, T., & Finno, R. J. (2012). Anisotropy Evolution and Irrecoverable Deformation in Triaxial Stress Probes. Journal of Geotechnical and Geoenvironmental Engineering, 138(2).

Kim, T., & Finno, R. J. (2014). Elastic Shear Modulus of Compressible Chicago Clay. KSCE Journal of Civil Engineering (2014) 18(7):1996-2006.

Kokusho, T., Yoshida, Y., & Esahi, Y. (1982). Dynamic Properties of Soft Clay for Wide Strain Range. Soils and Foundations, 22(4). doi:10.3208/sandf1972.22.4_1

Kramer, S. (1996). Geotechnical Earthquake Engineering. Prentice Hall, Upper Saddle River, New Jersey.

Kumar, S. S., Krishna, A. M., & Dey, A. (2013). Parameters Influencing Dynamic Soil Properties: A Review Treatise. National Conference on Recent Advances in Civil Engineering.

Ladd, C.C. and DeGroot D.J. (2003). Recommended practice for soft ground site characterization: Arthur Casagrande Lecture. 12th, PCSMGE, MIT, Cambridge, Massachusetts.

Landon, M. M., & DeGroot, D. J. (2006). Measurement of small strain shear modulus anisotropy on unconfined clay samples using bender elements. In: GeoCongress 2006: Geotechnical engineering in the information technology age. American Society of Civil Engineers. doi:10.1061/40803(187)20

Landon, M. M., DeGroot, D. J., & Sheahan, T. C. (2007). Nondestructive Sample Quality Assessment of a Soft Clay Using Shear Wave Velocity. Journal of Geotechnical and Geoenvironmental Engineering, 133(4).

Langø, H. (1991). Cyclis shear modulus on natural intact clays. Trondheim.

Lee, & Santamarina. (2005). Bender Elements: Performance and Signal Interpretation. Journal of Geotechnical and Geoenvironmental Engineering, 131(9). doi:10.1061/(ASCE)1090-0241(2005)131:9(1063)

Leong, E. C., J. Cahyadi and H. Rahardjo (2009). Measuring shear and compression wave velocities of soil using bender-extender elements. Canadian Geotechnical Journal, 46(7), pp. 792-812.

Leong, E. C, Yeo, H.S & Rahardjo.H (2005). Measuring Shear Wave Velocity Using Bender Elements. Geotechnical Testing Journal, Vol. 28, No. 5.

Leroueil, S., & Hight, D. W. (2003). Behaviour and properties of natural soils and soft rocks. International Workshop on Characterisation and Engineering Properties of Natural Soils, (ss. 29-254). Rotterdam, Netherlands.

L'Heureux, J.-S., & Long, M. (2016). Correlations between shear wave velocity and geotechnical parameters in Norwegian clay. Proceedings of the 17th Nordic Geotechnical Meeting. Reykjavik.

References

L'Heureux, J.-S., & Long, M. (2017). Relationship between Shear-Wave Velocity and Geotechnical Parameters for Norwegian Clays. Journal of Geotechnical and Geoenvironmental Engineering, 143(6).

L'Heureux, J.-S., Lindgård, A., & Emdal, A. (u.d.). (2019) The Tiller-Flotten research site: Geotechnical characterisation of a very sensitive clay deposit. AIMS Geosciences.

Li, X. S. (2003). Effective stress in unsaturated soil: a microstructural analysis. Ge´otechnique 53, No. 2, 273–277.

Lings, M. L., Pennington, D. S., & Nash, D. F. (2000). Anisotropic stiffness parameters and their measurement in a stiff natural clay. Géotechnique, 50(2), 109-125. doi:10.1680/geot.2000.50.2.109

Long, M., & Donohue, S. (2007). In situ shear wave velocity from multichannel analysis of surface waves (MASW) tests at eight Norwegian research sites. Canadian Geotechnical Journal. doi:10.1139/t07-013

Long, M., & Donohue, S. (2010). Characterisation of Norwegian marine clays with combined shear wave velocity and piezocone cone penetration test (CPTU) data. Canadian Geotechnical Journal, 47, 709-718. doi:10.1139/T09-133

Lunne, T., Berre, T., Andersen, K. H., Strandvik, S., & Sjursen, M. (2006). Effects of sample disturbance and consolidation procedures on measured shear strength of soft marine Norwegian clays. Canadian Geotechnical Journal, 43(7), 726-750. doi:10.1139/t06-040

Maja, M. (2019). An Experimental Study of Anisotropic Stiffness of Tiller-Flotten Quick Clay Using Bender Elements. Master's thesis, NTNU, Trondheim, Norway.

Mayne paul W., (2000). Enhanced geotechnical site characterization by seismic piezocone penetration test. Invited Lecture, Fourth International Geotechnical Conference, Cairo University, January 2000, pp. 95-120.

Mayne paul w.,&Rix Gleen j.,(1995). Correlation between shear wave velocity and cone tip resistance in natural clays. Japanese Society of soil Mechanics and Foundation Engineering. Vol 35, No. 2, 107-110.

Masin, D., & Rott, J. (2014). Small strain stiffness anisotropy of natural sedimentary clays: review and a model. Acta Geotechnica. doi:10.1007/s11440-013-0271-2

Mitaritonna,G., Amorosi, A., Cotecchia, Federica.(2010). Technical University of Bari.

Mitchell, J., & Soga, K. (2005). Fundamentals of soil behavior. John wiley and sons. Third edition.

Meirovitch L. (1967). Analytical methods in vibrations. Macmillan, New York.

Mui, T. S. (2005). The shearing effect of suction. MPhil thesis, Hong Kong University of Science and Technology.

NGI. (2019). Available at: https://www.ngi.no/eng/Projects/NGTS-Norwegian-Geo´-Test-Sites (accessed: May 2019).

NGU. (2019). Available at: http://geo.ngu.no/kart/minkommune/?kommunenr=5001 (accessed: May 2019).

NTNU. (2015). Geotechnics. Field and Laboratory Investigations. Lecture notes MSc course TBA 4110. Trondheim: Geotechnical Division, NTNU.

Pennington, D. S., Nash, D. F., & Lings, M. L. (1997). Anisotropy of G0 shear stiffness in Gault Clay. Géotechnique, 47(3), 391-398. doi:10.1680/geot.1997.47.3.391

PLAXIS. (2018). Material Models Manual. Build 9462.

Rio, J. F. (2006). Advances in Laboratory Geophysics Using Bender Elements. PhD thesis, University College London.

References

Roesler, S. K. (1979). Anisotropic Shear Modulus due to Stress Anisotropy. Journal of the Geotechnical Engineering Division, 105(7), 871-880.

Sanchez-Salinero, I., Roesset, J., & Stokoe, K. (1986). Analytical studies of body wave propagation and attenuation. Austin: University of Texas.

Santamarina Jc, Klein KA,Fam MA. Soils and waves. New York: John Wiley & Sons Ltd: (2001). P. 238-82

Satoshi nishimura. (2005). A thesis submitted to the University of London in partial fulfilment for the degree of Doctor of Philosophy and Diploma of Imperial College London. A thesis submitted to the University of London in partial fulfilment for the degree of Doctor of Philosophy and Diploma of Imperial College London

Sayers, C. M., & Den Boer, L. D. (2016). The elastic anisotropy of clay minerals. Geophysics, 81(5). doi:10.1190/geo2016-0005.1

Shirley, D. J., & Hampton, L. D. (1978). Shear-wave measurements in laboratory sediments. The Journal of the Acoustical Society of America, 63(2), 607-613. doi:10.1121/1.381760

Stokoe.K.H, & Santamarina, J. C. (2000). Seismic-Wave-Based Testing in Geotechnical Engineering.In GeoEng. An International Conference In geotechnical And Geological Eng.

Sully, J. P., & Campanella, R. G. (1995, June). Evaluation of in situ anisotropy from crosshole and downhole shear wave velocity measurements. Géotechnique, 45(2), 267-282. doi:10.1680/geot.1995.45.2.267

Tan, T.-S., Lee, F.-H., Chong, P.-T., & Tanaka, H. (2002). Effect of sampling disturbance on properties of Singapore clay. Journal of Geotechnical and Geoenvironmental Engineering, 128(11), 898-906. doi:10.1061/(ASCE)1090-0241(2002)128:11(898)

Teng, F., Ou, C., & Hsieh, P. (2014). Measurements and Numerical Simulations of Inherent Stiffness Anisotropy in Soft Taipei Clay. Journal of Geotechnical and Geoenvironmental Engineering, 140(1), 237-250. doi:10.1061/(ASCE)GT.1943-5606.0001010

T. G. Sitharam, L. GovindaRaju and A. Sridharan. (2004). Dynamic properties and liquefaction potential of soils. GEOTECHNICS AND EARTHQUAKE HAZARDS, CURRENT SCIENCE, VOL. 87, NO. 10, 25

Tonje Eide Helle1, Per Aagaard, Steinar Nordal, Michael Long and Sara Bazin5.(2019). A geochemical, mineralogical and geotechnical characterization of the low plastic, highly sensitive glaciomarine clay at Dragvoll, Norway. AIMS Geosciences, 5(4): 704–722.

Toki.S, Shibuya.S, & Yamashita .S.(1995). Standardization of Laboratory test Methods to determine The Cyclic Deformation Properties Of Geomaterials In Japan. Pre-failure Deformation of Geomaterials, Volume 2, Pages 741-784. Balkema. Rotterdam.

Towhata, I. (2008). Geotechnical Earthquake Engineering. Springer. doi:10.1007/978-3-540-35783-4

Viggiani, G., & Atkinson, J. H. (1995a). Interpretation of bender element tests. Géotechnique, 45(1), 149-154. doi:10.1680/geot.1995.45.1.149

Viggiani, G., & Atkinson, J. H. (1995b). Stiffness of Fine Grained Soil at Very Small Strains. Géotechnique, 45(2), 249-265. doi:10.1680/geot.1995.45.2.249

Vucetic, M., & Dobry, R. (1991). Effect of Soil Plasticity on Cyclic Response. Journal of Geotechnical Engineering, 117(1), 89-107.

Wang, Y. H., & Mok, C. M. (2008). Mechanisms of Small-Strain Shear-Modulus Anisotropy in Soils. Journal of Geotechnical and Geoenvironmental Enginnering, 134(10), 1516-1530. doi:10.1061/(ASCE)1090-0241(2008)134:10 (1516)

Wang, Y. H., & Siu, W. K. (2011). Structure characteristics and mechanical properties of kaolinite soils. II. Effects of structure on mechanical properties. Canadian Geotechnical Journal, 43(6), 601-617. doi:10.1139/t06-027.

Won, J. Y. (2013). Anisotropic strength ratio and plasticity index of natural clays. Proceedings of the 18th International Conference on Soil Mechanics and Geotechnical Engineering. Paris.

Wongsaroj, J., Soga, K., Yimsiri, S., & Mair, R. J. (2004). Stiffness anisotropy of London Clay and its modelling: Laboratory and Field. Advances in Geotechnical Engineering: The Skempton Conference. London.

Yamashita, S., Kawaguchi, T., Nakata, Y., Mikami, T., Fujiwara, T., & Shibuya, S. (2009). Interpretation of international paralel test on the measurement of Gmax using bender elements. Soils and Foundations, 49(4), 631-650.
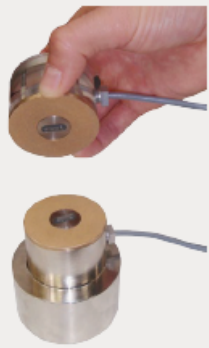
Yuanqiang cai.,Quanyang Dong, Jun Wang.,Chuan Gu, Changjie Xu.(2015). Measurement of small strain shear modulus of clean and natural sands in saturated condition using bender element test.

Wood, Tara. (2016). On the Small Strain Stiffness of Some Scandinavian Soft Clays and Impact on Deep Excavations. PhD thesis, Chalmers University of Technology. Gothenburg, Sweden.

APPENDIX A – Bender Element Specifications

World leaders in the manufacture of laboratory systems for soil & rock

Bender Element System (BES)

The GDS Bender Element system enables easy measurement of the maximum shear modulus of a soil at small strains in a triaxial cell. Measurement of soil stiffness at very small strains in the laboratory is difficult due to insufficient resolution and accuracy of load and displacement measuring devices. The capability exists to regularly carry out measurements of small strain stiffness in the triaxial apparatus using local strain transducers, but this can be expensive and is generally confined to research projects.

The addition of Bender Elements to a triaxial testing system makes the routine measurement of Gmax, maximum shear modulus, simple and cost effective.

Key Features:	Benefits to the User:
USB interface:	Allows the system to be swapped to any PC in the lab with a USB interface.
Titanium element inserts:	Reduces the weight of the top-cap.
Utilising existing products:	Pedestals and top-caps can be made for other manufacturers' cells as well as GDS cells, so upgrading is potentially simple.
The GDS Bender elements are bonded into a standard insert:	This makes the bender element insert a modular device that can then be easily fitted into a suitably modified pedestal/top-cap. Should an element fail, it is simple and quick for the complete insert to be replaced by the customer
2 Mega Samples/Second, 16bit Data Acquisition:	High speed data acquisition is essential as the sample interval provides the resolution for determining wave speeds.
Elements are manufactured to allow S and P wave testing to be performed:	Determining both S & P wave velocities allows additional specimen parameters to be calculated, such as Youngs Molulus, E.
Vertical and horizontal elements are available:	Specimen anisotropy can be studied with the use of both vertical and horizontal elements on the sample.

Tests that can be Performed:

Determination of Shear Wave Velocity, determination of P-Wave Velocity, vertically propogating horizontally polarised (vertical elements), horizontally propogating horizontally polarised (horizontal elements), horizontally propogating vertically polarised (horizontal elements).

Upgrade Options:

- Combined pedestals for unsaturated testing and bender elements (ie with bonded high air entry porous disc).

Technical Specification:

|	
Data acquisition speed:	2,000,000 samples/second, simultaneous sampling of both source and received signals.
Resolution of data acquisition (bits):	16
Operating Pressure Range:	Up to 3.5MPa. Above 3.5MPa Acoustic Velocity transducers are required for P&S waves.
Computer Interface:	USB
Available gain ranges for data acquisition:	From x10 to x500
Operating Temperature:	-10°C to 50°C
Sample Sizes:	Up to 300mm

APPENDIX B – Bender Element Equipment
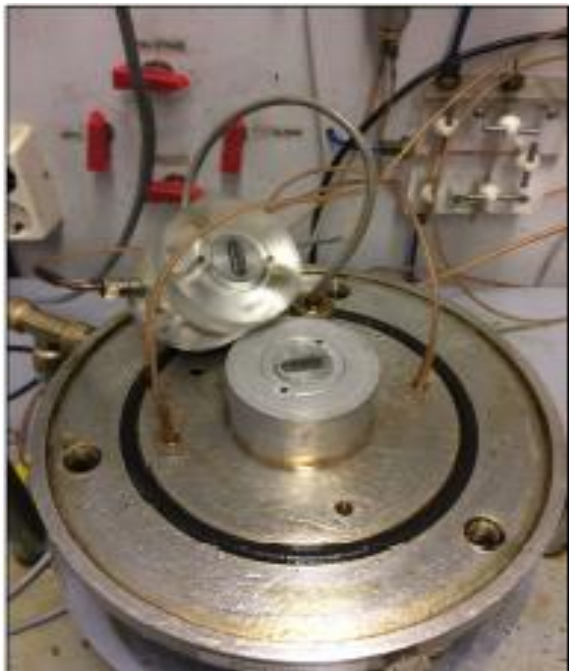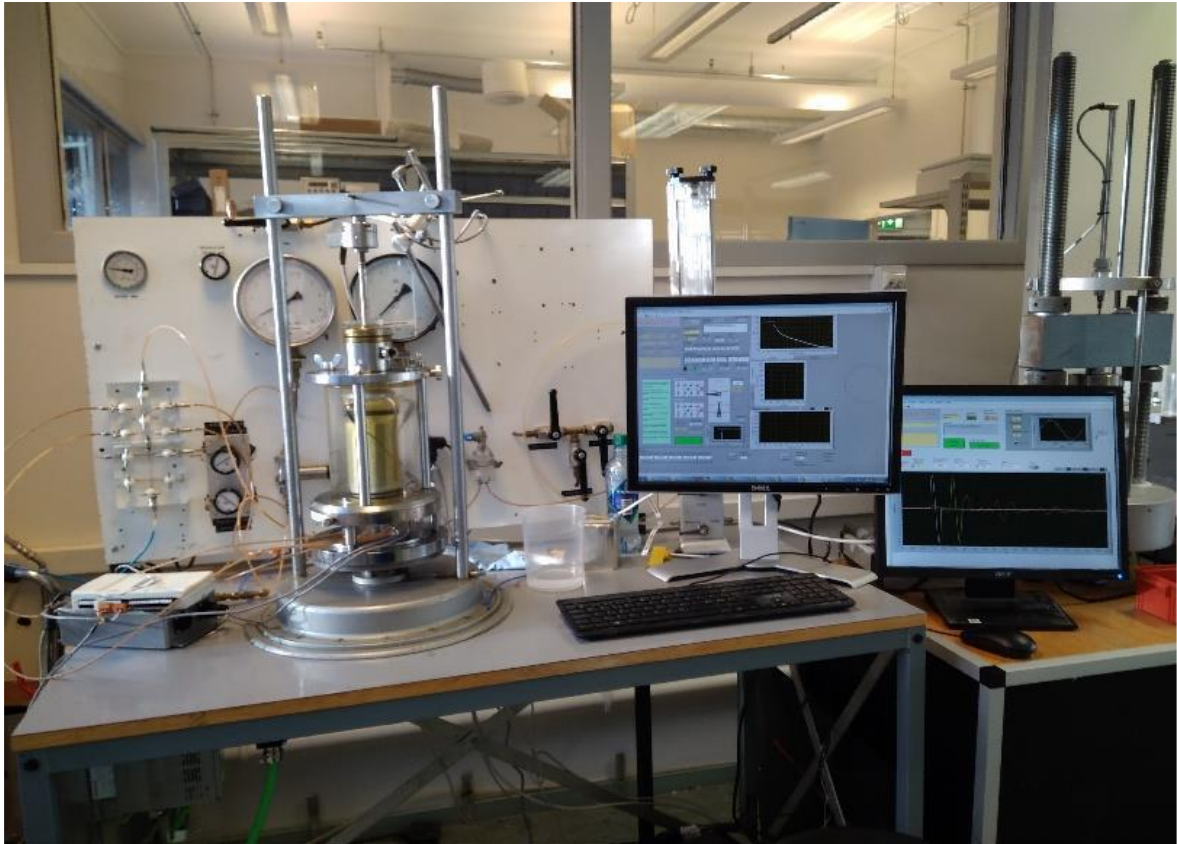
Photo by Maja (2019) and Beeston (2018)

APPENDIX C –Sample Preparation Apparatus